I.O.S.

SIZEWELL - DUNWICH BANKS FIELD STUDY

TOPIC REPORT 5

B J LEES AND A D HEATHERSHAW

OFFSHORE SEDIMENT MOVEMENT AND ITS RELATION TO OBSERVED TIDAL CURRENT AND WAVE DATA

REPORT NO 123

1981

NATURAL ENVIRONMENT RESEARCH COUNCIL

INSTITUTE OF OCEANOGRAPHIC SCIENCES

In most cases (c) and (d) will be modified by the effects of wave activity.

2.2 Non-linear effects

Heathershaw and Hammond (1979) consider that the principal difficultly involved in measuring and predicting sediment transport is its extreme non-linearity. From a dynamic point of view bedload transport (q_{sb}) is related to the friction velocity u_* times the excess shear stress $(\tau - \tau_{cr})$ at high transport rates and to u_* times the excess shear stress squared $(\tau - \tau_{cr})^2$ at low transport rates. Suspended sediment transport (q_{ss}) is dynamically related to the friction velocity u_* to a power greater than unity, times the excess shear stress. Here τ is the shear stress exerted on the sea bed and τ_{cr} is a critical value of τ related to the threshold of movement of material as bedload or in suspension.

Since $u_* = \left(\frac{\tau}{\rho}\right)^{-2}$, where ρ is the density of seawater

$$q_{sb} \propto \begin{cases} u_*(\tau - \tau_{cr}) \propto u_*^3 & \text{at high transport rates} \\ u_*(\tau - \tau_{cr})^2 \propto u_*^5 & \text{at low transport rates} \end{cases}$$

and $$q_{ss} \propto u_*^n(\tau - \tau_{cr}) \propto u_*^{n+2}$$

where $n = 1$ at least.

Further difficulties arise in computing bed load transport on rippled beds due to the uncertainty in partitioning the bed shear stress into that part which overcomes form drag and that part which is due solely to skin friction (see, eg Smith 1977; Smith and McLean 1977).

SIZEWELL - DUNWICH BANKS FIELD STUDY

TOPIC REPORT 5

B J Lees and A D Heathershaw

Offshore sediment movement and its relation to observed tidal current and wave data

Report No 123

1981

This project was supported financially by the Department of the Environment

Institute of Oceanographic Sciences
Crossway
Taunton
Somerset

CONTENTS

CONTENTS (Contd)

SUMMARY

This is the fifth in the Topic Report series concerning the Sizewell-Dunwich Banks area.

Observed and predicted transport rates have indicated that for sand size particles (d_{50} = 2.9Ø, 130 μm) sediment is moved mainly in the suspended mode. Measured suspended sand concentrations reach maxima of 423 mg l^{-1} at 175 cm above the seabed (ASB) and 1892 mg l^{-1} at 15 cm ASB. The calculated net suspended sediment transport rate for the total water column during a spring tide was 5.66 g $cm^{-1}s^{-1}$ in the ebb direction, ie to the NNE. The rate is likely to be 1/5 of this during neap tides.

Grain size analyses and subsequent calculations of transport rates for separate sand fractions show that the material transported is predominantly very fine sand. There is a relatively stable concentration of silt and clay present, with a depth mean concentration in 10 m of water of 230 mg l^{-1}. Overall the suspended particles do not affect the velocity profiles in the bottom 2 m, which fit the Karman-Prandtl logarithmic relationship well. From 2 m to the surface a power law expression, with an exponent of 0.1, is more representative.

Bed load rates have been measured using a fluorescent tracer, showing a depth of mixing of 17 cm after equilibrium with the background had been reached. In the short term, the rates were dependent on the tidal flow pattern, with a rate of 0.012 g cm^{-1} s^{-1} to the S, between 5 and 50 days after the injection, ie when equilibrium had been reached. During a period which included the recording of high waves (Hs = 2.5 m, Tz = 10s) the rate increased to 0.015 g cm^{-1} s^{-1}, and the direction changed to shoreward. These rates are at least 2 orders of magnitude smaller than the instantaneous rate given above for suspended load.

The logarithmic and power law relationships have been used to predict bed load sediment transport rates from mid-water current meter data. Comparison with the tracer experiment results has shown that of 5 widely used sediment transport formulae, Yalin's (1963) equation gives the best predictions. Although bed load transport paths predicted using this equation are shown to be mainly to the S, some transport is also indicated towards the N, in the vicinity of the Dunwich Bank, with a bed load parting offshore at Walberswick. The rates overall are of

the order of 0.02 g cm^{-1} s^{-1}, predicted from 2 month's current meter data at each site.

The location of the banks is geologically controlled by the outcrop of Coralline Crag at Thorpe Ness. Their trend and growth to the N over time appear to be in direct contrast to the bed load transport to the S. However, as already noted, it is suspended load transport which dominates and the evidence points to an ebb or northerly residual in the measured suspended rates. Thus the maintenance of the banks is likely to be dependent on a tidal suspended sediment mechanism. At the present time there is very little sediment supplied from the adjacent coastline and the presence of a sand comprising well-rounded grains, d_{50} = 2.5Ø, 180 μm, in suspension during the flood tide, different from that on the seabed, suggests that at least some material is entering the area from the N. Flushing of sediment to the SE probably occurs between Thorpe Ness and the Sizewell Bank in the S.

1. INTRODUCTION

This report is the fifth in the series of Topic Reports concerning the Sizewell-Dunwich Banks Field Study. It describes measurements of sediment transport rates and prediction of the sediment circulation pattern in the Sizewell-Dunwich area (Figure 1). The work parallels a similar study carried out in Swansea Bay (Heathershaw and Hammond, 1979). One area of interest concerning the two studies is the possibility of the general application of different sediment transport prediction formulae. Such considerations have broader implications with respect to sediment transport processes in the sea and will be discussed further below.

Observed transport rates have been used to determine the relative magnitudes of suspended and bedload transport, principally under tidal currents. The observed bedload sand transport rate has been used in the selection of a suitable sediment transport formula for the prediction of sediment transport rates and paths in the area. The role of surface wave activity in modifying the sediment transport processes is also briefly considered.

For a description of the long-term objectives of the Sizewell-Dunwich research programme, reference should be made to Lees (1980).

2. DYNAMICS OF SEDIMENT TRANSPORT

2.1 Fundamental processes

Sediment may be moved on or above the sea bed in two modes:

(a) bedload in which grains roll or saltate along the sea bed, perhaps at heights of up to a few grain diameters;
(b) suspended load in which grains are transported within the body of the fluid at some distance (many grain diameters) from the boundary.

Under tidal currents the motile agencies of these modes consist respectively of:

(c) the action of an applied stress at the sea bed by the action of the tidal current flowing above it;
(d) the production of turbulent kinetic energy by shear in the bottom boundary layer.

In most cases (c) and (d) will be modified by the effects of wave activity.

2.2 Non-linear effects

Heathershaw and Hammond (1979) consider that the principal difficultly involved in measuring and predicting sediment transport is its extreme non-linearity. From a dynamic point of view bedload transport (q_{sb}) is related to the friction velocity u_* times the excess shear stress $(\tau - \tau_{cr})$ at high transport rates and to u_* times the excess shear stress squared $(\tau - \tau_{cr})^2$ at low transport rates. Suspended sediment transport (q_{ss}) is dynamically related to the friction velocity u_* to a power greater than unity, times the excess shear stress. Here τ is the shear stress exerted on the sea bed and τ_{cr} is a critical value of τ related to the threshold of movement of material as bedload or in suspension.

Since $u_* = \left(\frac{\tau}{\rho}\right)^{-2}$, where ρ is the density of seawater

$$q_{sb} \propto \begin{cases} u_*(\tau - \tau_{cr}) \propto u_*^3 & \text{at high transport rates} \\ u_*(\tau - \tau_{cr})^2 \propto u_*^5 & \text{at low transport rates} \end{cases}$$

and $$q_{ss} \propto u_*^n(\tau - \tau_{cr}) \propto u_*^{n+2}$$

where $n = 1$ at least.

Further difficulties arise in computing bed load transport on rippled beds due to the uncertainty in partitioning the bed shear stress into that part which overcomes form drag and that part which is due solely to skin friction (see, eg Smith 1977; Smith and McLean 1977).

Whereas it is possible to calculate bedload transport from a knowledge of the sediment and flow characteristics alone, calculation of suspended load transport also requires a knowledge of the concentration at a specified height above the sea bed, the so-called reference concentration. This information, which requires special measuring techniques, is frequently not available, and successful suspended load prediction in the sea is one of the major difficulties presently confronting engineers, sedimentologists, geologists and oceanographers.

3. DISTRIBUTION OF SEDIMENTS

In the Sizewell-Dunwich study as in Swansea Bay (Heathershaw and Hammond, 1979) it will be seen that the overall diversity and changing distribution of sediments make the prediction of sediment transport rates difficult.

The coarser fraction is almost entirely fine to very fine sand (Wentworth scale), with the mean grain diameter varying from 3.38Ø (96 μm) to 2.19Ø (219 μm) in the samples measured. The main body of sand forms the two banks, extending over an area approximately 13 km long and 3 km wide, parallel to the coast and about 2 km away from it. Figure 2 shows typical grain size analysis curves of boxcore samples obtained mainly from the eastern slope of the banks, with their locations depicted in Figure 3.

Although the banks may be considered morphologically as one, the sediment distribution along their length does appear to vary seasonally. In winter clean , well-sorted sand forms both the banks and the col between (Figure 4), but in the spring, summer and autumn, clean sand is restricted to the banks. In summer the finer sands have been found towards the crests, and the standard deviations ranging from 0.26Ø to 0.71Ø indicate well-sorted to moderately well-sorted sediments (Folk, 1968). At the same time the col between the banks has been found to consist of intercalated sands, silts and clays, giving a much greater range of grain sizes (Figure 3).

These unconsolidated sediments lie on a gently sloping platform which falls from 0 m to 15 m in approximately 5 km along a line normal to the shore. In the S the oldest bedrock forming part of the platform is a WSW to ENE aligned ridge, which is almost completely buried. It comprises Coralline Crag, which was

deposited during the Pliocene, and is an offshore continuation of the core of Thorpe Ness. Lying against this crag are sediments of the Norwich Crag Series, underlying the remainder of the area. In the N the Crag is overlain by sticky blue-grey alluvial clay, well exposed offshore from Southwold and for 7 km to the SW. Further S the alluvium becomes browner as the silt content increases. In the vicinity of the Dunwich Bank the clay is either exposed or buried by the margins of the bank sand, according to the time of year (Figures 3 and 4).

Further offshore, below 15 m depth, there is an area of stable gravel, and S of this another area of sand, but these lie outside the region of study.

A more detailed description of the sediments is given in Lees (1980).

4. BEDLOAD TRANSPORT

4.1 Prediction of bedload transport rates

Various formulae have been developed to predict sediment transport paths and rates from current meter data, largely as a result of work in flumes and rivers. A major aim of the present project has been to compare such formulae with the direct measurement of bedload transport rates in the field. For a discussion on the selection of potentially useful formulae for such comparisons see Heathershaw and Hammond (1979). The 5 formulae ultimately selected for evaluation here are described in Appendix A, and the methods of calculating the required threshold velocities are given in Appendix D of Heathershaw and Hammond (1979).

Current meter measurements in the Sizewell-Dunwich area have been made at mid-water level at a number of locations (Figure 5). These measurements were originally planned to provide data for validating a two-dimensional numerical model of the water circulation (Lees, 1977). Consequently it was decided that the current at mid-depth would give the best parameterisation of the depth mean flow for the model and throughout the study current measurements have been made at this level. Justification for using mid-depth readings to predict sediment transport rates along the seabed is given in Heathershaw and Lees (1980) and Soulsby (1978). The conventional recording current meter techniques used are described in the former report.

However, to predict sediment transport rates from mid-depth current measurements it has been necessary to extrapolate from this level down to the seabed to obtain friction velocity and bed shear stress estimates. Heathershaw and Lees (1980) have shown and illustrated in their Figure 15 that velocity profiles over the bottom half of the flow do not follow any of the accepted forms, except in the lowest 2 m where there is reasonable evidence (Lees, 1981) to suggest that the distribution is logarithmic. Consequently in this study an empirical approach has been adopted, in which a power law has been used to extrapolate from the mid-depth current measurement down to the top of a notionally logarithmic layer, at a height of 2 m above the sea bed. This approach cannot take account of any veering in the water column, due to bottom friction and the Earth's rotation, which from theoretical considerations (Heathershaw and Hammond, 1980) is of the order of 2° for these water depths and flow speeds. This figure may be compared with values of 2 - 3° obtained by Soulsby (1978) from current measurements in the Sizewell-Dunwich Banks area and in any case it is within the error of the current measurements. Furthermore, where regional scale predictions are required it is doubtful whether the results from detailed current measurements at one site would have general applicability when applied to the area as a whole. This is because velocity profiles and veering effects are likely to be strongly influenced by topography. It was, therefore, considered that the two-layer model approach adopted in this study had the greatest general validity.

In the top half of the model the power law velocity profile is given by

$$\frac{u}{u_r} = \left(\frac{z}{z_r}\right)^p \qquad (1)$$

where u is the velocity at height z, u_r the velocity at the reference height z_r and p the exponent normally considered to be between $^1/7$ and $^1/10$ (Dyer, 1970). In the bottom layer the velocity distribution is logarithmic and of the form

$$u = \frac{u_*}{k} \cdot \ln \frac{z}{z_0} \qquad (2)$$

where u_* is the friction velocity, k von Karman's constant and z_0 the roughness length. Matching these distributions at the top of the logarithmic layer and writing the friction velocity in terms of the height of the logarithmic layer z_2, the height of the mid-depth current measurement z_6 and the mid-depth current u_6, gives

$$u_* = \frac{u_6 k}{\left(\frac{z_6}{z_2}\right)^p \ln\left(\frac{z_2}{z_0}\right)} \qquad (3)$$

Equation (3) was therefore used to obtain friction velocity u_* and bed shear stress estimates ($\tau = \rho u_*^2$ where ρ is the water density) for input to the various sediment transport equations. u_6, the mid-depth current, was usually measured at a height of 6 m (see Table 1) and similarly to the Swansea Bay Study (Heathershaw and Hammond, 1979) it was necessary to prescribe the roughness length z_0 at each of the locations where predictions were required and where current measurements had been made. This was achieved by comparison of the known sediment types in the area (Figures 3 and 4) with those from other areas described in the literature, where roughness length measurements had been made. The values adopted for this study are shown in Table 1.

The value of the exponent p in equation (1) was taken as 0.1 and this was based upon velocity profile measurements from the Marconi current meter system (Heathershaw and Lees, 1977) (Figure 5). Figure 6 shows exponent (p) values obtained from hourly averages of the more comprehensive Marconi data and these show some tendency for p to decrease with increasing flow (shown in terms of the current a height of 100 cm above the bed, u_{100}). However, it should be noted that in most cases power law profiles could only be fitted to the measured currents with correlation coefficients less than the 10% significance level. The value of $p = .1$ is close to the mean value of p for all the profiles shown in Figure 6.

Sediment transport predictions were made using the same formulae examined in the Swansea Bay Study (Table 2), full details of which are given in Appendix A.

To obtain net transport rates from the predictions based upon current meter records, successive 10 minute samples of current speed and direction were

converted to sediment transport rates and directions and then vector averaged over a large number of tidal cycles, the exact number being determined by the length of the current meter record. Smoothed progressive vector diagrams of sediment transport rates and directions are shown in Appendix B, Figures B.1 to B.34. The net transport rates used in the comparisons of sediment transport formulae and in the eventual prediction of sediment transport paths, as described in this report, are thus the resultants of the appropriate progressive vector diagrams, examples of which are shown in Appendix B. The sediment transport progressive vector diagrams may be compared with those for the water movements given by Heathershaw and Lees (1980). It is clear from these comparisons that residual sediment and water movements can be in significantly different directions.

4.2 Measurement of bedload transport rates

A fluorescent tracer experiment undertaken at a site on the SE corner of the Dunwich Bank enabled bedload transport estimates to be made. They have been compared with predicted rates using current measurements from nearby current meter moorings (Stations A, N and P). Details of the tracer experiment, during which the dispersion of fluorescent tracer was monitored over a period of 7.5 months, are given in Lees (1979) and Lees (1981).

Examples of the tracer dispersion patterns are given in Figure 7A and B. The first three contour maps, covering the tracer dispersion up to 51 days after the injection, show elongation of the tracer cloud on the seabed parallel to the bank, reflecting the almost rectilinear tidal flow pattern. In spite of strong currents of up to 120 cms^{-1} measured at mid-water near the injection site, the recorded tracer sand did not move far. After Day (D) 51, lateral spreading became apparent, particularly towards the bank in a westerly (shorewards) direction. Table 3 shows the maximum excursions for the different surveys, using a concentration of 10 grains kg^{-1} as the criterion for the boundary.

The concentration results were converted to sediment transport rates using the method described by Heathershaw and Carr (1977), based on similar methods used for radioactive tracer by Courtois and Monaco (1969) and other workers. The method involves calculating the centroid, or centre of gravity of each tracer cloud, knowing the depth to which the tracer has become mixed and combining the two. The x and y coordinates of the centroid of each cloud are given by:

$$\bar{x} = \frac{\sum_{i=1}^{M} C_i x_i}{\sum_{i=1}^{M} C_i} \quad \text{and} \quad \bar{y} = \frac{\sum_{i=1}^{M} C_i y_i}{\sum_{i=1}^{M} C_i} \tag{4}$$

where C_i is the concentration of the tracer at a measured sampling point, x_i and y_i are its coordinates, and M is the number of sample points.

Table 4 shows that the measured depth of mixing and the concentration of tracer in the cores varied in both sets of observations with the greatest depths and highest concentrations near the injection site, as would be expected. A typical variation of concentration with depth, using measurements from one vibrocore, is shown in Figure 8. It has been assumed that the depth of burial increases exponentially with time, and that by D231, the system is close to equilibrium. The mean depth from the 7 box cores taken at the end of the experiment is 16.86 cm and therefore the equilibrium depth has been taken as 17.0 cm. The computed depths of mixing for the various surveys are then as shown in Table 5.

Sediment transport rates have been calculated using the relationship

$$q_{sb} = \rho_s VE \tag{5}$$

where q_{sb} is the sediment transport rate per unit width, E is the depth of mixing, and V is the velocity of the centroid. The bulk density of the sediment ρ_s, was taken as 2.03 g cm^{-3} (Terzaghi and Peck, 1967).

The method depends on the recovery rate of the tracer being high, and calculations indicate that at least 60% of the tracer can be accounted for in each survey. Table 5 shows the results. For each survey the distance and bearing of the centroid from the injection site is given, the centroid velocity, or drift rate, and also the mean rate of daily transport since the injection. Table 6 gives the same information in a slightly different form where the sediment transport rates are calculated from survey to survey rather than the original injection time. The figures are displayed graphically

in Figure 9.

The initial dispersion shown in Figure 7 reflects the tidal flow pattern, with elongation in the directions of the tidal currents, and very little lateral dispersion. The tracer injection was made at high water slack and therefore by D2 the centroid was slightly E of N of the injection site, having moved first with the ebb tide (Figure 9). The calculated transport rate of 0.012 g cm^{-1} s^{-1} (Tables 5 and 6) was not particularly high at this stage, being a resultant of movement first with the ebb, and then with an equal number of flood and ebb tides. As the tracer gradually attained equilibrium with the background sediment, the rate changed from 0.040 g cm^{-1} s^{-1} between D3 and D5 to 0.012 g cm^{-1} s^{-1} between D5 and D50 and the centroid had moved to 33 m S of the injection site. This time taken to reach equilibrium is consistent with the value of 10-20 days suggested by Heathershaw and Carr (1977).

Wave records from a frequency modulated pressure recorder located at Dunwich (Figure 5) show that at some time between D50 and D164.5 gales gave rise to a maximum significant wave height of 2.5 m, with a mean zero crossing period of 9.9 s. The wind direction at the time measured at Gorleston Meteorological Station was NE/ENE. The effect of wave action on the seabed was shown by the rate of transport increasing to 0.015 g cm^{-1} s^{-1} integrated over the period 10 - 12 October 1978 to 2 - 3 February 1979, and the change in direction of centroid movement to a point with a bearing of 241° and 55 m distance from the injection site (Figure 9).

A seventh survey took place in April 1979 (D229), but only isolated patches of tracer in low concentrations, less than 10^2 grains kg^{-1}, were found.

4.3 Comparisons of measured and predicted rates

Using the mid-depth current measurements and equation (3) bedload transport rates were predicted at all locations using the five formulae given in Table 2 and an appropriate roughness length (Table 1). At any one location the predictions show very nearly a two order of magnitude spread while individual equations show up to a factor of 50 difference between highest and lowest rates (Figure 10) which may be attributed partly to seasonal differences in the wave and tidal current regime.

In this study it was not possible to make comparisons between measured and predicted sediment transport rates in correspondingly identical flow regimes. The results shown in Figure 10 were obtained from measurements at the long term current meter mooring (Station A, Figure 5) located about 1 km seaward of the tracer zone. Figure 7A and B shows that the tracer was dispersed, principally by tidal currents in a narrow strip along the crests of the Banks and that stations N and P (Figure 5) probably afford the best comparisons. Taking these (Figure 11) and the remaining results into account it is apparent that Yalin's (1963) equation (Appendix A) gives the best agreement with the measured bedload transport rates. This result may be contrasted with similar comparisons from the Swansea Bay study (Heathershaw and Hammond, 1979) which showed that for measured bedload transport rates, about a factor of 2 higher than those from the Sizewell-Dunwich Banks study, a modified form of Bagnold's (1963) equation gave the best predictions. Figure 10 shows that in this study Bagnold's equation over-predicts the measured rates by very nearly two orders of magnitude and in fact gives the worst prediction of all the equations which were examined. Furthermore Ackers' and White's (1973) equation which performed poorly in the Swansea Bay study (Heathershaw and Hammond, 1979), together with that of Engelund and Hansen (1967) slightly over predicts transport rates for Sizewell-Dunwich (Figure 10). Both these formulae are total load expressions and therefore also include suspended sediment rates in an area where it has been recognised that transport in the suspended mode is dominant (Lees, 1981).

The reasons for these differences between the equations are not clear although it is apparent that the equations may be far more sensitive to the differences in flow regime between the two sites than are the actual measured sediment movements. The sensitivity of the formulae to various parameters is examined in more detail in Heathershaw (1981).

On the basis of the comparisons shown in Figures 10 and 11, Yalin's (1963) equation was chosen for prediction of sediment transport paths in the Sizewell-Dunwich Banks area and this aspect of the work is discussed in a later section of this report.

5. SUSPENDED LOAD TRANSPORT

5.1 Suspended sediment transport formulae

Ways of predicting suspended sediment transport rates directly from a knowledge of the near bottom velocity field, and the sediment characteristics alone, are discussed in Heathershaw and Hammond (1979). The authors conclude that no satisfactory method is presently available.

The suspended sediment transport rate for the total water column (q_{ss}) is better obtained by numerically integrating the product of the equations which represent both the velocity and sediment concentration profiles throughout the water column. Particular emphasis is placed on the near bottom behaviour in both cases.

The velocity distribution can be described by the Karman-Prandtl relationship.

$$u = \frac{u_*}{k} \ln \frac{z}{z_0} \tag{6}$$

where u is the velocity at a height above the seabed z , u_* is the friction velocity, z_0 is the roughness length (the height at which the velocity equals zero) and k is von Karman's constant, generally accepted as equal to 0.4.

The Rouse sediment concentration profile, which has been developed from steady state diffusion equations (Yalin, 1972), gives the mass concentration C_z in terms of a reference concentration C_a , where a is the height above the seabed.

$$\frac{C_z}{C_a} = \left(\frac{h-z}{z} \frac{a}{h-a} \right)^{\frac{W_s}{k u_*}} \tag{7}$$

where C_z is the concentration at height z , C_a is the reference concentration, and h is the total water depth. The Stokes' settling velocity W_s modified according to Shepard (1967) depends on the mean grain size and density of the particles. The numerical integration of the product of equations

(6) and (7) then gives

$$q_{ss} = \frac{C_a U_*}{k}\left(\frac{a}{h-a}\right)^{\frac{w_s}{kU_*}} \int_{z_o}^{h} \left(\frac{h-z}{z}\right)^{\frac{w_s}{kU_*}} \cdot \ln\frac{z}{z_o} \cdot dz \qquad (8)$$

5.2 Techniques

Near bottom velocity and concentration profile measurements were made using the apparatus shown in Figure 12 and described in detail in Appendix F of Heathershaw and Hammond (1979). The heights above the seabed of the sampling nozzle and flowmeters are shown in Table 7.

Profiles were measured approximately once every half hour through one tidal cycle at each of 5 stations during spring tides (Figure 4). Nylon filters with a 40 μm mesh trapped the sand-sized material. It was noted that as sand accumulated on the filter it began to act as a filter itself, trapping increasingly smaller particles. Therefore on return to the laboratory the samples were dried and sieved, primarily to separate the sand from the silt and clay, the former comprising material >63 μm, 4.00Ø, and the latter <63 μm, 4.00Ø.

The velocity measurements were averaged over 10 minute intervals and the velocities and sediment concentrations were fitted to the appropriate equations (6) and (7), using a least squares technique.

The longest uninterrupted data series was obtained at PS4, located approximately 7 km NNE of the injection site for the bed load tracer experiment (Figure 4), and therefore the results from that station are presented in full.

Of 53 sets of velocity readings made at PS4, 50 fit Karman-Prandtl logarithmic profiles with a 95% confidence level, and 32 at a 98% confidence level (Figure 13A). Such high correlation coefficients do not necessarily mean that the profiles are strictly logarithmic, but Figure 13B shows that only those measured near slack water depart much from this ideal. A possible reason for this departure is discussed below.

Figure 14 shows examples of typical concentration profiles separated into the sand fraction (>63 μm, 4.00Ø) and the silt and clay fraction (<63 μm, 4.00Ø). Of the 21 sand fraction samples, two thirds fit Rouse profiles at the 95% confidence level, and 50% of these at 98% level. The ones which fit least well tend to be those measured as the tide was decelerating during the ebb flow, or when accelerating after turning, during both ebb and flood.

5.3 The "hysteresis" effect

An investigation of the relationship between the suspended solids concentration and the velocity at 100 cm above the seabed (u_{100}) shows that there is a difference between the rate at which sand particles are entrained during increasing flow and the fall velocity of excess sand particles returning to the bed during decreasing flow. This is expressed as a time lag of concentration with respect to u_{100} and is the so-called "hysteresis" effect (Thorn, 1975). It is expected that it will be more marked at a greater distance from the seabed (Thorn, 1975; Davies, 1977). At station PS4 during the ebb flow of a spring tide the effect is very marked at 10 cm above the seabed (ASB) and less so at a height of 15 cm, becoming progressively more apparent as the height increases to 175 cm (Figure 15). The anomaly at 10 cm ASB may be related to the structure of the rig (Figure 12), because the base of the frame, including the weights, is likely to affect the flow. The concentration maxima vary from 1181 mg l^{-1} at 15 cm ASB to 491 mg l^{-1} at 175 cm ASB. During the flood tide the effect may be masked by the presence of large quantities of sediment during deceleration, particularly at the lowest level (Figure 15). The maximum concentrations are 1892 gm l^{-1} at 10 cm, to 223 gm l^{-1} at 175 cm ASB. Grain size analysis curves for the suspended sediment, described in more detail below, show bi- and polymodality partly caused by the presence of grains centred on a 2.5Ø mean grain diameter. This material is coarser than the sand on the seabed at PS4 and at least two provenances may be considered. Firstly, sand grains may fall from higher levels during tidal deceleration, and secondly other sand grains may be carried to the sampling station from a different area by the tidal flow.

These complex effects preclude the use of a simple, unique relationship between the suspended sands and the water velocity.

5.4 Grain size analyses of suspended sediment

The samples retained on the filters for each level and each profile at station PS4 were sieved at ½ Ø intervals. Additional representative profiles from the remaining pumped sampling stations were also processed. The calculated grain size distributions of the sand sized material vary not only at the different heights above the seabed, but also through the tidal cycle at any one level. Figure 16 A-F illustrates these variations and Figure 17 and Table 8 depict the changes in means and standard deviations. All measurements were made during a spring tidal cycle.

In the early stages of the flood tide, when the tide was accelerating, the distributions were close to unimodal and the means for the 6 levels varied from 3.24Ø at 15 cm ASB, to 3.58Ø at 85 cm ASB. The samples were very well to well sorted (Folk, 1968) and profile 4.1 exemplifies this stage (Figures 16A and 17).

As the tide accelerated further, the curves began to exhibit bimodality and thus increasingly poorer sorting, showing first at the 15 cm height, with a particularly high concentration of the 2.5Ø fraction. Profile 4.4, (Figures 16B and 17) sampled at the peak of the flood tide, exhibits this phenomenon at the 3 heights of 15, 25 and 45 cm. However, it is not shown at any stage of the accelerating flood tide by samples from the lowest nozzle, 10 cm ASB. It is possible that this last unexpected feature was due either to an unidentified limitation of the pumped sampling instrument, or the structure of the rig itself (see above). At the peak of the flood tide, the means varied from 3.15Ø to 3.42Ø, only slightly larger than in the early stages of the flood.

From that stage onwards, the size distribution at 15 cm ASB became particularly interesting. Although the tide was decelerating, increasingly larger particles were found in suspension. (It should be noted that the current speeds were still well above the threshold velocities required to entrain particles of the sizes found). One hour after maximum velocities the mean at 15 cm ASB was 2.25Ø and the size distribution curve was polymodal (Figure 16C). It is suggested that suspensions derived from a source upstream of station PS4 had been sampled. It is also likely that during deceleration, particles in the upper parts of the water column would begin to settle towards the seabed thus entering the

sampling area. Curves for the remaining levels show what appear to be a truncation at 1.0Ø, but it seems likely that this was a result of the small size of the samples, making accurate separation of these larger grain sizes extremely difficult. Often there was less than 0.065 g remaining on the 1.0Ø sieve.

No samples were taken at slack water. As the ebb tide gained strength there was a return to the bimodal stage, still peaking at 2.5Ø, and also showing a certain amount of truncation at the 1.0Ø size (see above and Figures 16D and 17). By the time maximum velocities had been reached, the distributions were returning to the unimodal stage, with similar configurations at all levels. These conditions remained constant through most of the decelerating phase (Figures 16E and 17), but as slack water was approached, the curves again appear to be truncated artificially at the coarser end (Figure 16F). It is likely that grains larger than 0.5Ø diameter were present, although not detected by the particular sieving method used.

Microscopic examination, in reflected light, of representative samples showing the 2.5Ø peak, revealed high percentages of subangular to angular quartz grains of this mean size, mostly transparent, but some with surface frosting. A relatively small proportion was iron-stained. Other minerals present, in small quantities, included glauconite, silica in the form of diatom shells, and calcium carbonate as foraminiferid and ostracod tests, bivalve and gastropod shell fragments, and echinoid spines.

At PS1 (Figure 3) where the rig was placed on a sandy bottom, similar to that at PS4, the analysis of a sample obtained during an accelerating flood tide shows the curve to be bimodal. One of the peaks is caused by the presence of coarse to very coarse sand. The seabed, however, probably comprised medium to very fine sand (Figure 3). At stations PS2 and PS3, in contrast, where the rig was placed on clay or intercalated sands, silts and clays, the suspended sediments show near unimodal distributions during both accelerating and decelerating phases of flood and ebb tides, with a median grain size d_{50} = 2.75Ø (fine sand).

Carling (personal communication) finds that suspended sediment distributions measured in an intertidal environment show different features from the above. They are bimodal at the beginning and end of each half tidal cycle, and unimodal when the flow is well established. He attributes this to the influence

of wave activity when the tidal currents are weak near the time of slack water. A wave plus tidal current induced suspension is bimodal and that induced by tidal currents only is unimodal.

The Sizewell-Dunwich material smaller than 4.0Ø mean diameter was also examined. This showed that a small washload was present at all times, some having been trapped on the filters, as mentioned above, whilst the remainder was in the water samples. Figure 18, showing concentrations of sediments through a tidal cycle $\geq$4.0Ø, and those <4.0Ø, serves to illustrate this point, showing that the concentration of silt and clay remained relatively constant throughout, with a depth mean value of 230 mg l^{-1} in 10 m water. U_* (friction velocity) and U_{100} (velocity at height 100 cm ASB) are also included in the diagram.

5.5 Suspended sediment transport rates

Figures 19 and 20 show the variation of reference concentration and total suspended sediment through one tidal cycle at PS4.

As noted above, q_{ss} , the suspended sediment transport rate, has been calculated using equation (8). When concentration data for each phi range are used separately, the results are seen to be particularly sensitive to the exponent $\frac{W_s}{k U_*}$. This expression represents the slope of the straight line fitted to the concentration data using equation (7). The equation assumes that the eddy diffusivity of the grains, ε_s , is equal to the eddy viscosity of the fluid, ε , but the relationship may be proportional (Graf, 1972),

$$\text{with} \quad \varepsilon_s = \beta \varepsilon \tag{9}$$

He then shows that $\frac{W_s}{k U_*}$ can be written as $\frac{W_s}{\beta k U_*}$.

By using the slope of the straight line fitted to the velocity data and using equation (6) to eliminate U_*, β can then be expressed in terms of k, w_s, and the straight line slopes m_1 and m_2 related to equations (6) and (7).

$$u_* = \frac{k}{m_1}$$

$$\frac{w_s}{\beta k u_*} = m_2$$

then

$$\frac{w_s m_1}{\beta k . k} = m_2$$

and

$$\beta = \frac{w_s m_1}{k^2 m_2} \qquad (10)$$

Table 9 and Figure 21 give the computed values of β for the different phi ranges through a spring tidal cycle. Table 10 and Figure 22 show the total suspended sediment transport rates for each sand fraction throughout a tidal cycle, using the appropriate values of β . Where the data were considered inadequate for the computation of β a mean value for the particular phi range was used. It may be noted that generally β >1 for these data. Swart (1976) cites workers who have found β <1, and others with β >1.

The method of computation assumes that the Karman-Prandtl and Rouse equations are the best representations of the velocity and concentration profiles. Criteria given by Stanford (1976) were used to define the limits beyond which these equations were not applied.

Table 11 compares the sums of the transport rates of the separate phi ranges for each profile, with those calculated from the sample before sieving. The agreement is good. There are no calculations for some of the larger phi ranges, 2.0Ø to 1.5Ø and 1.5Ø to 1.0Ø, where the fractions for a profile did not fit equation (7). This may be due to the fact that the fractions were so small that they were not representative (see above, 5.4). The apparent increase in sediment transport in phi ranges 2.0Ø to 3.0Ø as the ebb tide decelerates (Figure 22) may also be the result of small samples.

5.6 Transport during spring and neap tides

Measurements for the calculation of suspended sediment transport rates were made during maximum spring tides, and some estimation is required of how such rates might vary during neap tides. A consistent feature of sediment transport is its extreme non-linearity, and suspended sediment transport rates are dynamically related to the friction velocity to a power of $n + 2$, where n is at least one. Bagnold (1963) and Yalin (1972) both suggested that the rates vary as U_*^3, but more recent work by Dyer (1980) indicates that in certain cases q_{ss} varies as U_* to a power between 4 and 7.

In the case of the Sizewell-Dunwich data the total suspended sediment transport rate for PS4 has been found to vary as $U_*^{2.8}$, which is near U_*^3 (Figure 23). The friction velocity amplitude varies with the tidal flow, and therefore as the principal astronomical tidal constituents ie the M_2 and S_2 tides. Analysis of the current meter data for the study area (Heathershaw and Lees, 1980) shows that if spring tide amplitudes to the power of 2.8 are compared with neap tide amplitudes to the power of2.8, there is a 5-fold difference. This suggests that the total suspended sediment rate for a neap tide is likely to be in the order of one fifth of that calculated for springs.

6. BED LOAD SEDIMENT TRANSPORT PATHS

Sediment transport rates and directions calculated using Yalin's (1963) bedload equation (Appendix A) are given in Table 12 and Figure 24. The results show that in general there is an increase in predicted transport rates towards the shore associated with an increase in the tidal residuals. Unlike the Swansea Bay study, the increase in transport rates is also associated with a decrease in the tidal current amplitudes (Heathershaw and Lees, 1980). Sediment transport rates vary typically from .004 gm cm^{-1} s^{-1} offshore to .069 gm cm^{-1} s^{-1} inshore which is less than the 100 fold variation seen in Swansea Bay (Heathershaw and Hammond, 1979).

A schematic representation of the sediment transport paths in the Sizewell-Dunwich area, based upon midwater current measurements, is shown in Figure 25. An apparent bedload parting seaward of Dunwich may be compared with the bedload

parting further offshore which has been identified by Stride (1973) from sedimentological data. This feature appears to be related to the presence of an amphidromic point in the southern Bight of the N Sea and is also revealed in bed shear stress distributions from numerical models of the tidal circulation in this area (Pingree and Griffiths, 1979).

From the point of view of the relationship between offshore banks and adjacent coastlines, the Sizewell-Dunwich Banks study shows that unlike Swansea Bay the predicted directions of net bedload transport are opposite to the direction of the Banks' trend from their point of attachment to the coast. This is also true of residual currents in this area (Heathershaw and Lees, 1980), and does not preclude the possibility, therefore, of transfer of material between Banks and coast. However, this is likely to be limited by the strong flushing action of currents between Thorpe Ness and Sizewell Bank where the residual transport is high. Only in the N of the study area (ie Dunwich Bank) is the direction of predicted net bedload movement similar to the trend of the Banks which Carr (1979) has shown to be extending in a northerly direction. Calculations of suspended sediment transport rates at PS4 (Figure 3) also give a net northerly movement of sediment in this area.

Although the tidal current data (Heathershaw and Lees, 1980) and the predicted directions of bedload sediment movement (Figure 24) hint at an eddy in the mean water and sediment circulations in the S part of the area, it is not centred over the Sizewell Bank. Therefore, it is not a likely mechanism for the maintenance of the bank in its present position, in the manner described by Pingree and Maddock (1979) for the Shambles, off Portland. They show that vorticity generated by tidal streaming at a point of abrupt change in the coastal geometry leads to secondary circulation effects. These give rise to a near-bottom convergence and mid-depth divergence in the mean circulation on the flanks of the sandbank. Bank maintenance by this type of tidal process was identified in Swansea Bay, where the long axes of the banks lie normal to the coastline, and where the coast itself undergoes the required sharp change in direction. In contrast, the banks on the E coast lie parallel to the N-S shoreline. It is also likely that waves play a more dominant role in determining overall Bank morphology than in Swansea Bay, demonstrated to some extent by fluorescent tracer work, which showed shoreward movement of sediment during storms. At present it is not possible to resolve the problem of the

displacement seawards of the centre of the "eddy" relative to the axis of the bank.

Finally it should be stated that the data in Table 12 and Figure 24 need to be treated with some caution since they relate to bedload transport only. Measurements and calculations (see Section 5) show clearly that suspended load transport is the dominant mode of transport on the E coast with measured rates at least 2 orders of magnitude greater than those for bedload. Therefore the overall sediment circulation pattern (ie bedload plus suspended load) may be different from the pattern given in Figure 25.

7. THE EFFECTS OF WAVES

7.1 Bijker's formula

The theory of wave tidal current interaction is still poorly understood although recent theoretical developments (eg Grant and Madsen, 1979) go some way towards improving our understanding of the physical processes involved. The effect of this interaction on sediment transport is still more tenuous since sediment transport theories, as we have seen, can in themselves give widely differing estimates. Present approaches are largely empirical (eg Owen and Thorn, 1979) and it is likely to be some time before theories are available which are capable of dealing with the wide range of conditions encountered on the continental shelf.

One approach which has been used is that developed by Bijker (1967) which, although semi-empirical, does attempt to deal with the physical interaction of the waves and the currents, The theory consists of making a vector addition of the orbital velocity (u_o) of the wave and the velocity due to the tidal current alone, at a height above the sea bed equivalent to the thickness of the viscous sublayer. The resultant velocity is converted to a bed shear stress using Prandtl mixing length theory in which the bed shear stress is given by

$$\tau = \rho l^2 \left[\frac{\partial u_z}{\partial z}\right]^2_{z \to o} \qquad (11)$$

where u_z is the combined velocity at a height z above the bed, ρ is the density, τ is the bed shear stress and ℓ is the mixing length given by $\ell = kz$ for small values of z. Thus, according to Bijker's theory, the maximum enhancement of the bed shear stress is given by,

$$\psi = \frac{\tau_{wc}}{\tau_c} = 1 + \frac{1}{2}\left(\xi \frac{u_0}{\hat{u}}\right)^2 \qquad (12)$$

where τ_{wc} is now the resultant bed shear stress due to waves and currents, τ_c is the bed shear stress due to currents alone, ξ is given by $\xi = \beta_b \sqrt{[(h/z_0) - 1]}$, h is the mean depth, β_b is an empirically determined constant, which Bijker (1967) found equal to 0.45, and $\hat{u}$ is the steady depth mean current. In this report ψ is referred to as the Bijker magnification factor.

To obtain an upper limit to the enhancement of the bed shear stress due to wave activity, equation (12) has been evaluated for typical and extreme wave conditions. ξ has been calculated with a roughness length z_0 of .05 cm, appropriate to Station A and the depth mean current in (12) has been calculated in terms of the current at a height of 1 m above the sea bed by integrating the logarithmic velocity profile (2) from the sea bed to a height 2 m, and the power law profile (1) from 2 m to the surface. The variation of ψ with wave height H, for a wave period of 6s (typical for the area, see Fortnum and Hardcastle, 1979) and water depth of 12 m is plotted in Figure 26. This shows for example that even moderate wave conditions (H = 1 m) increase sediment transport rates (calculated using Yalin's formula) by a factor of about 2 at peak tidal flows (ie 100 cm s^{-1}) with the effect becoming more pronounced as the steady current ($\bar{u}_{100}$) decreases in strength.

7.2 Thresholds of movement under waves and currents

In considering the effects of waves, it should be borne in mind that sediment particles which are suspended by enhanced bed shear stresses, are likely to move in a direction which is governed principally by the tidal currents. Furthermore, the waves are not a persistent feature of the nearbed water movements.

This is illustrated in Figure 27 which shows exceedance curves for wave induced and tidal currents. Typical current threshold values are also indicated, that for the waves having been calculated using Komar and Miller's (1974) threshold criterion,

$$\frac{\rho}{\rho_s - \rho} \cdot \frac{u_{ocr}^2}{gd} = .21 \left(\frac{u_{ocr} T}{\pi d} \right)^{\frac{1}{2}} \qquad (13)$$

where u_{ocr} is the critical near bed orbital velocity and T the wave period. For these calculations T has been taken as 6s. The grain size d has been taken as the median grain size of 130 μm and the steady current threshold, u_{cr}, calculated from Shields' curve. A roughness length of z_o = .05 cm has been assumed in calculating the corresponding current at 2 m above the sea bed from the logarithmic velocity profile (2). A roughness length of z_o = .05 cm corresponds to the value which was prescribed for sediment transport calculations at Station A. This figure gives a threshold velocity (u_{cr}) at 200 cm above the bed of about 27 cm s^{-1}.

These results suggest that in the offshore areas (water depth $\simeq$ 10 m) the threshold due to waves is on average exceeded for 30% of the time and that if waves were capable of directly influencing sediment movement then the effect would be limited in duration. This observation is corroborated to some extent by the enhancement of tracer movement towards the coast when the wind blows from the NE/E. However, this movement may well have occurred due to a wave induced mass transport effect (see below). The figure of 30% exceedance for the threshold of movement under waves may be compared with exceedance levels of over 85% for the threshold of sediment transport in a unidirectional tidal flow at Station A (Figure 27).

7.3 Mass transport effects due to waves

From observation and theory it appears that on average the direction of sediment movement is controlled by the tidal currents with perhaps some intensification of transport by wave activity. It is interesting to note that in Figures 10 and 11 the observed transport rates are consistently lower than those predicted by most of the theories examined. This may be due to the fact that transport in the

area is dominantly in the suspended mode, whereas three of the formulae predict bedload rates only. The fluorescent tracer experiments (see 4.2 and above) suggest that transport is enhanced in the presence of large waves. The effect arises from the fact that wave particle orbits are not closed, giving rise to a steady movement of the water particle at the surface and near the bed in the direction of wave propagation. Heathershaw and Hammond (1979) have examined the Stokes drift u_s at different depths using Longuet-Higgins' (1953) solution for flow in the interior of the fluid. At the bed this gives the well known expression

$$u_s = \frac{5}{4} \cdot \frac{a_w^2 \sigma k}{\sinh^2(kh)} \qquad (14)$$

where a_w is the wave amplitude, σ its angular frequency, k its wave number equal to $2\pi/\lambda$, where λ is the wavelength, and h the total depth. Equation (15), which strictly speaking is only valid for laminar flow, but which Longuet-Higgins (1957), in an appendix to the paper by Russell and Osorio (1957), has shown may also apply to turbulent flow, predicts a steady forward mass transport at the sea-bed.

We must conclude therefore that during periods of prevailing NE/E wave activity there is likely to be a steady shoreward drift at the bed and for a wave height of 2 m, wave period of 6s and water depth of 10 m, equation (15) predicts that this will be in the order of 3.5 cm s^{-1}, which is a similar order of magnitude to the tidal residuals.

8. CONCLUSIONS

Observed and predicted transport rates have indicated that for sand size material (d_{50} = 2.9Ø, 130 μm) transport in the suspended mode is likely to be dominant in the area. Concentrations of sand reached maxima of 423 mg l^{-1} at 175 cm above the seabed (ASB), and 1892 mg l^{-1} at 15 cm ASB during a spring tidal cycle at station PS4. Silt and clay is present in addition to the sand as a relatively constant "washload", but with a depth mean concentration of only 230 mg l^{-1}.

The sand is suspension does not always comprise a unimodal population with respect to grain size, and shows a definite pattern of change through a tidal cycle (Figure 16). At PS4 bimodality during the decelerating flood tide is related to an additional population of well rounded quartz grains, centred around a mean of 2.5Ø,180 μm. Because they appear on the flood tide, their provenance is likely to be an area to the N of PS4 (Figure 4).

Perhaps surprisingly, the turbulent structure of the bottom boundary layer is not obviously modified by these suspensions, and the measured velocity profiles fit the Karman-Prandtl logarithmic relationship well. The exception is during the decelerating flood tide, when the velocity profiles are almost certainly modified causing overprediction of the roughness length (z_o) and, to a slight extent, of the friction velocity (u_*).

The presence of complex suspensions means also that the concentration profiles do not always fit the Rouse relationship. The complexity is added to by the hysteresiseffect, where a time lag is evident in the response of suspended solids concentrations to changes in velocity. In spite of these problems, the integrated product of the Karman-Prandtl and Rouse equations has been used to calculate the total suspended sediment transport rates, with a resultant of 5.66 g cm^{-1} s^{-1} in the ebb direction at PS4. However, modifications were necessary to compute suspended sediment transport rates for the separate grain sizes, involving the calculation of β , the factor of proportionality relating the eddy diffusivity to the eddy viscosity. These results show that the main transport of sediment is in the very fine sand range. Of the five stations (Figure 4) where sediment concentrations and velocity profiles were measured, PS1 and PS4 which are in line with the banks, and PS3 close inshore, showed ebb residuals. At PS2, seaward of the banks, flood and ebb rates approximately balanced, and at PS5, between the banks and the shore, the direction of the residual was unclear. It should be noted that the rates are for spring tides, and neap values are likely to be only $^1/5$ of these rates.

Sediment transport occurs to a lesser extent as bedload. The rates have been estimated using Yalin's (1963) formula, shown by tracer measurements to give the best predictions. They are within the maximum and minimum limits of the observed values, and overall are of the order of 0.02g cm^{-1} s^{-1}. Comparison may be made with the Swansea Bay area, where a modified version of Bagnold's (1963) formula

gave the best predictions. The overprediction by the Bagnold and other formulae in Sizewell-Dunwich is consistent with the fact that bedload transport is the subordinate of the two modes, whereas in Swansea Bay it is the dominant one.

The overall picture of the study area is one of active transport, mainly in the suspended mode showing measured rates at least 2 orders of magnitude greater than those for bedload. However, under stormy conditions, it has been shown that bedload transport of a tracer can be enhanced by wave effects. During a 114 day period the mean rate of tracer transport was increased by a factor of 1.25 and the direction changed, when the significant wave height was >1.5 m for 5% of the time.

Predicted bedload transport paths for the area are presented schematically in Figure 25. Transport is shown to be mainly to the S, but with some to the N, forming a bedload parting offshore at Walberswick (Figure 25). This agrees with the very limited geophysical evidence (Lees, 1980).

The above S trending bedload residuals are in direct opposition to the trend of the banks. The banks are related to the shoreline at Thorpe Ness, demonstrated particularly by historical surveys (Carr, 1979), and the two facts suggest the possibility of transfer of sand from the banks to the shore at the ness. This would be strongly supported by Robinson (1980). A contrary view is held by McCave (1978) and for an analysis of these opposing views reference should be made to Carr (1981). The last author, on balance, tends towards the view of McCave for this particular area, ie if sediment transference takes place it is likely to be from Thorpe Ness to the banks. A further important factor is that of geological control. An outcrop of Coralline Crag, aligned in a WSW-ENE direction occurs immediately inland of Thorpe Ness, and continues offshore through the ness. Its presence accounts for the stability of this particular ness over time. (Lees, 1980; Carr, 1981).

At present the banks protect the shore from attack by waves >2.2 m in height (Carr, 1981) and hence the sediment supply from that area is minimal. Currently the growth of the banks to the N is either very small or has ceased. The bed load sediment transport paths shoreward of the Sizewell Bank show particularly strong trends to the S during the summer. The source may be the "col" area of the banks, where the beginning of separation into two banks is more apparent

during the summer. With the flushing action to the S and SE between Thorpe Ness and the Sizewell Bank, some sand deposition in this direction might be expected and a southerly tongue is recorded as having been present earlier this century and may be a frequently occurring short lived feature (Carr, 1979).

Although the relationship of the bank structure to the bedload transport pattern is difficult to define, it must be remembered that suspended load transport is dominant, and therefore it is more likely to be a suspended load mechanism maintaining the banks overall. The existing evidence points to ebb residuals in the transport system ie in the direction of bank growth. Enhancement of sediment transport in a shoreward direction is effected by waves from the NE and E.

The contrasting results from the comparative study of two areas, Swansea Bay and Sizewell-Dunwich, with differing coastline geometry, sediment distribution, tidal current and wave climate characteristics, clearly demonstrates the necessity of assessing these features in some depth before sediment transport predictions can be reasonably made. It is notable that, as shown above, of 5 commonly used sediment transport formulae, Bagnold's modified (1963) equation gave the closest correspondence to the observed rates for Swansea Bay, and that of Yalin (1963) for Sizewell-Dunwich. In both areas there were two orders of magnitude difference in the results from these two formulae.

9. ACKNOWLEDGEMENTS

We would like to acknowledge the support and cooperation of our colleagues at the Institute of Oceanographic Sciences, Taunton. This work was supported financially by the Department of the Environment.

NOTATIONS (Not applicable to Appendix A)

a	height of reference concentration
a_w	wave amplitude
β	factor of proportionality
C_a	reference concentration
C_i	concentration of tracer at one sample point
C_z	mass concentration at height z
d	grain diameter
d_{50}	median grain diameter
E	depth of mixing
ε	eddy viscosity
ε_s	eddy diffusivity
g	acceleration due to gravity
H	wave height
h	total water depth
k	wave number
K	von Karman's constant
ℓ	mixing length
λ	wavelength
M	number of sample points
M_2	principal lunar tide
m_1	slope of straight line fitted to Karman-Prandtl equation
m_2	slope of straight line fitted to Rouse equation
μm	micron
n	exponent used in sediment transport equations
A_b	Bijker empirically determined constant
p	exponent, different from n
q_{sb}	bedload transport rate
q_{ss}	suspended load transport rate
ρ	density of seawater
ρ_s	density of quartz
S_2	principal solar tide
σ	angular frequency of wave
T	wave period
τ	bed shear stress
τ_{cr}	critical bed shear stress
τ_{wc}	bed shear stress due to waves and currents
u	velocity at height
u_o	orbital velocity of wave at bed
u_6	mid depth current
u_{100}	velocity at 100 cm above seabed
u_*	friction velocity
$\bar{u}$	steady depth mean current
u_{ocr}	critical bed orbital velocity
u_{cr}	steady current threshold
u_R	velocity at reference height
u_s	mass transport velocity near bed
u_z	combined velocity at height z
V	velocity of centroid
ϕ	$-\log_2$ grain diameter in mm
ψ	Bijker magnification factor
w_s	settling velocity
x, y	coordinates of centroid
x_i, y_i	coordinates of sampling point
z	height
z_o	roughness length
z_2	height of logarithmic layer
z_6	mid-depth height
z_R	reference height

REFERENCES

ABRAMOWITZ, A and STEGUN, I A, 1965. Handbook of Mathematical Functions. Dover Publications, New York, NY, 1046 pp.

ACKERS, P, 1972. Sediment transport in channels: an alternative approach. Hydraulics Research Station Report No INT 102, 31 pp.

ACKERS, P and WHITE, W R, 1973. Sediment Transport: New approach and analysis. Proceedings of the American Society of Civil Engineers, Journal of the Hydraulics Division HY 11, 2041-2060.

BAGNOLD, R A, 1963. Mechanics of marine sedimentation, in Hill, M N (ed), The Sea. Interscience Publications, Vol 3, 507-582.

BIJKER, E W, 1967. Some considerations about scales for coastal models with moveable beds. Delft Hydraulics Laboratory Report No 50, 142 pp.

CARR, A P, 1979. Long-term changes in the coastline and offshore banks. Sizewell-Dunwich Banks Field Study Topic Report 2. Institute of Oceanographic Sciences Report No 89, 25 pp.

CARR, A P, 1981. Evidence for the sediment circulation along the coast of East Anglia. Marine Geology, 40, M9-M22.

COURTOIS, G and MONACO, A, 1969. Radioactive methods for the quantitative determination of coastal drift rate. Marine Geology, 7, 183-206.

DAVIES, A G, 1977. A mathematical model of sediment in suspension in a uniform reversing tidal flow. Geophysical Journal of the Royal Astronomical Society, 51, 27 pp.

DYER, K R, 1970. Current velocity profiles in a tidal channel. Geophysical Journal of the Royal Astronomical Society, 22, 153-161.

DYER, K R, 1980. Velocity profiles over a rippled bed and the threshold of movement of sand. Estuarine and Coastal Marine Science, 10, 181-199.

EINSTEIN, H A, 1950. The bedload function for sediment transportation in open channel flows. Soil Conservation Service, United States Department of Agriculture Technical Bulletin No 1026, 78 pp.

ENGELUND, F and HANSEN, E, 1967. A monograph on sediment transport in alluvial streams. Teknisk Vorlag, Copenhagen. 62 pp.

FLEMMING, C A and HUNT, J N, 1976. A mathematical sediment transport model for unidirectional flow. Proceedings of the Institute of Civil Engineers, 61. 297-310.

FOLK, R L, 1968. The Petrology of Sedimentary Rocks. The University of Texas, Hemphill's, 171 pp.

FORTNUM, B C H and HARDCASTLE, P J, 1979. Waves recorded at Aldeburgh, Dunwich and Southwold on the east coast of England. Institute of Oceanographic Sciences Report No 65, 9 pp + figures.

GADD, P E, LAVELLE, J W and SWIFT, D J P, 1978. Estimates of sand transport on the New York Shelf using near-bottom current meter observations. Journal of Sedimentary Petrology, 48. 239-252.

GRAF, W H, 1972. Hydraulics of Sediment Transport, McGraw-Hill, New York, 509 pp.

GRANT, W D and MADSEN, O S, 1979. Combined wave and current interaction with a rough bottom. Journal of Geophysical Research, 84, 1797-1808.

GUY, H P, SIMONS, D B and RICHARDSON, E V, 1966. Summary of alluvial channel data from flume experiments 1955-1961. United States Geological Survey Professional Papers, 4621. 92 pp.

HEATHERSHAW, A D, 1981. Comparisons of measured and predicted sediment transport rates in tidal currents. Marine Geology, 42, (in press).

HEATHERSHAW, A D and CARR, A P, 1977. Measurements of sediment transport rates using radioactive tracers. Coastal Sediments '77, American Society of Civil Engineers, Charleston, South Carolina, USA, 399-416.

HEATHERSHAW, A D and HAMMOND, F D C, 1979. Offshore sediment movement and its relation to observed tidal current and wave data. Swansea Bay (Sker) Project. Topic Report 6. Institute of Oceanographic Sciences Report No 93, 119 pp.

HEATHERSHAW, A D and HAMMOND, F D C, 1980. Secondary circulations near sand banks and in coastal embayments. Deutsche Hydrographische Zeitschrift, 33, 135-151.

HEATHERSHAW, A D and LEES, B J, 1980. Tidal currents: observed tidal and residual circulations. Sizewell-Dunwich Banks Field Study. Topic Report 4. Institute of Oceanographic Sciences Report No 104, 92 pp.

KACHEL, N V and STERNBERG, R W, 1971. Transport of bedload as ripples during an ebb current. Marine Geology, 10, 229-244.

KOMAR, P D and MILLER, M C, 1974. Sediment threshold under oscillatory waves. Proceedings of the 14th Coastal Engineering Conference. Copenhagen, 765-775.

LEES, B J, 1977. Progress report for the period January 1975 to December 1976. Sizewell-Dunwich Bank Project. Institute of Oceanographic Sciences Report No 38, 15 pp + figures.

LEES, B J, 1979. A new technique for injecting fluorescent sand tracer in sediment transport experiments in a shallow water marine environment. Marine Geology, 33, M95-M98.

LEES, B J, 1980. Introduction and geological background. Sizewell-Dunwich Banks Field Study. Topic Report 1. Institute of Oceanographic Sciences Report No 88, 24 pp + figures.

LEES, B J, 1981. Sediment transport measurements in the Sizewell-Dunwich Banks area, East Anglia, UK. Special Publications of the International Association of Sedimentologists, 5, 13 pp.

LOUGUET-HIGGINS, M S, 1953. Mass transport in water waves. Philosophical Transactions of the Royal Society of London, Series A, 245, 535-581.

LONGUET-HIGGINS, M S, 1957. The mechanics of the boundary-layer near the bottom in a progressive water wave. Appendix to Russell and Osorio (1957).

McCAVE, I N, 1978. Grain-size trends and transport along beaches: Examples from Eastern England. Marine Geology, 28, M43-M51.

OWEN, M W and THORN, M F C, 1979. Effect of waves on sand transport by currents. Proceedings of the 16th Coastal Engineering Conference, Hamburg (in press).

PINGREE, R D and GRIFFITHS, D K, 1979. Sand transport paths around the British Isles resulting from M_2 and M_4 tidal interactions. Journal of the Marine Biological Association of the United Kingdom, 59, 497-513.

PINGREE, R D and MADDOCK, L, 1979. The tidal physics of headland flows and offshore tidal bank formation. Marine Geology, 32, 269-289.

RAUDKIVI, A J, 1976. Loose Boundary Hydraulics, Pergamon, Oxford, 2nd ed, 397 pp.

ROBINSON, A H W, 1980. Erosion and accretion along part of the Suffolk coast of East Anglia, England. Marine Geology, 37. 133-146.

RUSSELL, R C H and OSORIO, J D C, 1957. An experimental investigation of drift profiles in a closed channel. Proceedings of the 6th Coastal Engineering Conference, Miami, 171-193.

SHEPARD , F P, 1967. Submarine Geology. Harper International Editions, New York, 2nd ed.

SMITH, J D, 1977. Modelling of sediment transport on continental shelves. In Goldberg, E D, McCave, I N, O'Brien, J J and Steele, J H (eds). The Sea. Wiley-Interscience Publications, Vol 6, 539-577.

SMITH, J D and McLEAN, S R, 1977. Spatially averaged flow over a wavy surface. Journal of Geophysical Research, 82, 1735-1746.

SOULSBY, R L, 1978. The use of depth-averaged currents to estimate bed shear stress, as applied to a numerical model of the Sizewell-Dunwich Bank area. Institute of Oceanographic Sciences Internal Document No 26, 40 pp.

STANFORD, P N, 1977. Data processing. Annual Progress Report, 1977, on Sedimentary Processes in the South West Approaches. Department of Geology, University of Bristol.

STRIDE, A H, 1973. Sediment transport by the North Sea. In North Sea Science, edited by E D Goldberg, Cambridge, Massachusetts, Massachusetts Institute of Technology Press.

SWART, D H, 1976. Coastal sediment transport. Delft Hydraulics Laboratory Report No R968, 61 pp.

TERZAGHI, K and PECK, R B, 1967. Soil Mechanics in Engineering Practice. Wiley and Sons, New York. 729 pp.

THORN, M F C, 1975. Hysteresis of fine sand suspensions in a tidal estuary. Hydraulics Research Station Notes, (17),2 pp.

WHITE, W R, 1972. Sediment transport in channels: a general function. Hydraulics Research Station Report No INT 104, 25 pp.

WHITE, W R, MILLI, H and CRABBE, A O, 1975. Sediment transport theories: a review. Proceedings of the Institute of Civil Engineers, pt 2, 59, 264-292.

WHITE, W R, MILLI, H and CRABBE, A O, 1978. Sediment transport theories: an appraisal of available methods (2 volumes). Hydraulics Research Station Report No IT 119, 101 pp.

YALIN, M S, 1963. An expression for bed load transportation. Proceedings of the American Society of Civil Engineers, Journal of the Hydraulics Division. 221-250.

YALIN, M S, 1972. Mechanics of Sediment Transport. Pergamon Press, Oxford, 290 pp.

TABLE 1

Roughness length (z_o), threshold velocity (u_{cR}) and water depth values used in calculating bedload transport rates for the Sizewell-Dunwich Banks area

Station	Substrate	Roughness length (z_o) (cm)	Threshold velocity (u_{cR}) at 200 cm above seabed (cm s^{-1})	Total water depth (m)	Height of current meter above seabed (m)
A	Fine, sands, silts, clays	.05	27	12.0	6.0
B	Sand and gravel	.10	25	24.0	10.0
C	Clay	.01	32	13.0	6.0
D	Clay	.01	32	12.0	6.0
E	Fine sand	.50	20	13.0	7.0
F	Sand and gravel	.10	25	17.0	8.0
G	Fine sand	.50	20	12.0	6.0
H	Fine sand	.50	20	12.5	6.0
J	Clay	.01	32	8.5	5.0
K	Sands, silts, clays	.05	27	12.5	6.0
L	Sand and gravel	.10	25	23.0	10.0
M	Fine sand	.50	20	11.5	6.0
N	Fine sand	.50	20	9.0	3.0
P	Fine sand	.50	20	5.0	2.0
Q	Fine sand	.50	20	12.0	6.0
R	Sand and gravel	.10	25	21.0	10.0
S	Clay	.01	32	9.0	5.0
T	Sands, silts, clays	.05	27	21.0	10.0
V	Sands, silts, clays	.05	27	11.5	6.0
W	Sands, silts, clays	.05	27	17.0	8.0
X	Fine sand	.50	20	13.0	6.0
Y	Sands, silts, clays	.05	27	12.0	6.0
Z	Sands, silts, clays	.05	27	17.0	8.0

TABLE 2

Sediment transport formulae used in comparisons of observed and predicted sediment transport rates in the Sizewell-Dunwich Banks area

Originators		Date	Type	Mode
Bagnold	a	1963	Deterministic	Bed load
Yalin	a	1963	Deterministic	Bed load
Einstein	a	1950	Stochastic	Bed load
Ackers and White	b,c	1973	Deterministic	Total load
Engelund and Hansen	b,c	1967	Deterministic	Total load

Used recently by (a) Gadd et al 1978
(b) Swart 1976
(c) Flemming and Hunt 1976

TABLE 3

Maximum observed excursion of fluorescent tracer cloud during each survey. Concentration 10 grains kg^{-1} used as boundary

Survey number	Maximum elongation (m)	Maximum width (m)
1 + 2	968	92
3 + 4	984	92
5	1072	112
6	c. 1070	c. 320
7	c. 360	c. 180

TABLE 4

Depth of mixing measurements

Date	Box core number	Maximum depth (m)	Mean tracer concentration (grains kg^{-1})
23 August 1978. Injection day + 2	60	0.003	412
"	61	0.003	1414
"	63	0.010	177
"	64	0.008	1966
"	65	0.004	1856
"	66	0.019	1172
"	67	0.018	1060
"	68	0.010	2050
"	69	0.016	12977
"	71	0.005	1979
"	72	0.010	2085
"	75	0.010	424
5 April 1979. Injection day + 226	Vibrocore VC 13	0.22	1861
10 April 1979. Injection day + 231	S1	0.22	1844
" (Day 231)	S2	0.18	882
"	S3	0.20	566
"	S4	0.12	409
"	S5	0.12	492
"	S7	0.16	931
"	S8	0.18	2984

TABLE 5

Drift rates and net sediment transport rates for each survey, referred to injection site

Survey Number	Days after injection (mean)	Distance from injection site (m)	Bearing from true N	Centroid velocity or drift rate ($m\ day^{-1}$)	Estimated depth of mixing (m)	q_{sb} ($g\ cm^{-1}\ s^{-1}$)
1 + 2	2	8.06	10°	4.03	0.013	0.012
3 + 4	5	14.32	171°	2.86	0.023	0.016
5	50	33.24	190°	0.66	0.112	0.017
6	164.5	55.07	244°	0.33	0.165	0.013

TABLE 6

Drift rates and sediment transport rates between surveys

Survey Numbers	Number of days between	Distance travelled (m)	Drift rate ($m\ day^{-1}$)	Estimated depth of mixing (m)	q_{sb} ($g\ cm^{-1}\ s^{1-}$)
1+2 from injection site	2	8.06	4.03	0.013	0.012
3+4 from 1+2	3	22.09	7.36	0.023	0.040
5 from 3+4	45	20.25	0.45	0.112	0.012
6 from 5	114.5	44.41	0.39	0.165	0.015

TABLE 7

Height of sampling nozzles and flowmeters in pumped sampling equipment

Sampling nozzle	Height above seabed (cm)	Flowmeter
*	175	*
*	85	*
*	45	*
*	25	*
*	15	
*	10	

TABLE 8

Pumped samples from station PS4. Means and standard deviations (sorting coefficients)

Profile number	Height above seabed (cm)											
	10		15		25		45		85		175	
	Mean (Ø)	Standard deviation (Ø)	Mean	St. dev.	Mean	St. dev.	Mean	St. dev.	Mean	St. dev.	Mean	St. dev.
4.1	3.45	0.46	3.38	0.45	3.40	0.48	3.54	0.34	3.58	0.32	3.52	0.36
4.2	3.49	0.39	3.24	0.60	3.45	0.42	3.40	0.46	3.46	0.37	3.50	0.34
4.3	3.45	0.39	3.31	0.51	3.42	0.40	3.47	0.38	3.49	0.32	3.47	0.33
4.4	3.46	0.34	3.10	0.52	3.19	0.50	3.33	0.44	3.42	0.38	3.44	0.37
4.5	3.38	0.36	3.15	0.56	3.17	0.53	3.34	0.42	3.42	0.37	3.42	0.37
4.6	3.25	0.51	2.92	0.70	3.13	0.56	3.30	0.47	3.41	0.40	-	
4.7	3.40	0.41	2.25	0.94	3.15	0.69	3.31	0.53	3.44	0.42	3.44	0.42
4.8	2.67	1.22	1.97	0.51	2.25	0.79	2.97	0.91	3.10	0.94	3.49	0.63
4.9	2.06	0.86	-		-		-		-		-	
4.11	3.46	0.40	3.15	0.65	3.22	0.64	3.46	0.47	3.51	0.41	3.60	0.37
4.12	3.11	0.70	3.04	0.69	3.18	0.64	3.43	0.45	3.46	0.43	3.49	0.42
4.13	3.43	0.42	2.16	0.61	2.99	0.71	3.24	0.64	3.41	0.41	3.41	0.39
4.14	3.03	0.69	3.05	0.64	3.29	0.52	3.29	0.54	3.46	0.36	3.49	0.35
4.15	3.20	0.56	3.26	0.50	3.26	0.47	3.38	0.38	3.51	0.30	-	
4.17	-		-		-		3.49	0.39	3.54	0.35	3.59	0.32
4.18	3.52	0.37	3.49	0.41	3.53	0.39	3.57	0.35	3.56	0.35	3.62	0.29
4.19	3.56	0.44	3.44	0.56	3.50	0.49	3.47	0.52	3.52	0.51	3.57	0.46
4.20	3.49	0.44	3.55	0.45	3.55	0.38	3.50	0.57	3.54	0.36	3.58	0.39
4.21	3.63	0.21	3.46	0.47	3.57	0.37	3.65	0.36	3.62	0.23	3.60	0.24

TABLE 9

Calculation of β , where β is the factor of proportionality relating the eddy diffusivity of the sediment to the eddy viscosity of the water

Time	Phi range: 4.0ϕ-3.5	3.5 -3.0	3.0 -2.5	2.5 -2.0	2.0 -1.5	1.5 -1.0ϕ
1930	1.5870	-	2.3287	1.8212	-	-
2000	1.3439	3.6835	-	-	-	4.4595
2030	1.0754	1.1051	1.4161	1.3836	1.7338	-
2100	1.2499	1.6487	2.3432	1.6809	1.7816	10.9445
2130	1.4250	1.4641	1.5619	-	-	-
2200	1.1210	1.7636	3.5579	-	-	-
2234	-	-	-	-	-	4.7154
0100	0.6823	0.9375	1.4185	-	-	-
0130	0.7170	0.8552	1.4436	1.3168	-	-
0200	1.6751	-	-	-	-	-
0230	-	1.6085	1.4310	1.3590	1.6066	18.4470
0448	-	2.5897	3.3994	3.7384	7.0942	9.9824
0502	3.4013	2.3955	10.2592	-	-	10.2704
0530	2.1448	3.1835	6.1765	-	19.4018	-

TABLE 10

Total suspended sediment transport rate for separate phi fractions ($g\ cm^{-1}\ s^{-1}$)

Time	Phi range 4.0Ø-3.5	3.5-3.0	3.0-2.5	2.5-2.0	2.0-1.5	1.5-1.0Ø
1930	3.8320	1.7361	0.2259	0.1156	0.0202	0.0106
2000	5.1765	1.9216	0.2920	0.0773	0.0124	0.0096
2030	7.1606	4.7322	0.7494	0.3814	0.2136	0.0058
2100	5.8541	3.7368	0.5738	0.2632	0.2375	0.0101
2130	4.9038	2.9244	0.6153	0.3356	0.1139	-
2200	2.9524	1.2011	0.1879	0.2202	0.0724	-
2234	1.1910	0.2535	0.1732	-	-	-
0100	2.3694	0.4835	0.1321	0.0251	0.0071	0.0049
0130	6.9195	2.0926	0.4077	0.3442	0.0396	0.0094
0200	8.3007	3.5110	0.6307	0.5052	0.1317	0.0305
0230	17.1988	8.7301	1.2823	1.0852	1.3853	0.0166
0448	4.3950	0.6642	0.0997	0.0430	0.0171	-
0502	2.1680	0.4801	0.0846	0.2344	0.1100	-
0530	0.7281	0.1169	0.0340	0.4334	-	-

NB: Where the concentration data does not fit the Rouse equation (equation (7)), a mean β (one for each phi range) is used.

TABLE 11

(suspended sediment transport rate) calculated as a total suspended load, and compared with the sums of the rates calculated separately for the various phi ranges

Time	(total) (= 0.4) ($g\ cm^{-1}\ s^{-1}$)	(sum of fractions) ($g\ cm^{-1}\ s^{-1}$)
1930	5.4186	5.9404
2000	7.0568	7.4894
2030	12.6266	13.2430
2100	10.7291	10.6755
2130	10.0351	8.8930
2200	5.5664	4.6340
2234	4.1041	1.6177*
0100	2.4856	3.0221
0130	8.6460	9.8130
0200	16.3838	13.1098
0230	27.8936	29.6983
0448	4.5881	5.2190
0502	2.8094	3.0771
0530	1.0207	1.3124

* 3 fractions not available

TABLE 12

Predicted sediment transport rates and directions using Yalin's (1963) formula

Current meter station	Direction from true N (°)	Transport rate x 10^{-1} (g cm^{-1} s^{-1})	Transport rate (tonnes $m^{-1}day^{-1}$)
A	204	0.156	0.13
B	27	0.129	0.11
C	61	0.027	0.02
D	216	0.137	0.12
E	22	0.605	0.52
F	64	0.128	0.11
G	14	0.601	0.52
H	326	0.077	0.07
J	199	0.089	0.08
K	222	0.209	0.18
L	341	0.034	0.03
M	188	0.690	0.60
N	205	0.183	0.16
P	199	0.140	0.12
Q	197	0.560	0.48
R	3	0.262	0.23
S	187	0.162	0.14
T	146	0.063	0.05
V	152	0.128	0.11
W	208	0.227	0.20
X	169	0.054	0.02
Y	285	0.053	0.05
Z	212	0.372	0.32

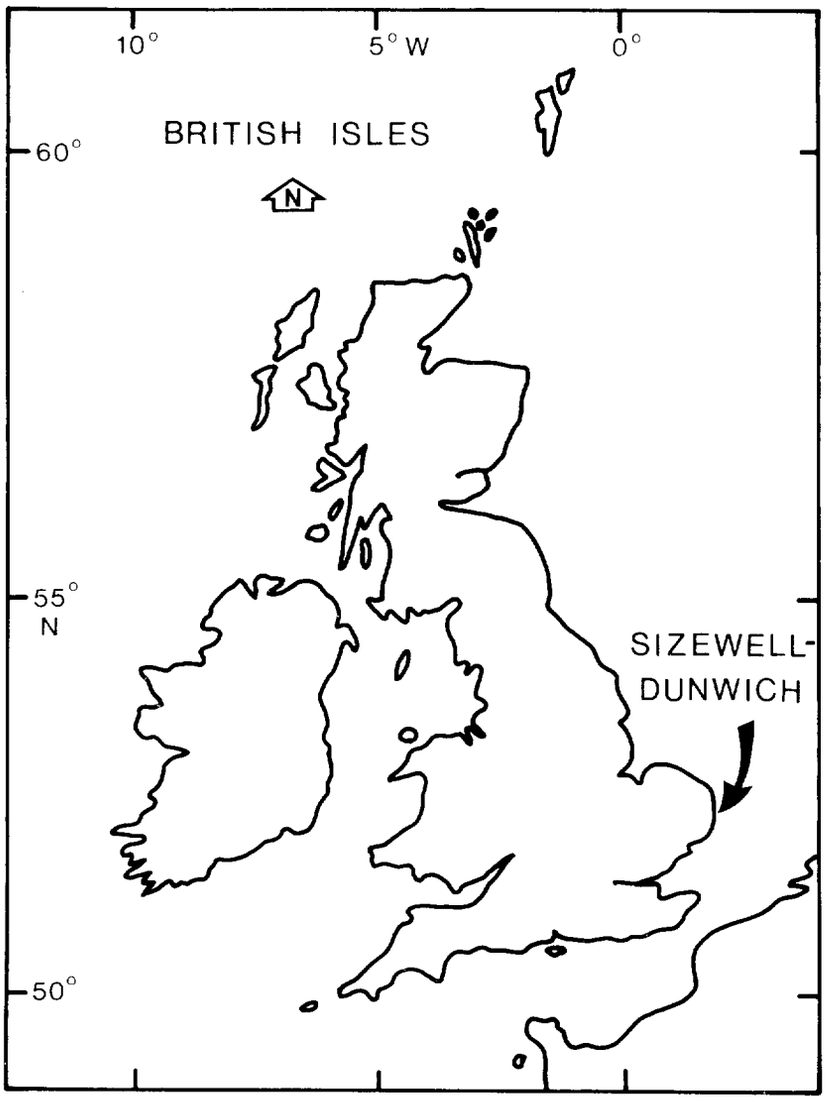

Figure 1 Location of study area.

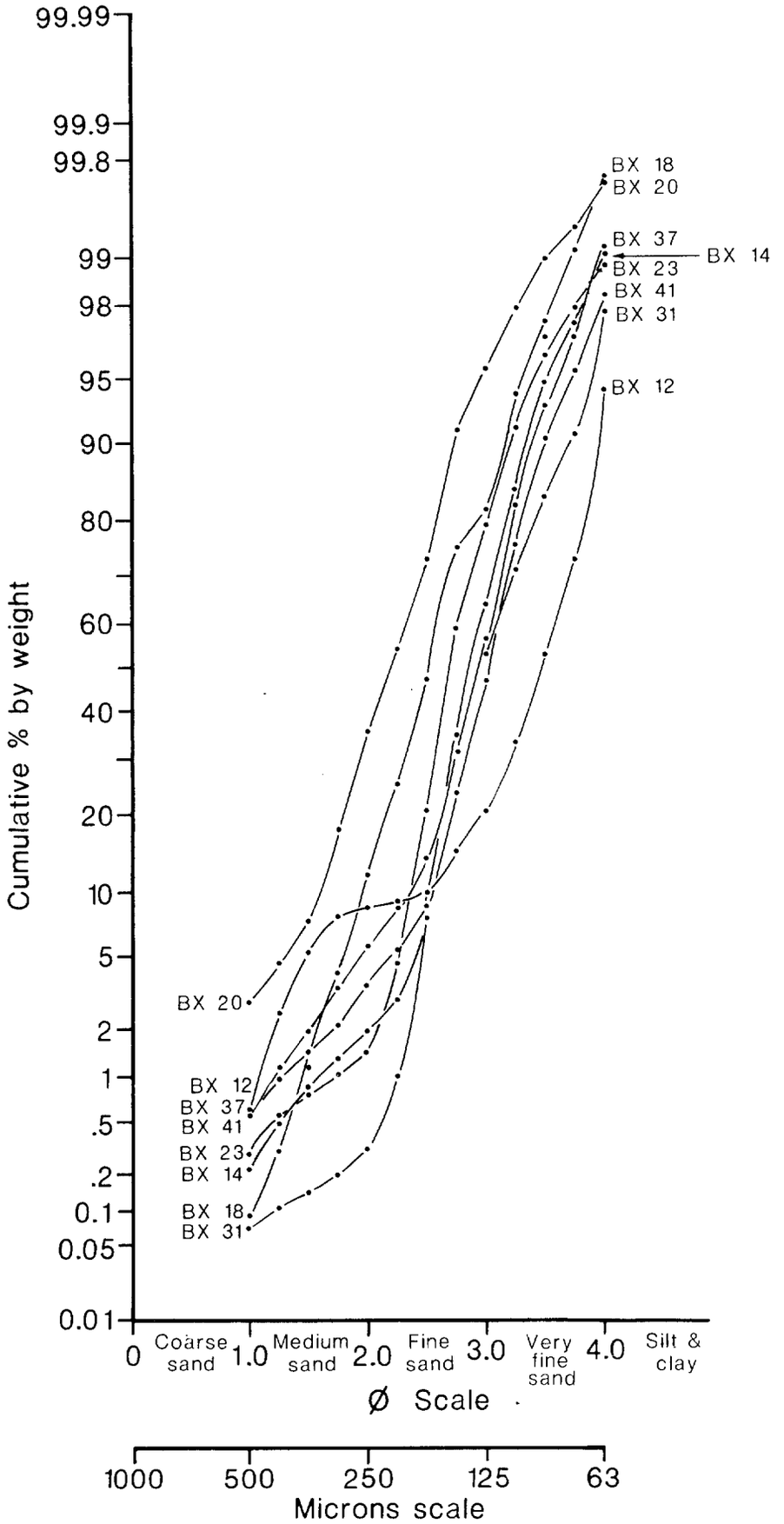

Figure 2 Grain size analyses of box core samples.

Key for figs 3 and 4

a Gravel. Angular and rounded pebbles, mainly orangey flints. Good fauna, mainly sessile forms.

b Medium sand)
c Fine sand) Clean, brownish to yellowish, firm.
d Very fine sand)

e Intercalated sands, silts and clays. Mainly grey. 'Fluid'.

f Sticky blue-grey clay, often with veneer of brown silt or sand.

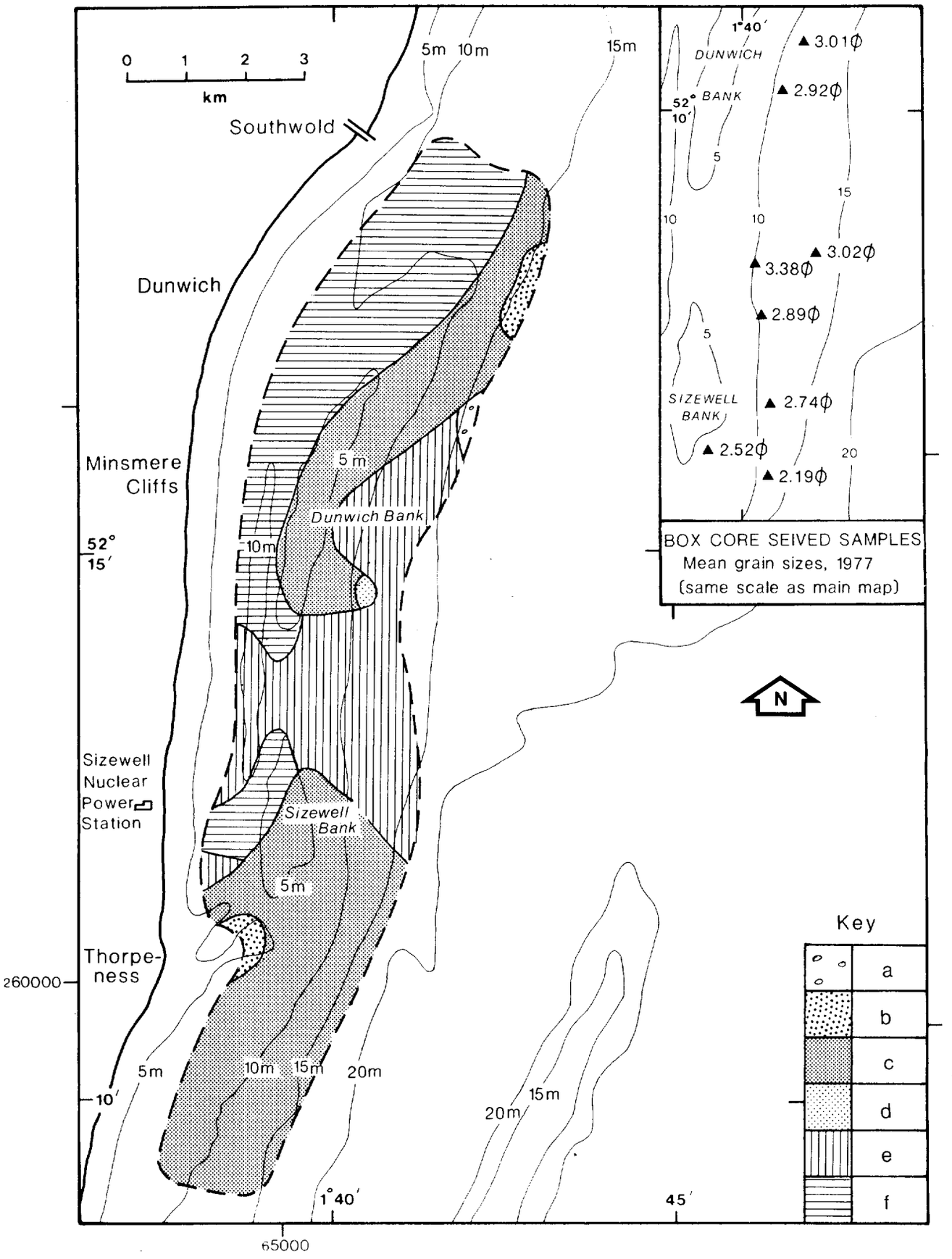

Figure 3 Sediment distribution, August 1978.

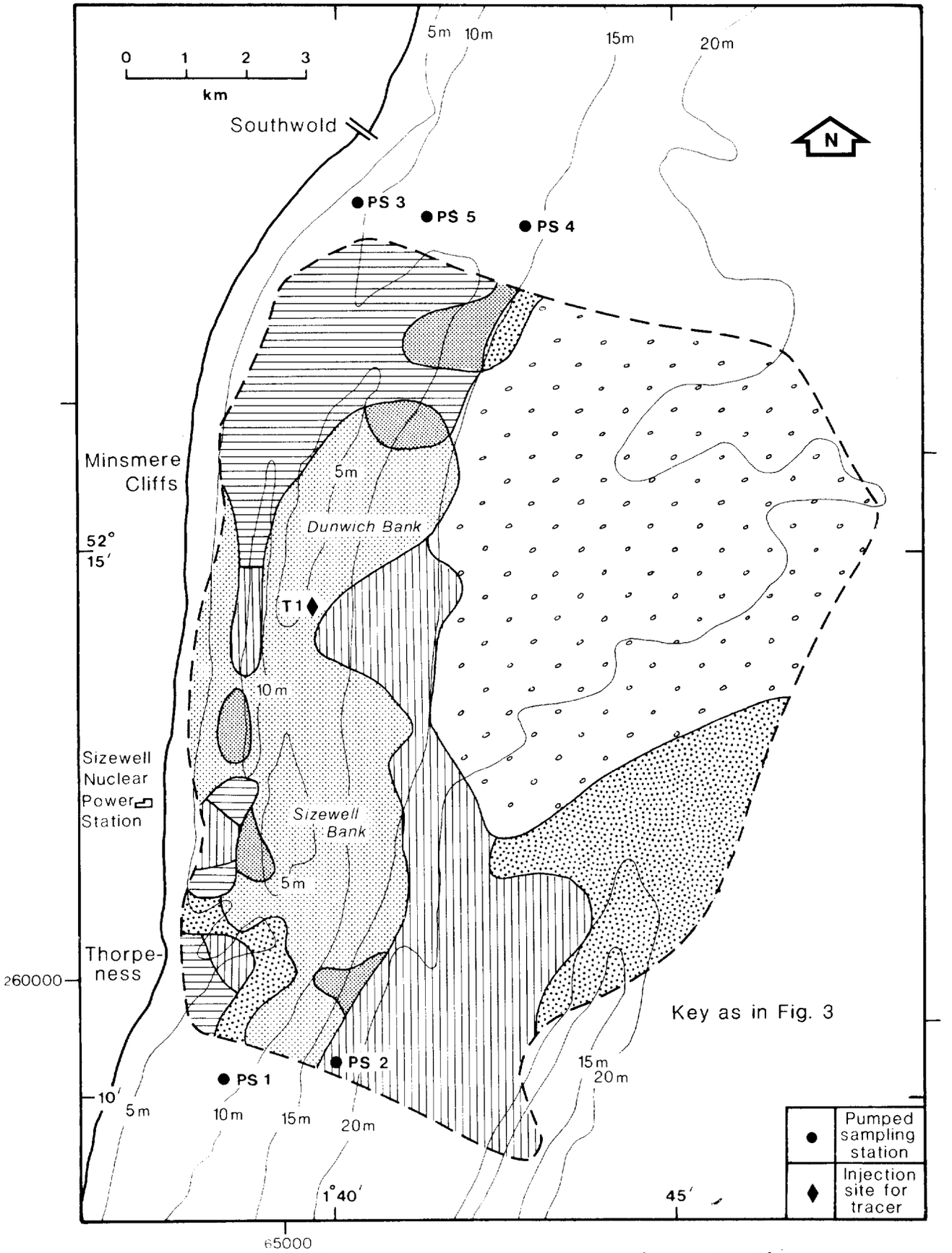

Figure 4 Sediment distribution 1975 and locations of sediment transport measurement sites.

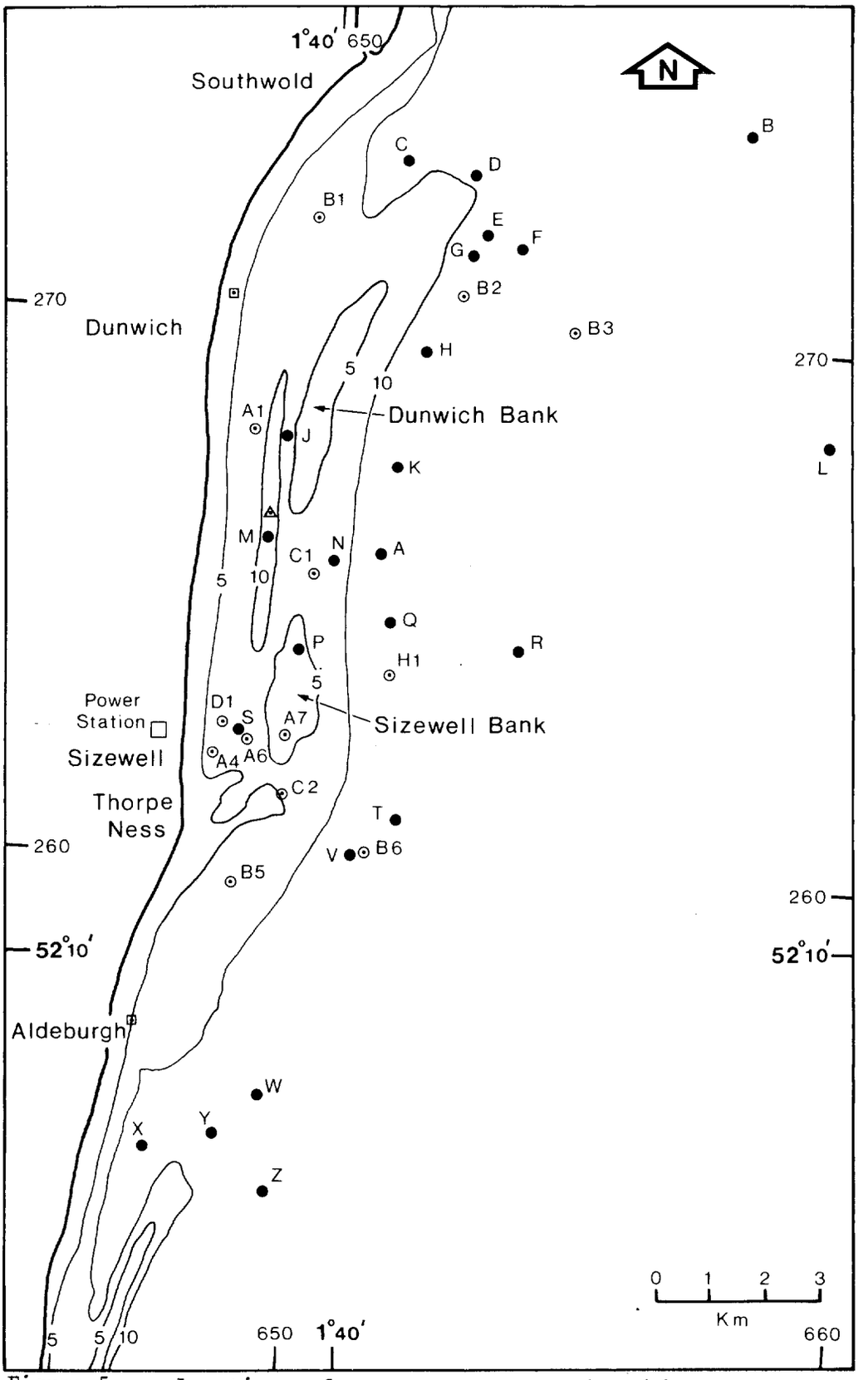

Figure 5 Locations of current meter moorings (●). For dates of deployment see Heathershaw and Lees (1980). Also shown are positions of Marconi current meter mooring (▲) and CEGB moorings (⊙).

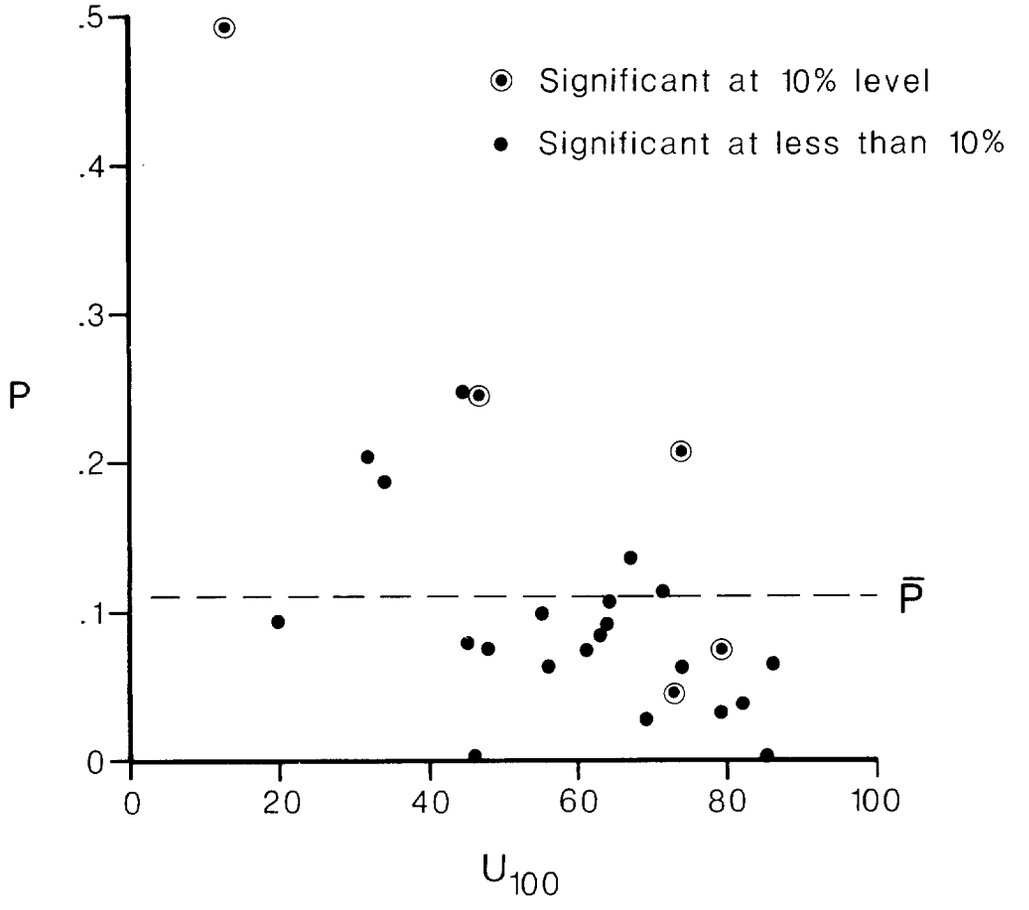

Figure 6 Power law velocity profile exponentiation from Marconi data. Uy (N-S) component only shown, using hourly averages of 10 minute values. $\frac{u}{u_1} = \left(\frac{z}{z_1}\right)^p$.

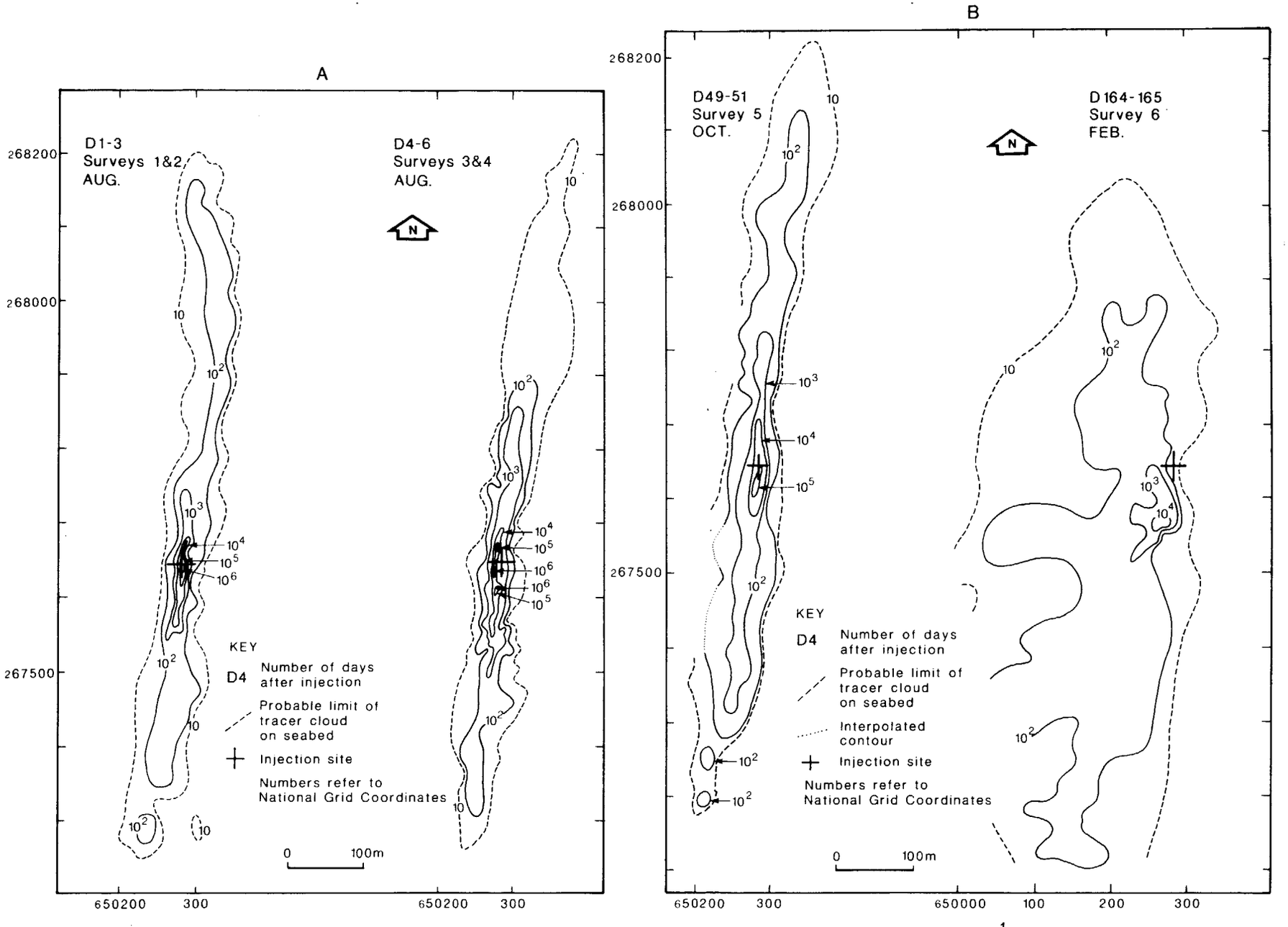

Figure 7 Contours of fluorescent tracer concentration in grains kg^{-1}, A for Surveys 1 + 2 and Surveys 3 + 4, B for Survey 5 and 6.

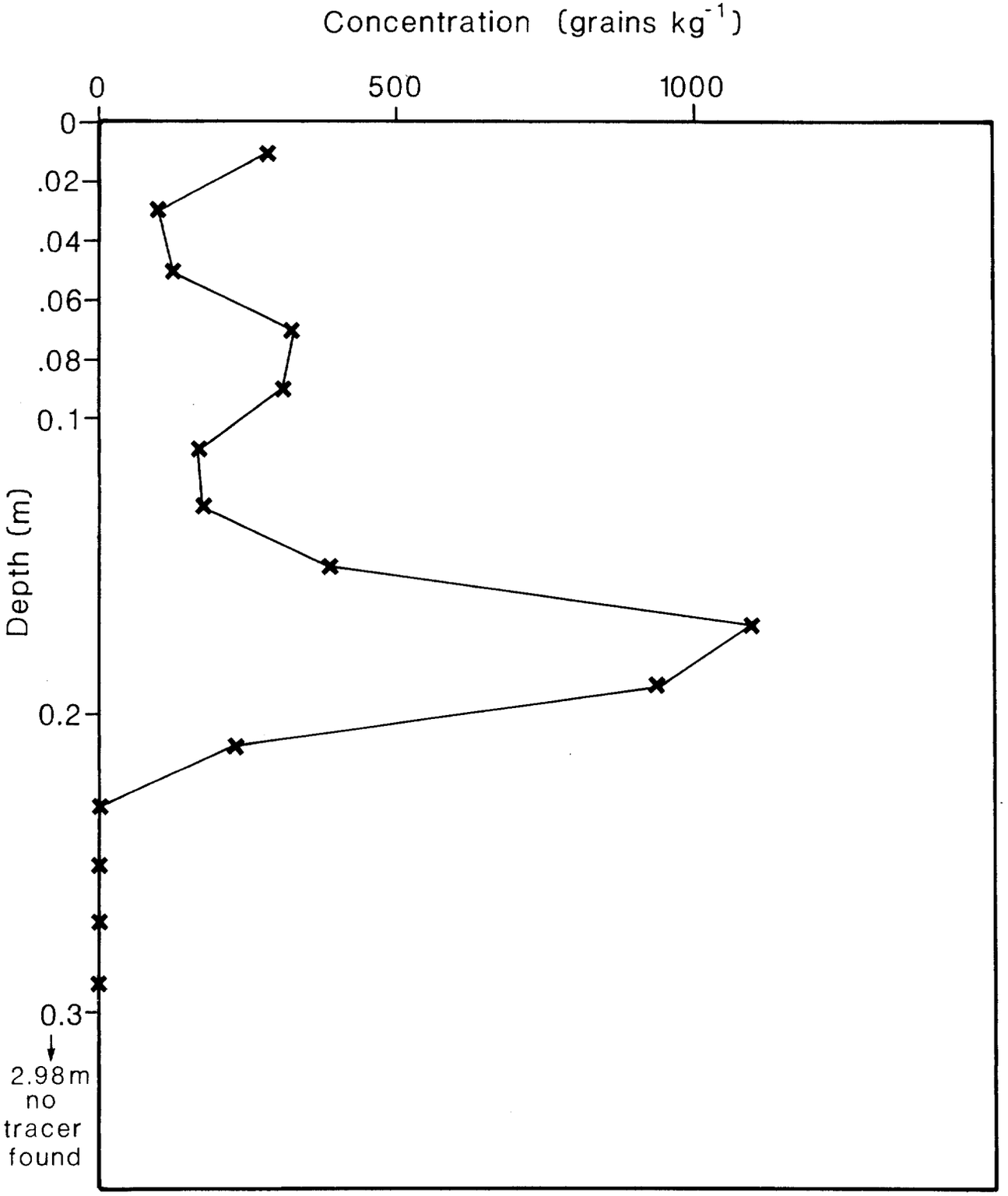

Figure 8 Variation of fluorescent tracer concentration with depth in vibrocore VC13.

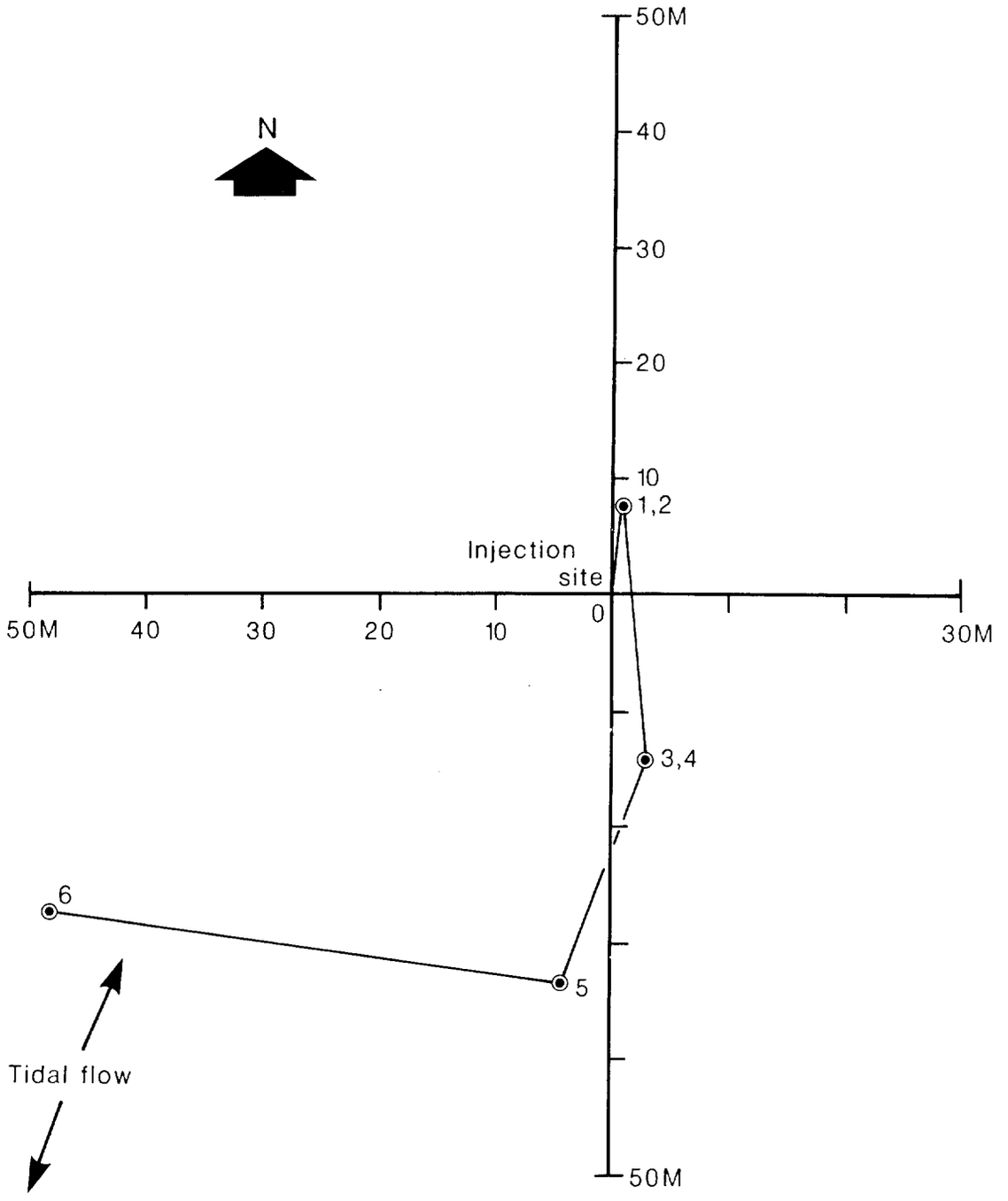

Survey No.	Days after injection (mean)	Transport rate between surveys q_{sb} (g cm^{-1} s^{-1})
1+2	2	0.012
3+4	5	0.040
5	50	0.012
6	164.5	0.015

Figure 9 Movement of tracer centroid observed over a period of 165 days. The value of the tidal residual at the nearest current meter station to the injection site (6 km to NNE), which was measured during surveys 1-3, was 0.043 m s^{-1} to WSW.

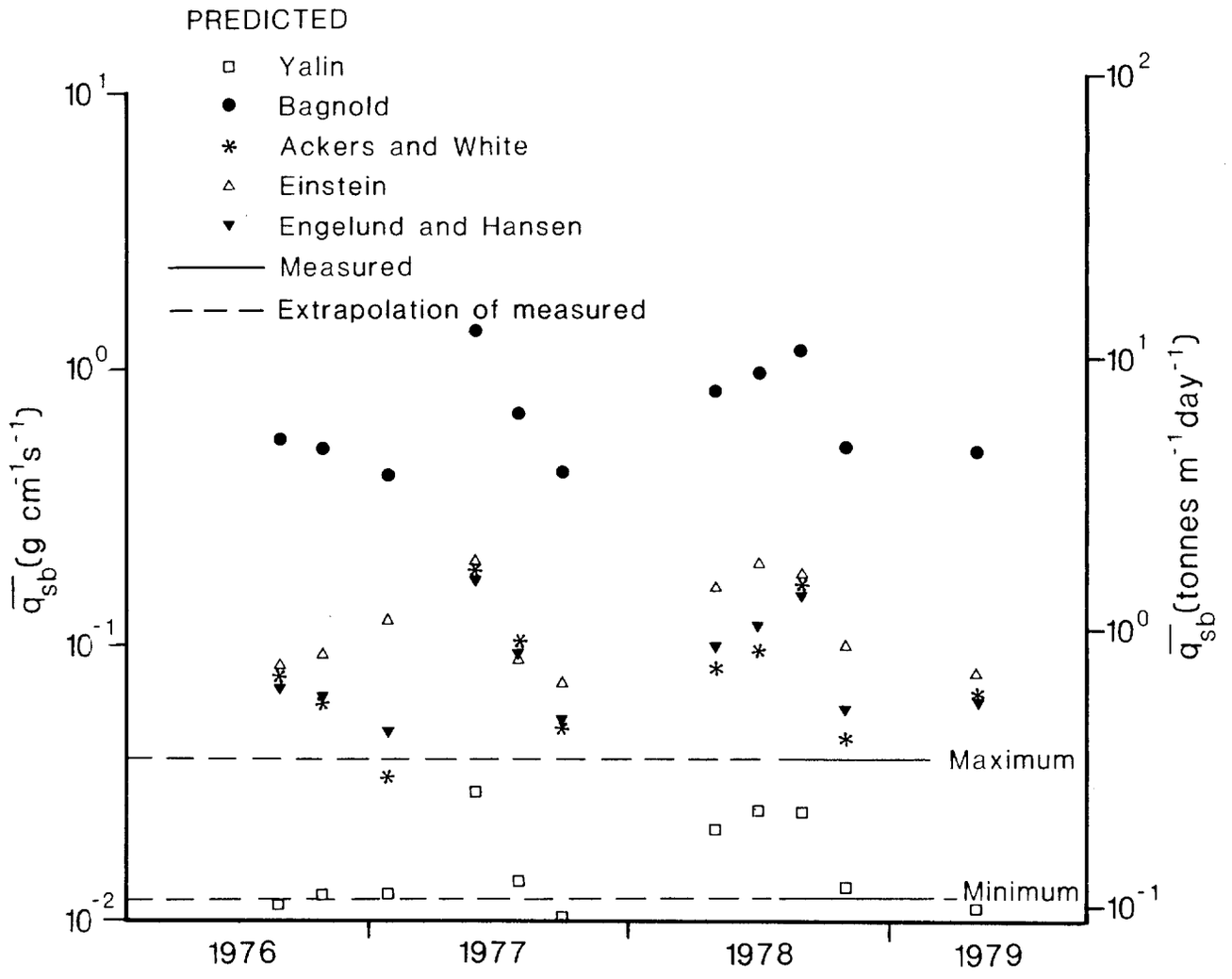

Figure 10 Comparisons of measured and predicted net transport rates ($\overline{q_{sb}}$). Strictly speaking Ackers and White's, and Engelund and Hansen's formulae are for total loads and q_{sb} in these cases is actually ($\overline{q_{sb} + q_{ss}}$).

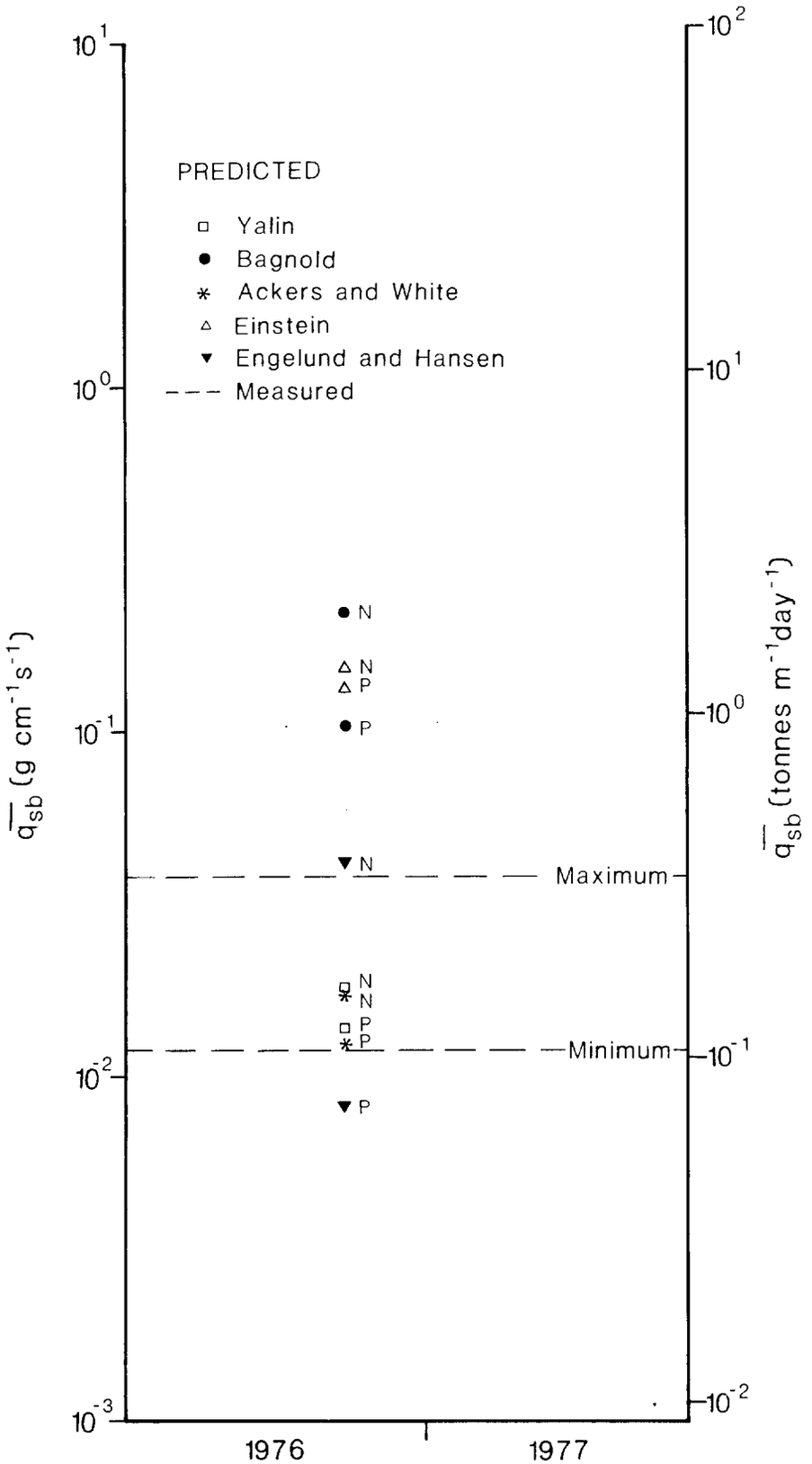

Figure 11 Comparison of measured net transport rates with those predicted at Stations N and P. The time scale on the horizontal axis is similar to that for Figure 10 and shows that the readings were made during September 1976.

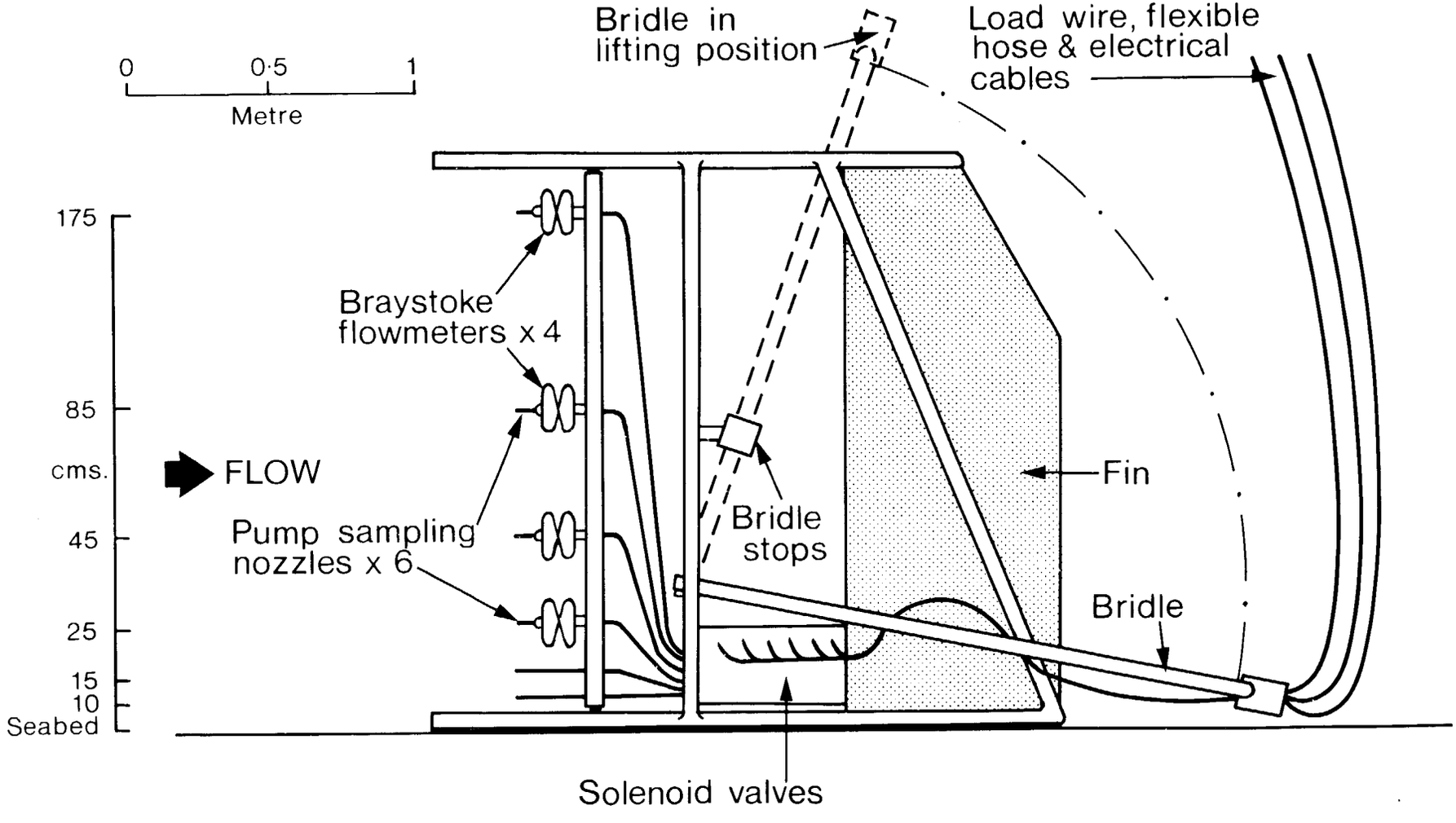

Figure 12 Schematic diagram of pumped sampling apparatus.

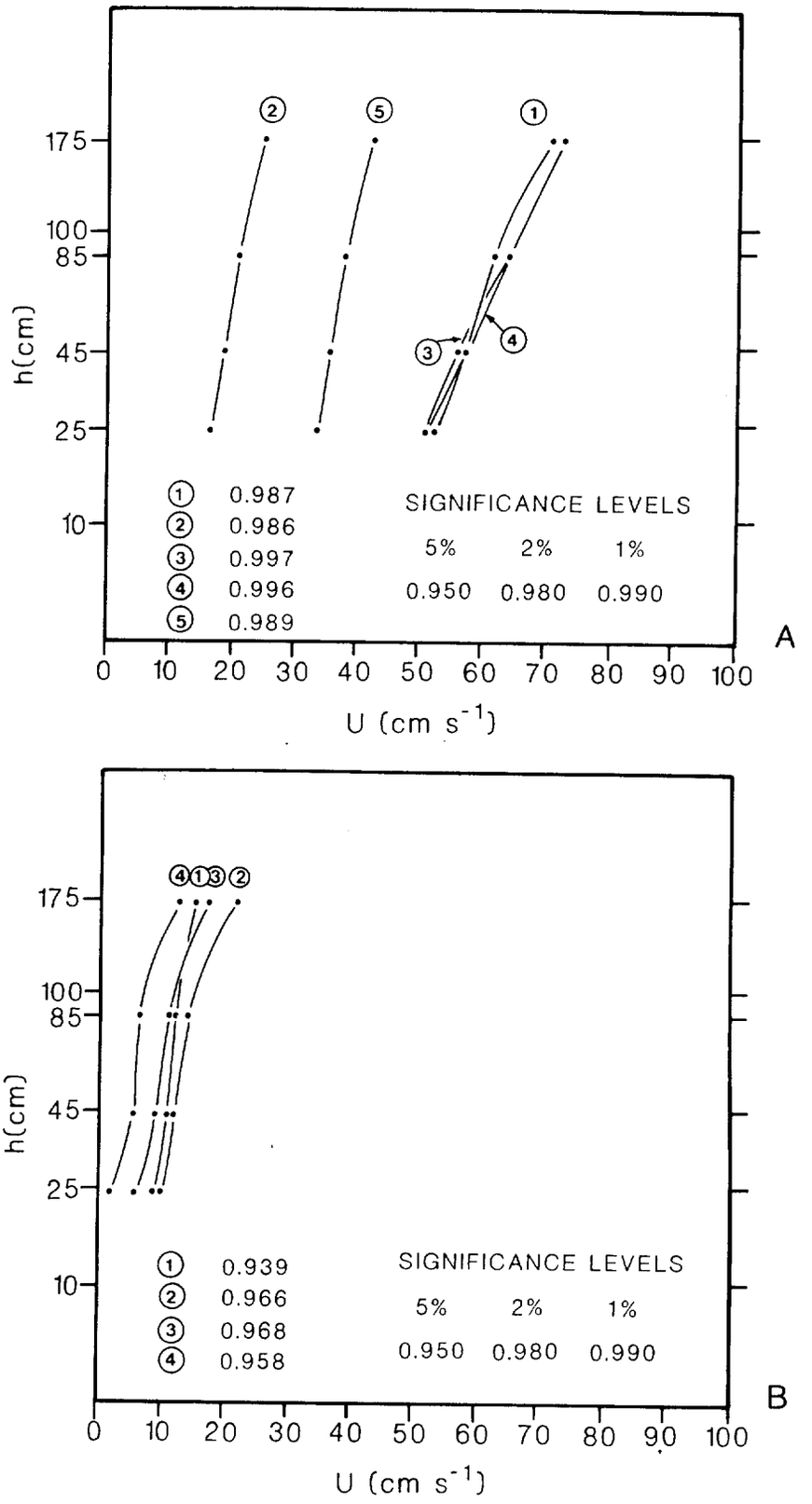

Figure 13 Typical velocity profiles, Station PS4, A with flow well established and B near slack water with decelerating flow. Correlation coefficients for fit to Karman-Prandtl logarithmic profiles are also shown.

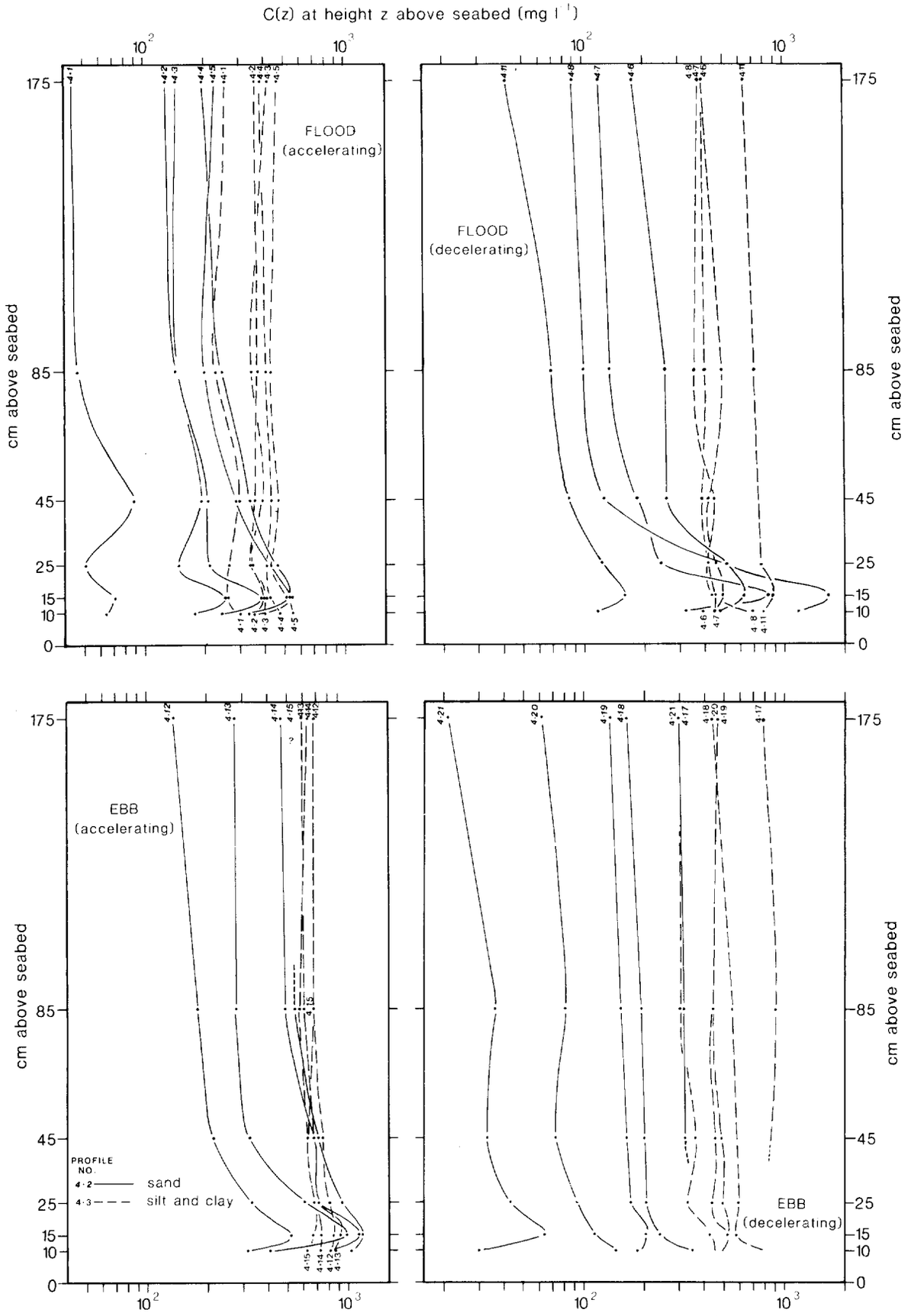

Figure 14 Suspended sediment concentration profiles for Station PS4.

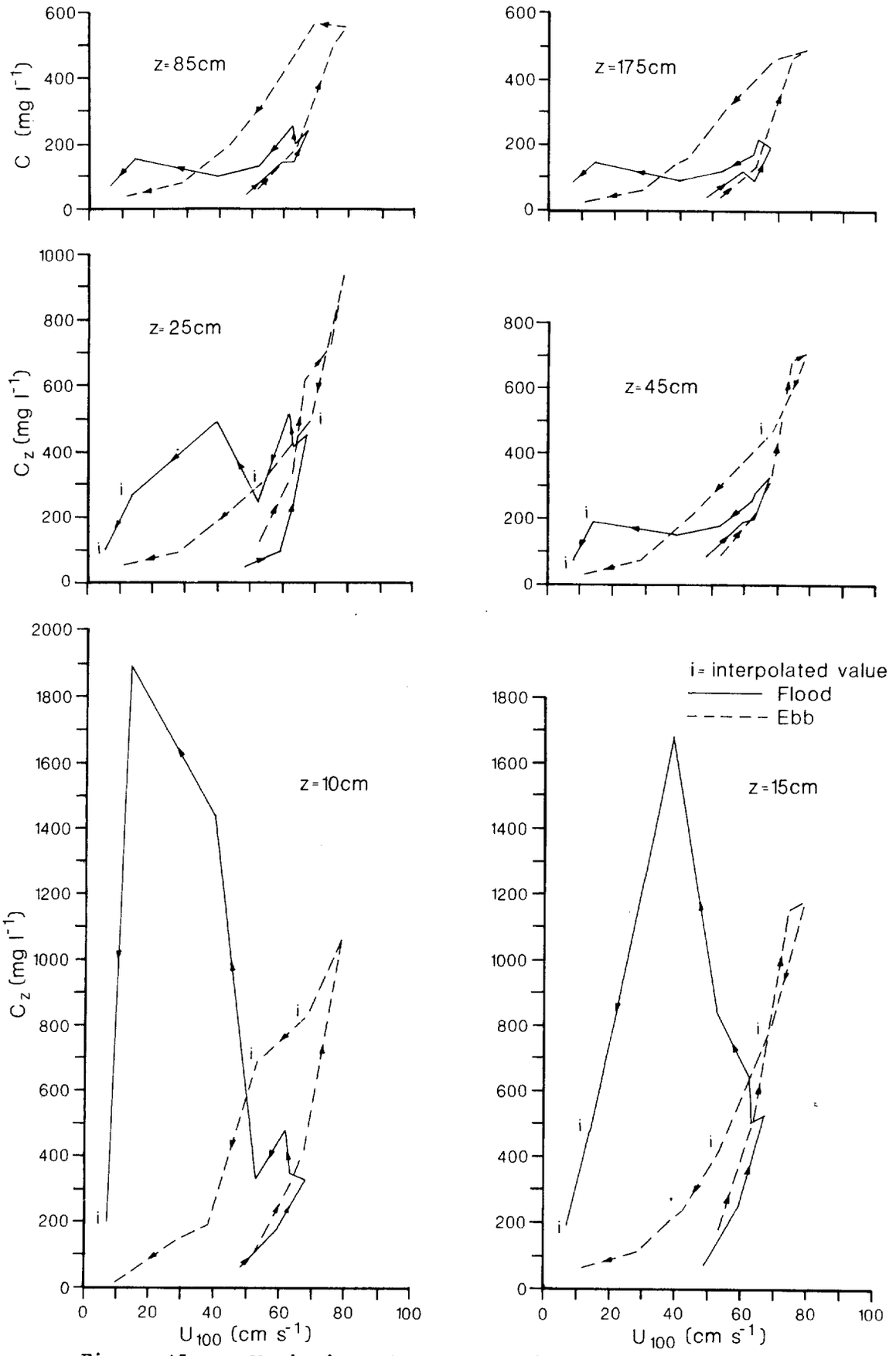

Figure 15 Variation of concentration with velocity at 100 cm above seabed.

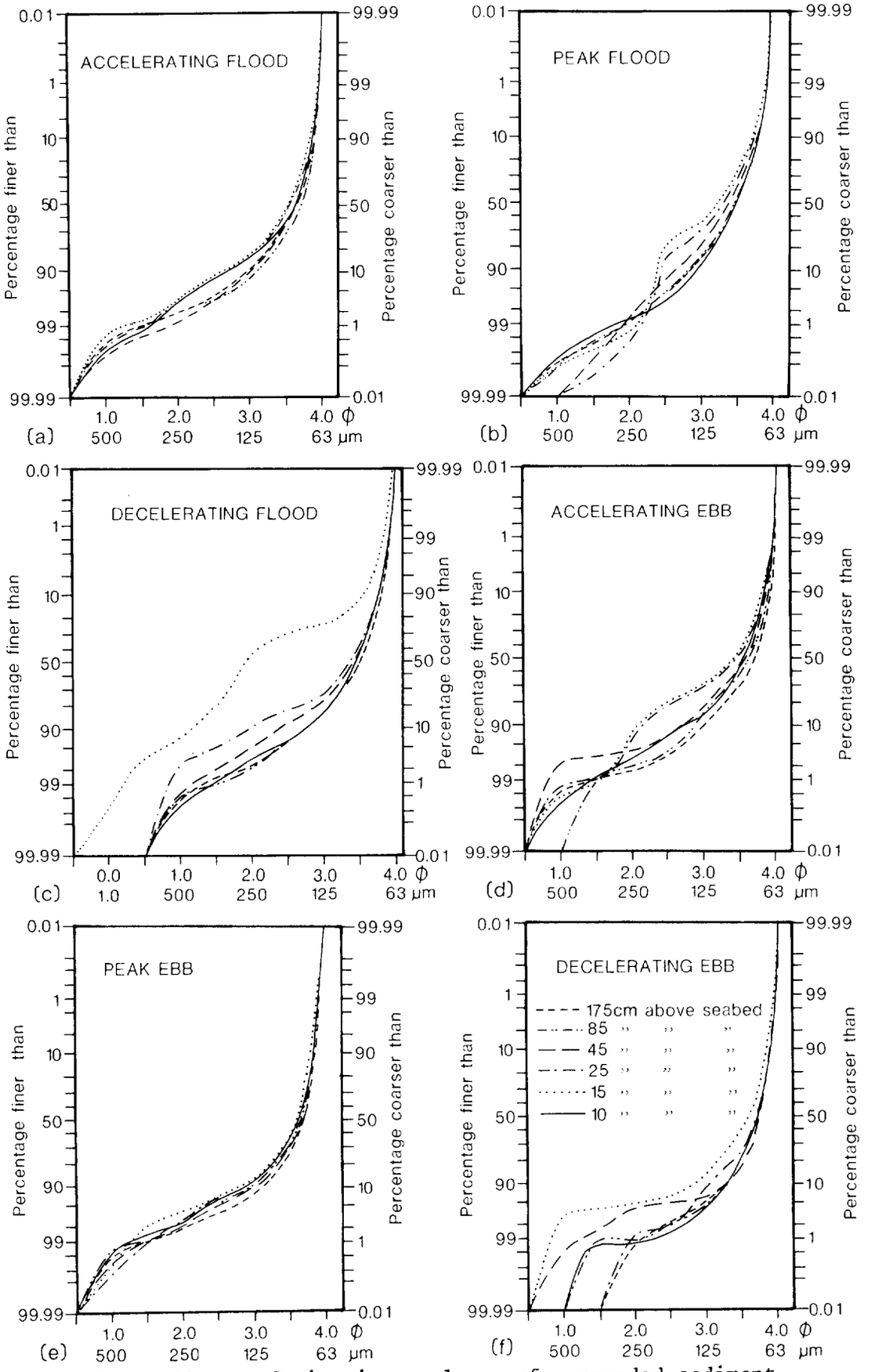

Figure 16 Grain size analyses of suspended sediment samples, showing variation through a tidal cycle.

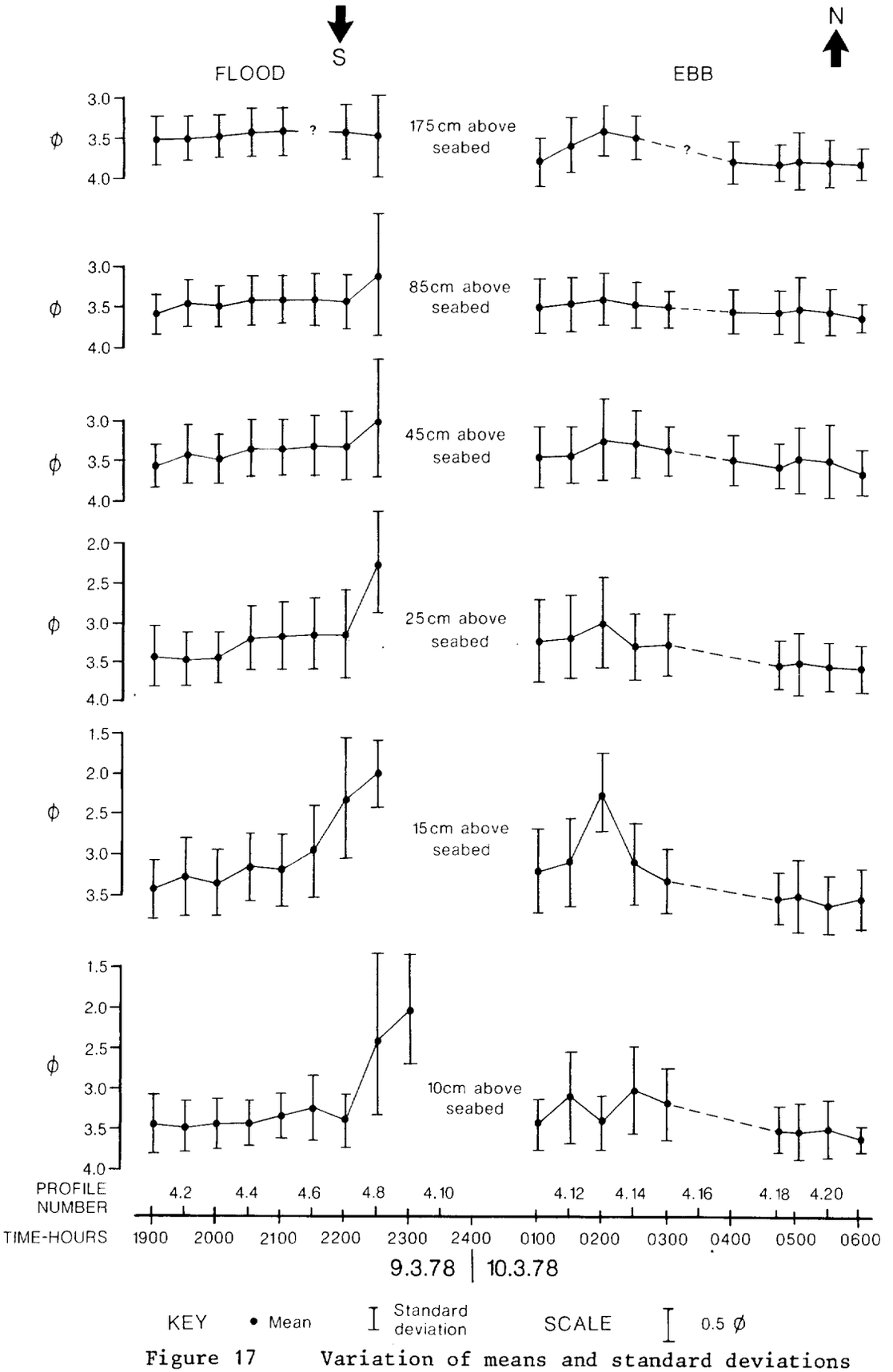

Figure 17 Variation of means and standard deviations of suspended sediments at different heights above seabed, through a tidal cycle.

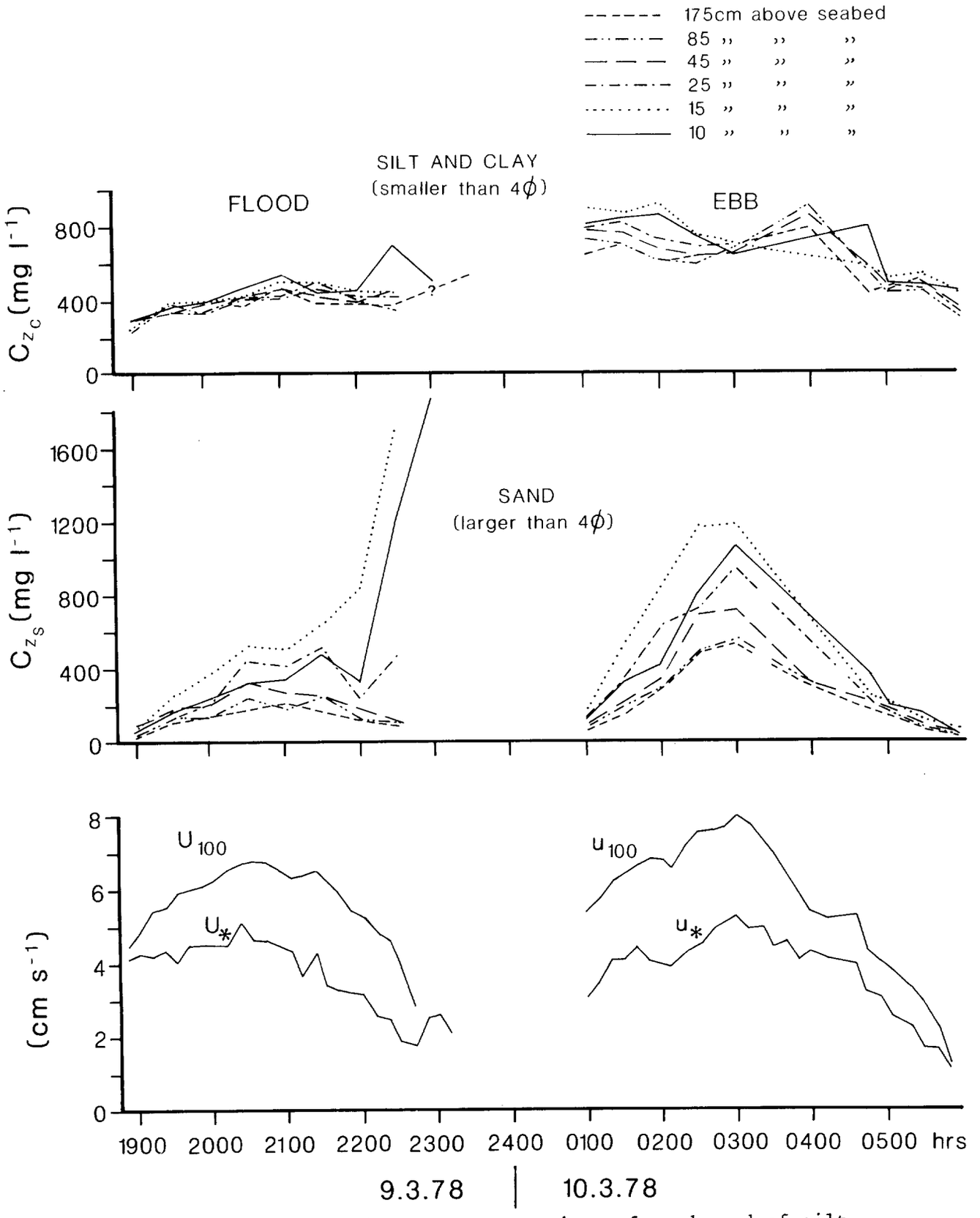

Figure 18 Variation of concentrations of sand, and of silt and clay through a tidal cycle. U_{100} (velocity at 100 cm above seabed) and U_* (friction velocity) are also shown.

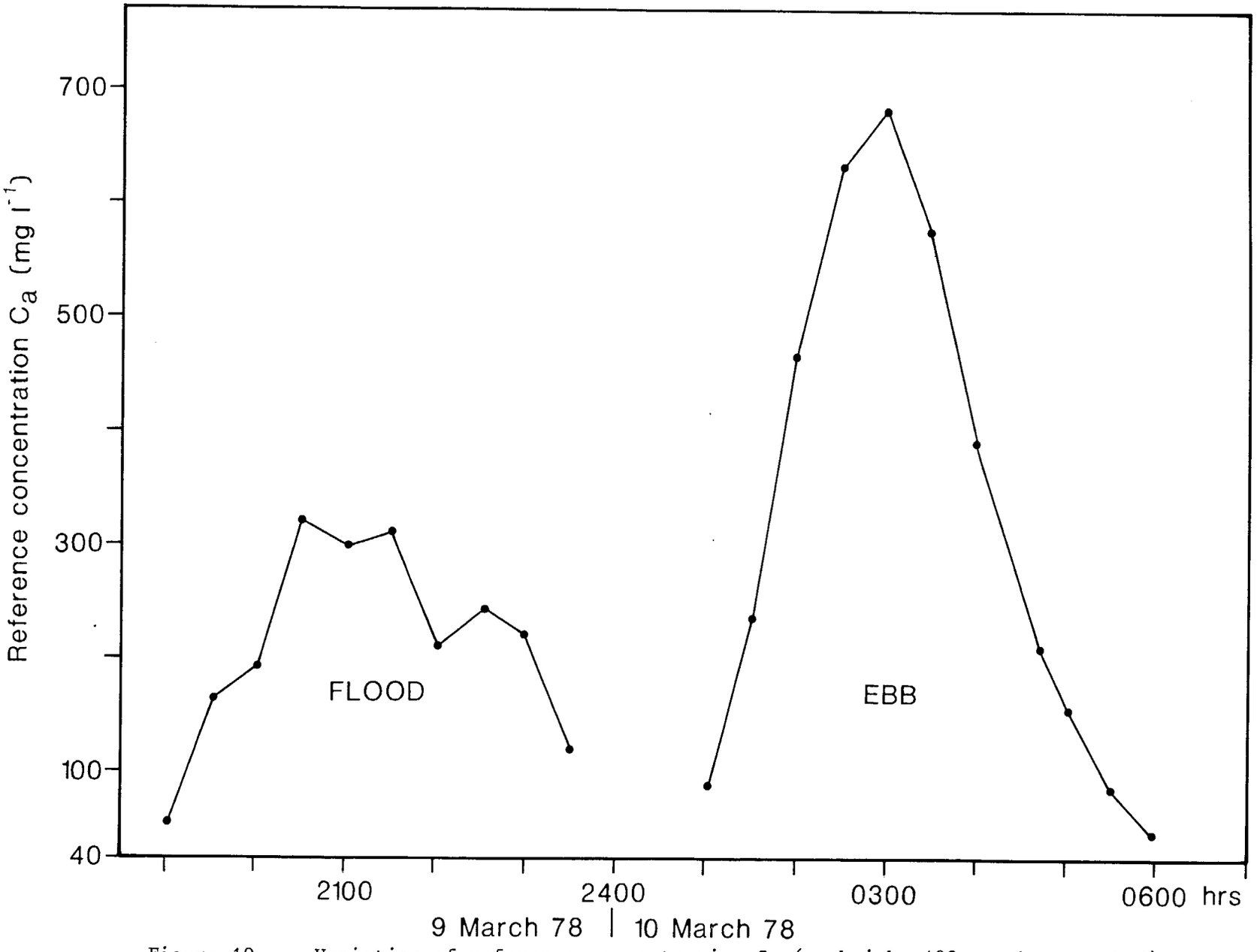

Figure 19 Variation of reference concentration Ca (at height 100 cm above seabed) with time during one tidal cycle.

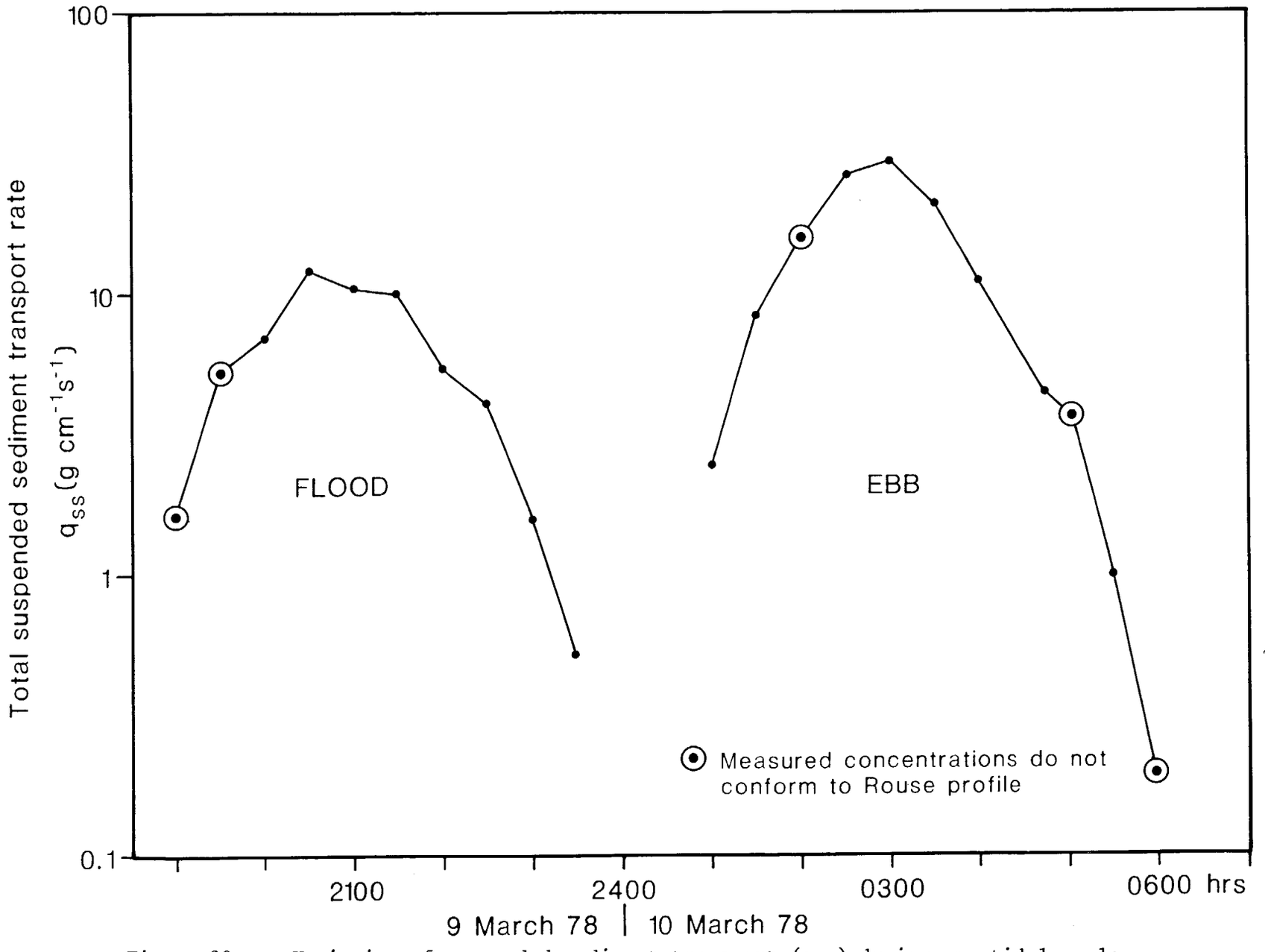

Figure 20 Variation of suspended sediment transport (q_{ss}) during one tidal cycle.

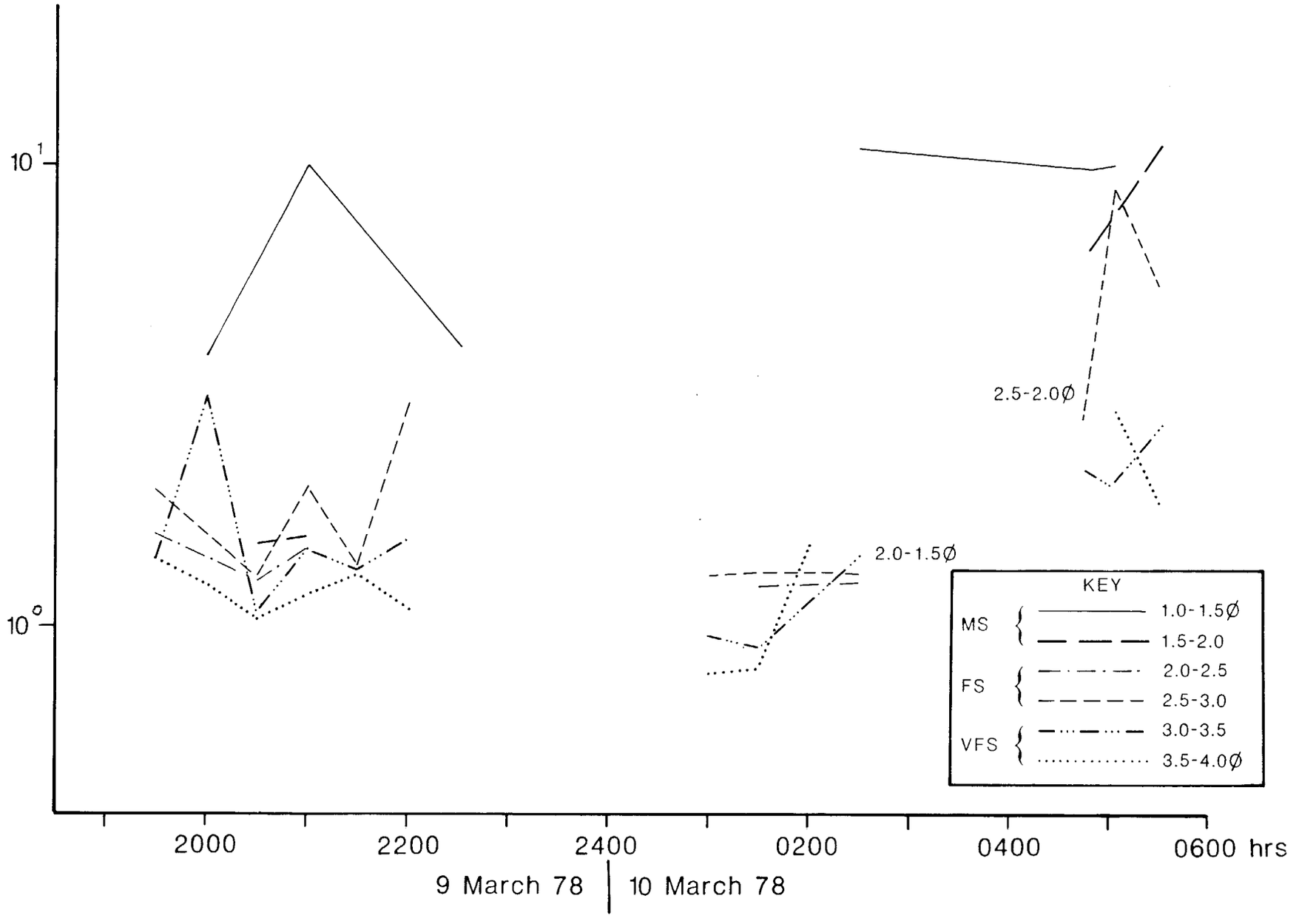

Figure 21 Calculated values for factor of proportionality β, where $E_s = \beta E_w$.

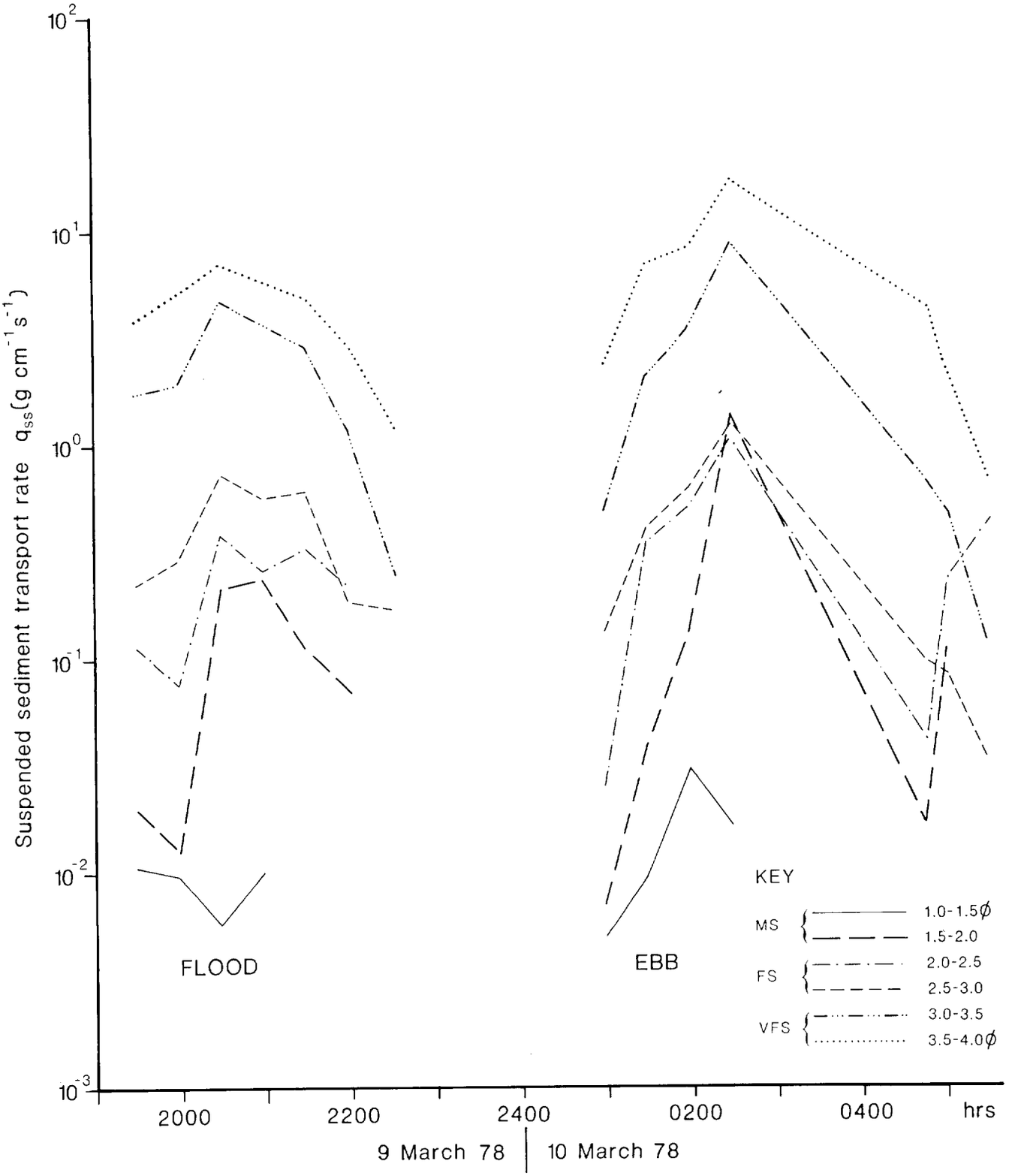

Figure 22 Variation of suspended sediment transport rates for varying phi ranges during one spring tidal cycle at Station PS4.

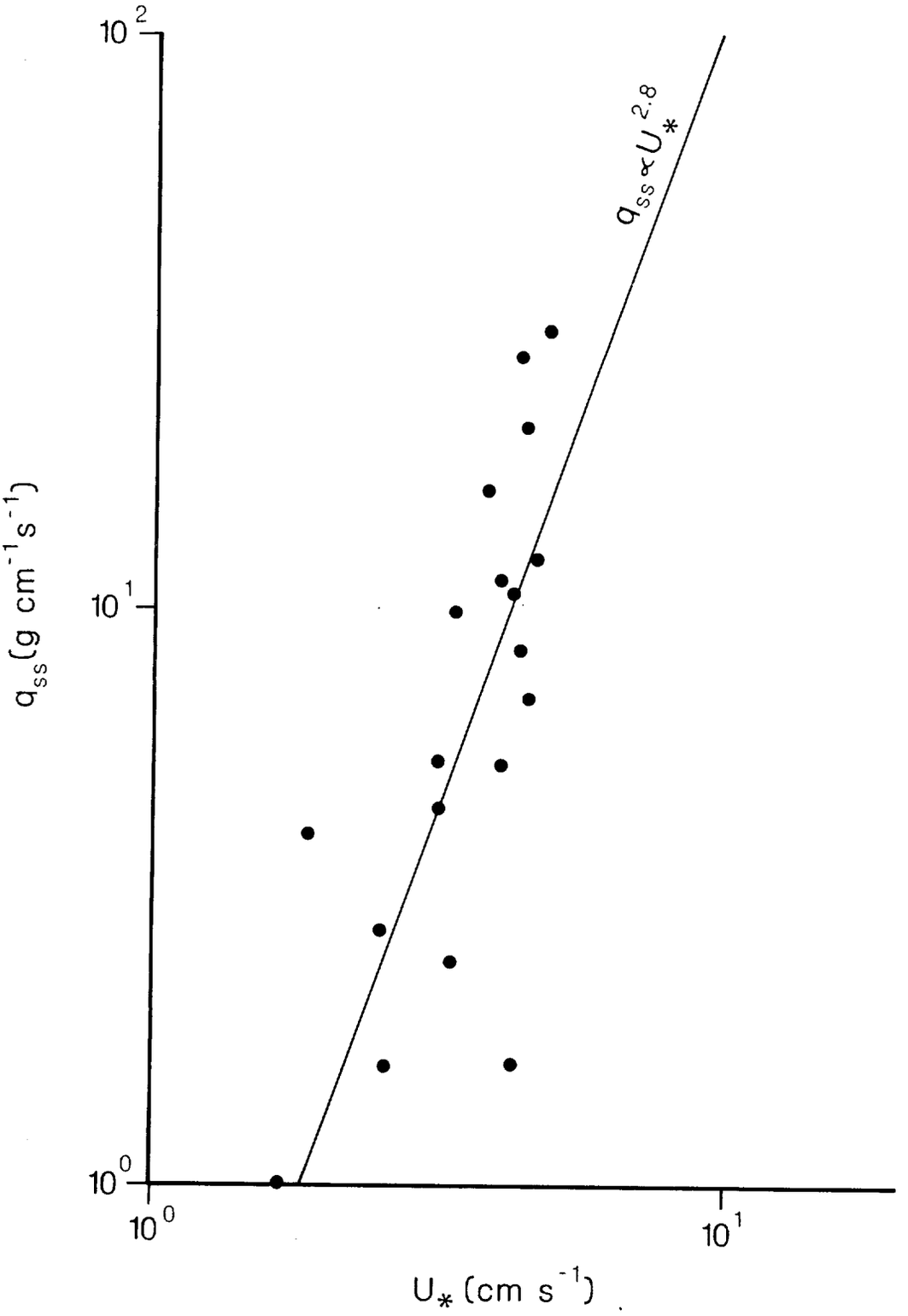

Figure 23 Variation of total suspended sediment transport rate (q_{ss}) with friction velocity (U_*). Linear regression analysis shows $q_{ss} \propto U_*^{2.8}$

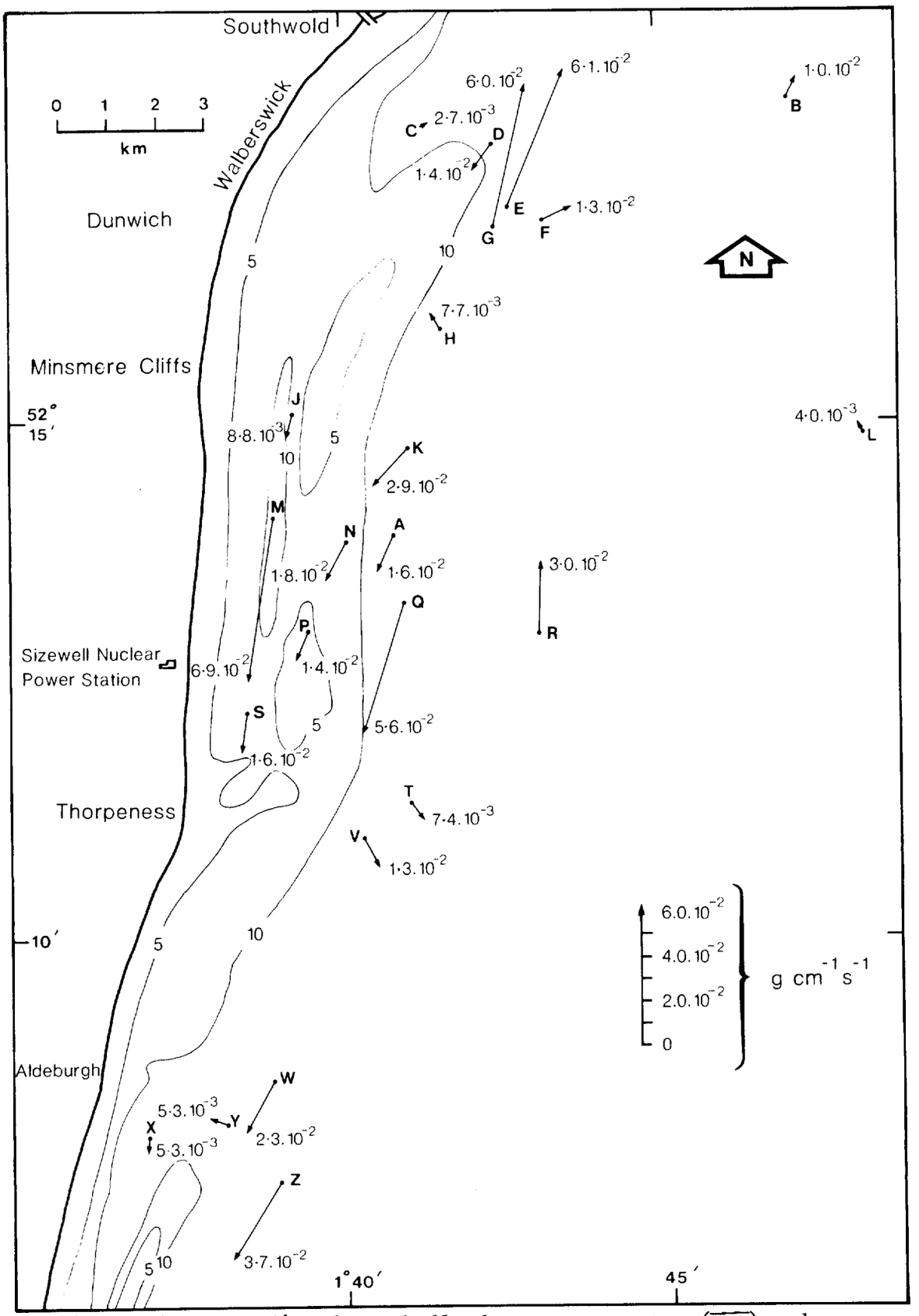

Figure 24 Predicted net bedload transport rates ($\overline{q_{sb}}$) and directions, using Yalin's (1972) sediment transport formula. Transport rates are given in g cm^{-1} s^{-1}.

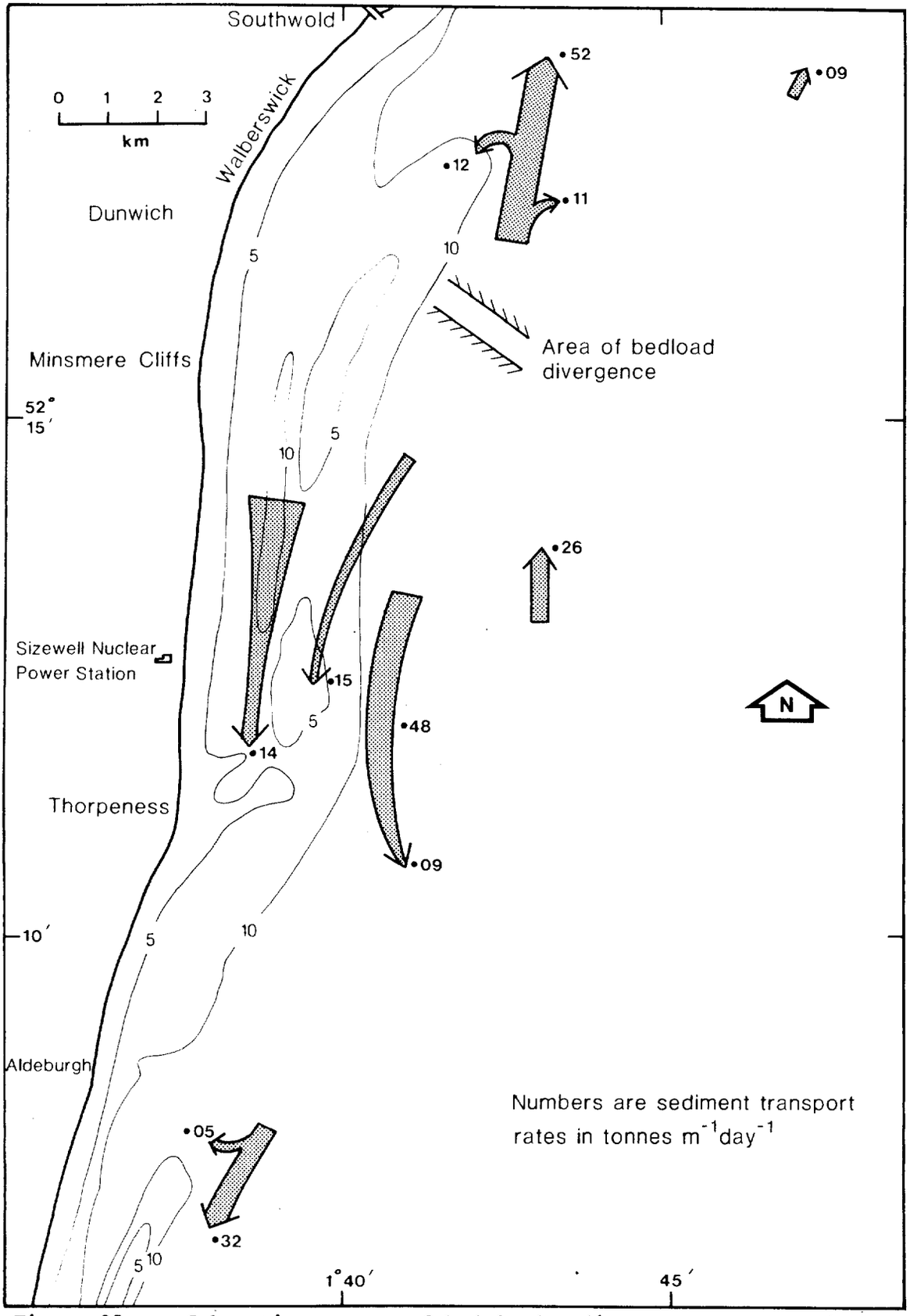

Figure 25 Schematic summary of bed load sediment transport paths, based on information given in Figure 24. Numbers are sediment transport rates in tonnes m^{-1} day^{-1}.

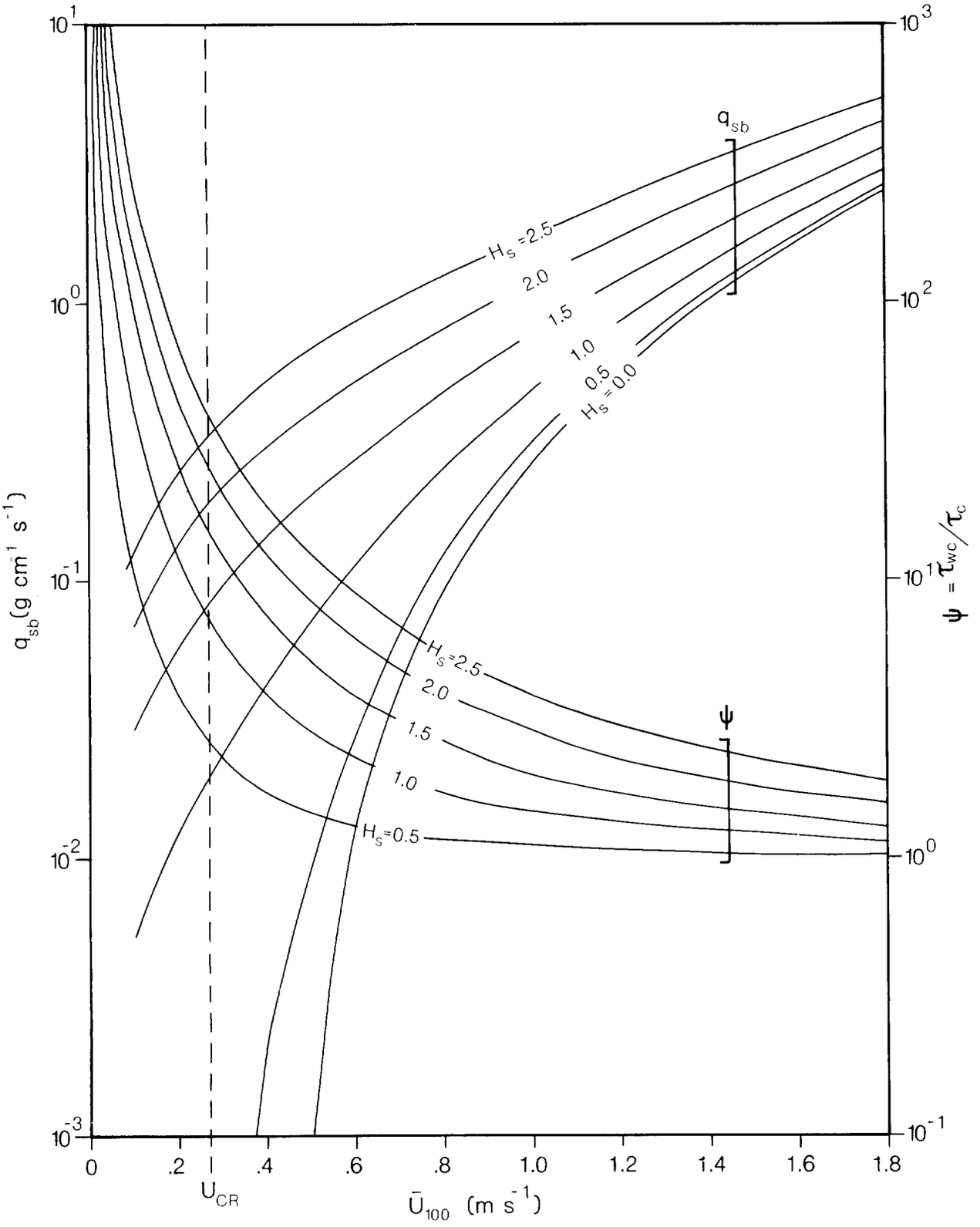

Figure 26 Effect of waves on sediment transport. Bijker's (1967) magnification factor (ψ), illustrating effect of increasing wave height (H) on bedload transport rates (q_{sb}), as function of current at height of 100 cm above sea bed (U_{100}). NB These calculations have been carried out for a wave of 6s period and water depth of 12 m, with roughness length of .05 cm, typical for fine sand.

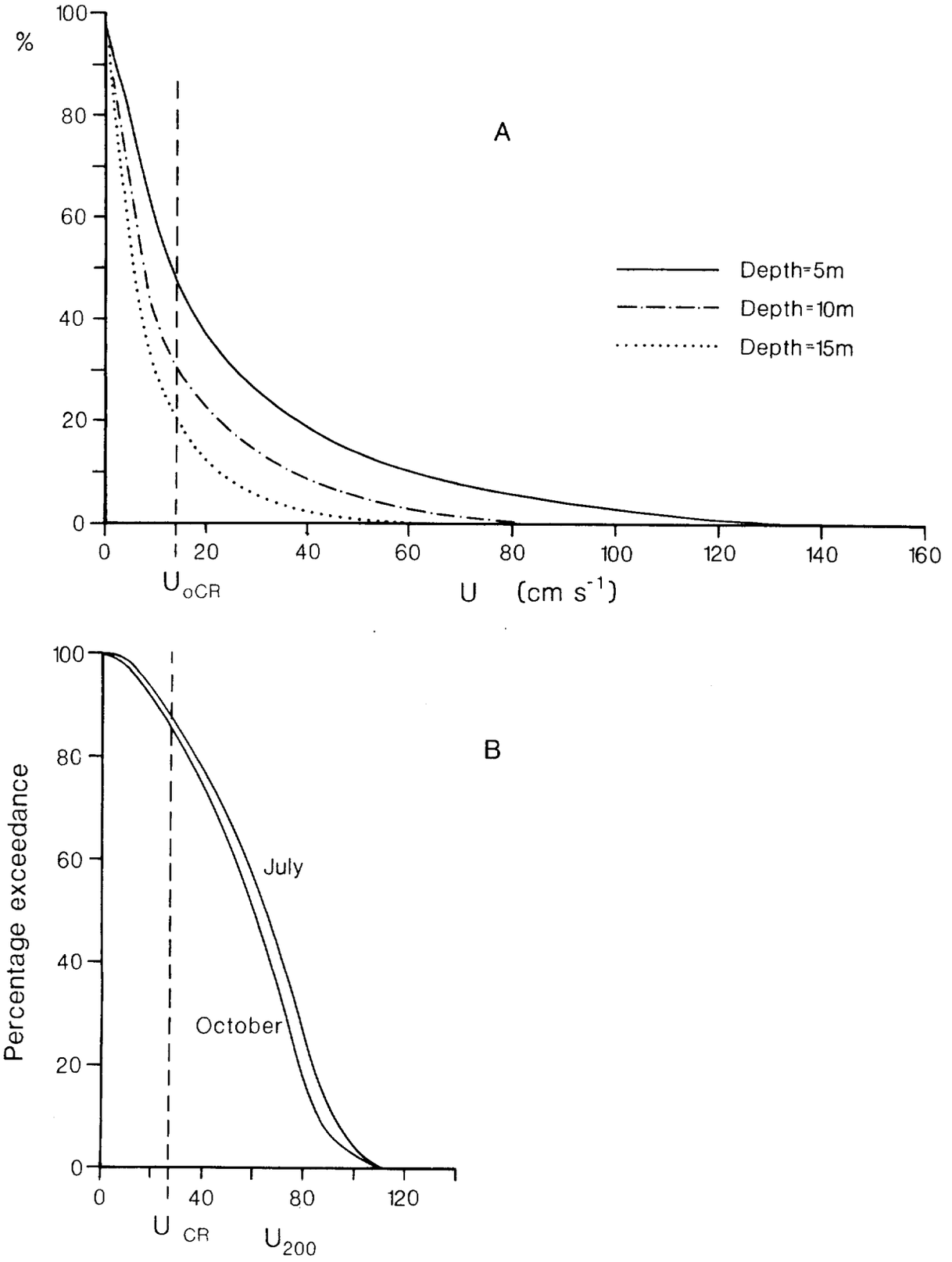

Figure 27 A. Wave induced current exceedance curves, based on 1 year's wave measurements made offshore from Southwold. U_{OCR} is indicated and has been calculated from equation (13).

B. Percentage exceedance curves for tidally induced currents, using 1 month's data in each case.

APPENDIX A

DETAILS OF SEDIMENT TRANSPORT EQUATIONS

(After Heathershaw, 1981)

On the basis of evidence presented by Swart (1976), Flemming and Hunt (1976), and Gadd et al (1978), five sediment transport equations were chosen for evaluation in this study. These are listed in Table II with details given below. The description of Einstein's (1950), Bagnold's (1963), and Yalin's (1963) equations follows that given by Gadd et al.

1.

Einstein's (1950) bedload equation. Einstein's equation differs from others in a number of ways. These are:

(a) the equation is stochastic and relates sediment transport to random velocity fluctuations rather than mean flow parameters;

(b) the equation contains no threshold criterion for sediment movement.

According to Einstein's equation the initiation of particle motion occurs when the instantaneous lift forces are greater than the immersed weight of sediment. The probability (P) of this occurring is given by the normal error law:

$$P = 1 - \frac{1}{\pi^{\frac{1}{2}}} \int_{-B_* \psi_* - 1/n_0}^{B_* \psi_* - 1/n_0} e^{-t^2} \, dt \qquad \text{(A1)}$$

where n_0 = 0.5 and B_* is a constant. ψ_* is the flow intensity given by:

$$\psi = g\left(\frac{\rho_s - \rho}{\rho}\right)\frac{d_{50}}{u_*^2} \qquad \text{(A2)}$$

Bedload transport q_{sb} is thus expressed in terms of a dimensionless sediment transport ϕ given by:

$$\phi = \frac{q_{sb}}{\rho_s}\left(\frac{\rho}{\rho_s - \rho} \cdot \frac{1}{g d_{50}^3}\right)^{\frac{1}{2}} \qquad \text{(A3)}$$

which is related to the probability of particle motion P by:

$$\frac{P}{1-P} = A_* \phi \qquad \text{(A4)}$$

where A_* is a constant. Thus the bedload transport may be expressed in terms of P and A_* as:

$$q_{sb} = \frac{P}{1-P} \cdot \frac{\rho_s}{A_*} \left(\frac{\rho_s - \rho}{\rho} \cdot g d_{50}^3 \right)^{\frac{1}{2}} \qquad \text{(A5)}$$

Einstein obtained the constants A_* and B_* from flume data for median particle sizes(d_{50}) of 785 μm and 2865 μm. These are considerably coarser than the sand-size material examined in this study (d_{50} of order 150-200 μm). Gadd et al (1978) found that Einstein's values of A_* = 43.5 and B_* = 0.143 gave unrealistic transport rates when compared with Guy et al's (1966) flume data for median grain sizes of 190 μm and 450 μm. Recalibration of Einstein's equation against Guy et al's flume data gave values of A_* = 60.0 and B_* = 0.07 which Gadd et al then took as being representative of the sediment sizes (110-560 μm) in their study area (the New York shelf).

To calculate q_{sb} from (A5) it is necessary to evaluate the integral in (A1). This was done using a rational approximation (see Abramowitz and Stegun, 1965).

2.

Bagnold's (1963) bedload equation. Bagnold's original equation expresses the bedload transport rate in terms of the stream power ω and an efficiency factor K . That is:

$$q_{sb} = \frac{\rho_s}{(\rho_s - \rho) g} \cdot K\omega \qquad \text{(A6)}$$

The power per unit area, ω , expended on the sea-bed by the fluid can be expressed as $\omega = \tau u_*$, or written as $\omega = \rho u_*^3$, because $\tau = \rho u_*^2$. K was originally thought to depend only on sediment characteristics

(see Bagnold, 1963). However, it has subsequently been shown (Kachel and Sternberg, 1971) that K depends not only on grain size but also on the excess shear stress $(\tau - \tau_{CR})/\tau_{CR}$, where τ_{CR} is the threshold shear stress, ie, that stress at which initial motion occurs. This dependence was removed by Gadd et al (1978), who, using Guy et al's (1966) flume data, expressed eq A6 in terms of the near-bed current (u_{100}) and a threshold velocity (u_{CR}) so obtaining:

$$q_{sb} = \beta (u_{100} - u_{CR})^3 \qquad \text{(A7)}$$

where β is a coefficient of proportionality obtained from the flume data. It is worth noting that Bagnold's original eq A6 contains no threshold condition and predicts sediment motion at all flow speeds. From a physical point of view this must be regarded as something of a shortcoming, and the formulation proposed by Gadd et al goes some way towards overcoming this difficulty. The value of β was obtained from Guy et al's flume data which gave $\beta = 7.22 \cdot 10^{-5}$ g cm^{-4} s^2 for $d_{50} = 190$ μm, and $\beta = 1.73 \cdot 10^{-5}$ g cm^{-4} s^2 for $d_{50} = 450$ μm. In the present study the value of β corresponding to $d_{50} = 190$ μm is assumed to be most representative of the sediments and the tracer particle-size range.

3.

Yalin's (1963) bedload equation. Yalin's equation is one of the simplest to apply, and considers the average lift forces exerted on a sediment particle. In Yalin's theory particles are assumed to move over the bed by saltation and any increase in transport is brought about by an increase in the particle path length and not necessarily an increase in the number of particles. The existence of a critical shear stress is assumed. Yalin thus obtained a bedload transport rate q_{sb} given by:

$$q_{sb} = 0.635 \rho_s d_{50} u_* s \left[1 - \frac{1}{a s} \ln (1 + a s)\right] \qquad \text{(A8)}$$

where

$$a = 2.45\left(\frac{\rho}{\rho_s}\right)^{0.4}\left(\frac{\tau_{cr}}{[\rho_s - \rho]\, g\, d_{50}}\right)^{\frac{1}{2}} \qquad \text{(A9)}$$

is a constant for given values of d_{50} and τ_{cr} and S is the non-dimensional excess shear stress given by: $S = (\tau - \tau_{cr})/\tau_{cr}$. Gadd et al (1978) found that Yalin's eq A8 for a grain size (d_{50}) of 450 μm gave good agreement with Guy et al's flume data for grain sizes of 190 and 450 μm at velocities near threshold. For higher velocities the predicted values are less than those obtained in the flume experiments. However, despite these differences, the empirically determined constants are used as they appear in eqs A8 and A9. Strictly speaking, Yalin's equation is restricted to plane beds, to fully developed flows, and to large flow-depth/particle-diameter ratios.

4.

Ackers and White's (1973) total load equation. It is beyond the scope of this report to review in full the derivation of Ackers and White's equation. Full details of the theory and calibration techniques can be found elsewhere, eg, Ackers (1972), White (1972), Ackers and White (1973), White et al (1975, 1978). The general function of Ackers and White is based on the physics of the stream power concept and dimensional considerations, and is expressed in terms of three dimensionless groups as follows:

$$G_{gr} = C\left\{\frac{F_{gr}}{A} - 1\right\}^{m} \qquad \text{(A10)}$$

where G_{gr} is the dimensionless sediment transport given by:

$$G_{gr} = \frac{c\rho h}{\rho_s d_{35}}\left(\frac{u_*}{\hat{u}}\right)^{n} \qquad \text{(A11)}$$

Here C is the concentration by weight of sediment which is related to the total load transport rate q_{st} by $q_{st} = c\rho\hat{u}/g$. F_{gr} is a dimensionless mobility number given by:

$$F_{gr} = \frac{u_*^{\,n}}{\left(g d_{35}\left[\frac{\rho_s}{\rho} - 1\right]\right)^{\frac{1}{2}}} \left(\frac{\hat{u}}{2.46\, h\left[10h/d_{35}\right]}\right)^{1-n} \qquad \text{(A12)}$$

The coefficients A, C, m, and n are given in terms of a dimensionless grain size:

$$D_{gr} = d_{35}\left\{\frac{g\left(\frac{\rho_s}{\rho} - 1\right)}{\nu^2}\right\}^{\frac{1}{3}} \qquad \text{(A13)}$$

For coarse sediments the coefficients take values $A = 0.17$, $C = 0.025$, $m = 1.50$ and $n = 0.0$. For intermediate fine sediments $A = (0.23/D_{gr}) + 0.14$, $\log C = 2.86 \log D_{gr} - (\log D_{gr})^2 - 3.53$, and h tends to unity.

Important points to note about Ackers and White's equation are:

(a) although it was calibrated against 1000 flume experiments, these were mostly in flow depths less than 0.4 m;

(b) the equation may be applied to particle sizes in the range 40-4000 μm;

(c) correlations with observed transport rates have shown that the transport of fine sediment is best related to gross shear (friction velocity, u_*, being the representative variable) and that transport of coarse material is best related to net shear (depth-mean flow, $\hat{u}$ being the representative variable);

(d) the equation is based upon experiments in which there was established sediment motion and the equations forecast initial movement conditions which gave reasonable agreement with previous threshold studies;

(e) the equation is not sensitive to bed form and may be applied to plain rippled and duned configurations for Froude numbers $F_r \leqslant 0.8$;

(f) the equation incorporates a transition exponent n which affects the change from friction velocity (u_*) to depth mean flow through intermediate particle sizes.

5.

Engelund and Hansen's (1967) total load equation. Engelund and Hansen's equation expresses the total load q_{st} in terms of a friction factor C_f a dimensionless sediment discharge ϕ, and a dimensionless bed shear stress θ. Thus:

$$C_f \phi = 0.1 \theta^{\frac{5}{2}} \tag{A14}$$

where:

$$C_f = 2u_*^2 / \hat{u}^2 \tag{A15}$$

$$\phi = q_{st} / \rho_s \left(g \left[\frac{\rho_s}{\rho} - 1 \right] d_{50}^3 \right)^{\frac{1}{2}} \tag{A16}$$

and:

$$\theta = \tau / (\rho_s - \rho) g d_{50} \tag{A17}$$

Substituting for C_f, ϕ, and θ in equation (A14) gives:

$$q_{st} = 0.05 \rho_s \hat{u}^2 \left(\frac{d_{50}}{g \left[\frac{\rho_s}{\rho} - 1 \right]} \right)^{\frac{1}{2}} \left(\frac{\tau}{[\rho_s - \rho] d_{50}} \right)^{\frac{3}{2}} \tag{A18}$$

Eq A18 is apparently only valid for dune-covered beds in which the boundary Reynolds number $u_* d_{50} / \nu > 12$ and $d_{50} > 150$ μm (see Raudkivi, 1976).

APPENDIX B

Smoothed progressive vector diagrams for residual sediment movements in the Sizewell-Dunwich area. Sediment transport rates have been calculated using Yalin's (1963) formula (see Appendix A).

Notes: (1) The header code on each progressive vector diagram indicates the following:

eg	Meter 238	:	Current meter number
	Date 30.8.76	:	Date record starts
	SWD	:	Area (Sizewell-Dunwich)
	STN A	:	Station
	HT 6M	:	Height above seabed
	Y SED	:	Sediment transport formula used in calculations
	TRANS GM/CM*10**5:		Scale x 10^5 gives transport in g cm^{-1}.

(2) The scales of the progressive vector plots are not the same.

(3) Origin represents day record starts. Small crosses indicate midday GMT each day, with a large cross every tenth day.

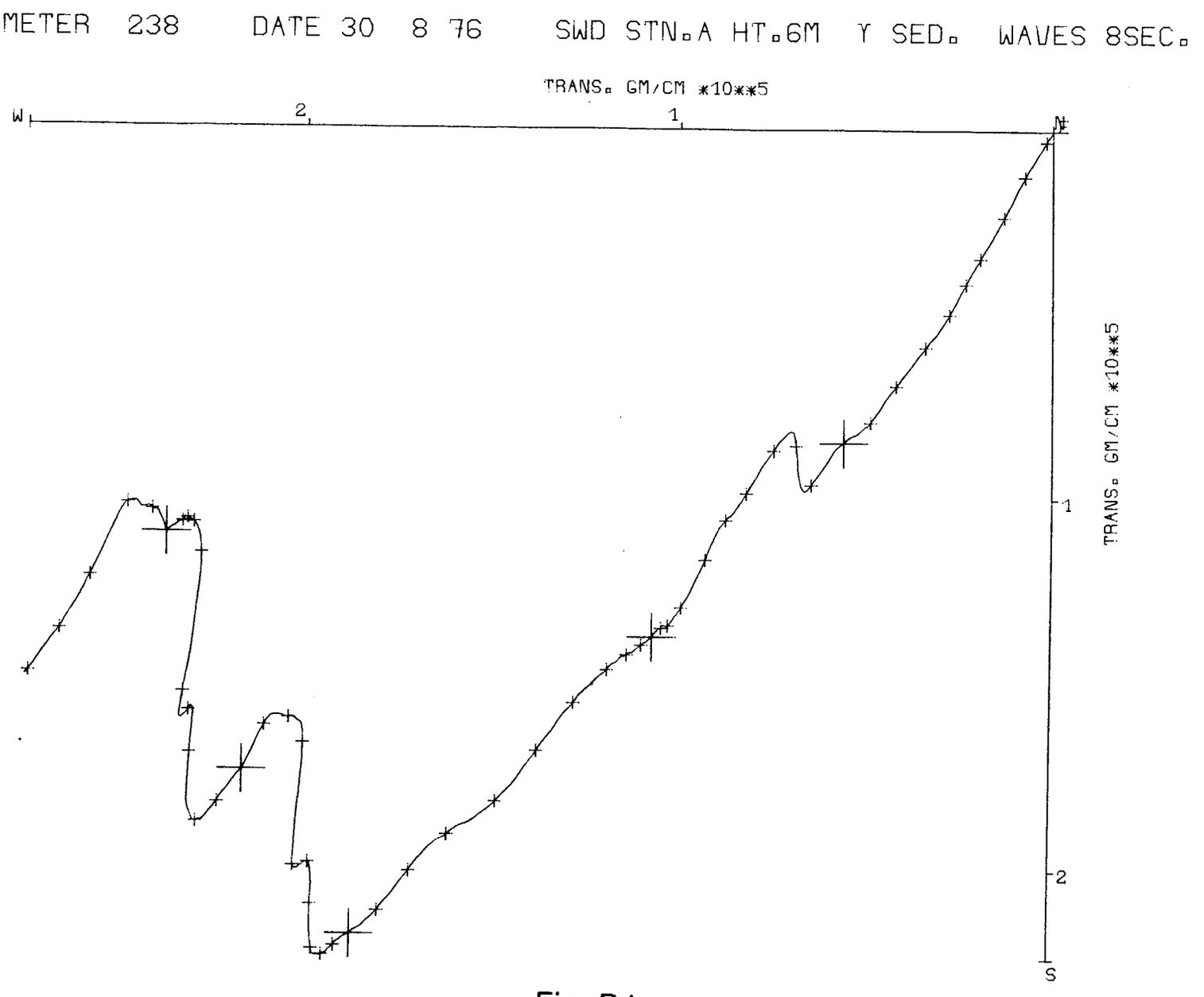
METER 238 DATE 30 8 76 SWD STN. A HT. 6M T SED. WAVES 8SEC.
TRANS. GM/CM *10**5
W
2
1
N
1
2
S
TRANS. GM/CM *10**5

Fig. B1

METER 232 DATE 29 10 76 SWD STN.A HT.6M Y SED. WAVES 8SEC.

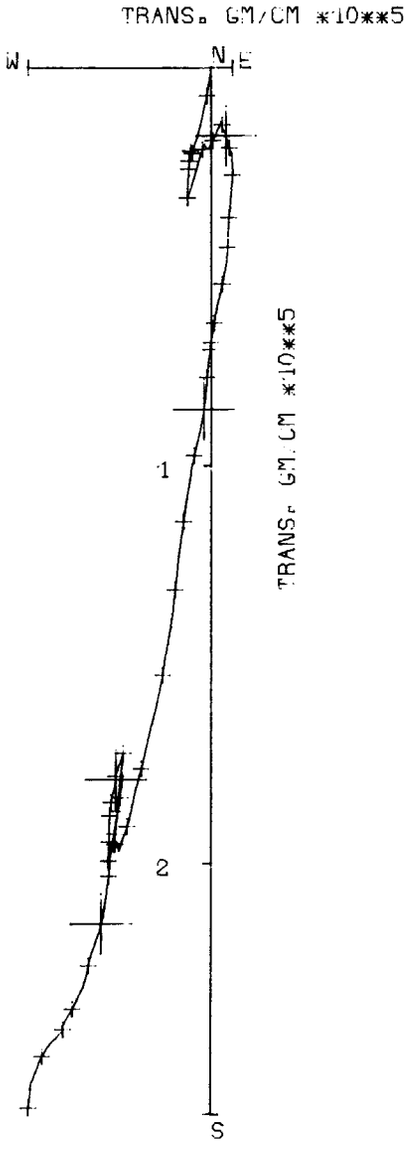

Fig. B2

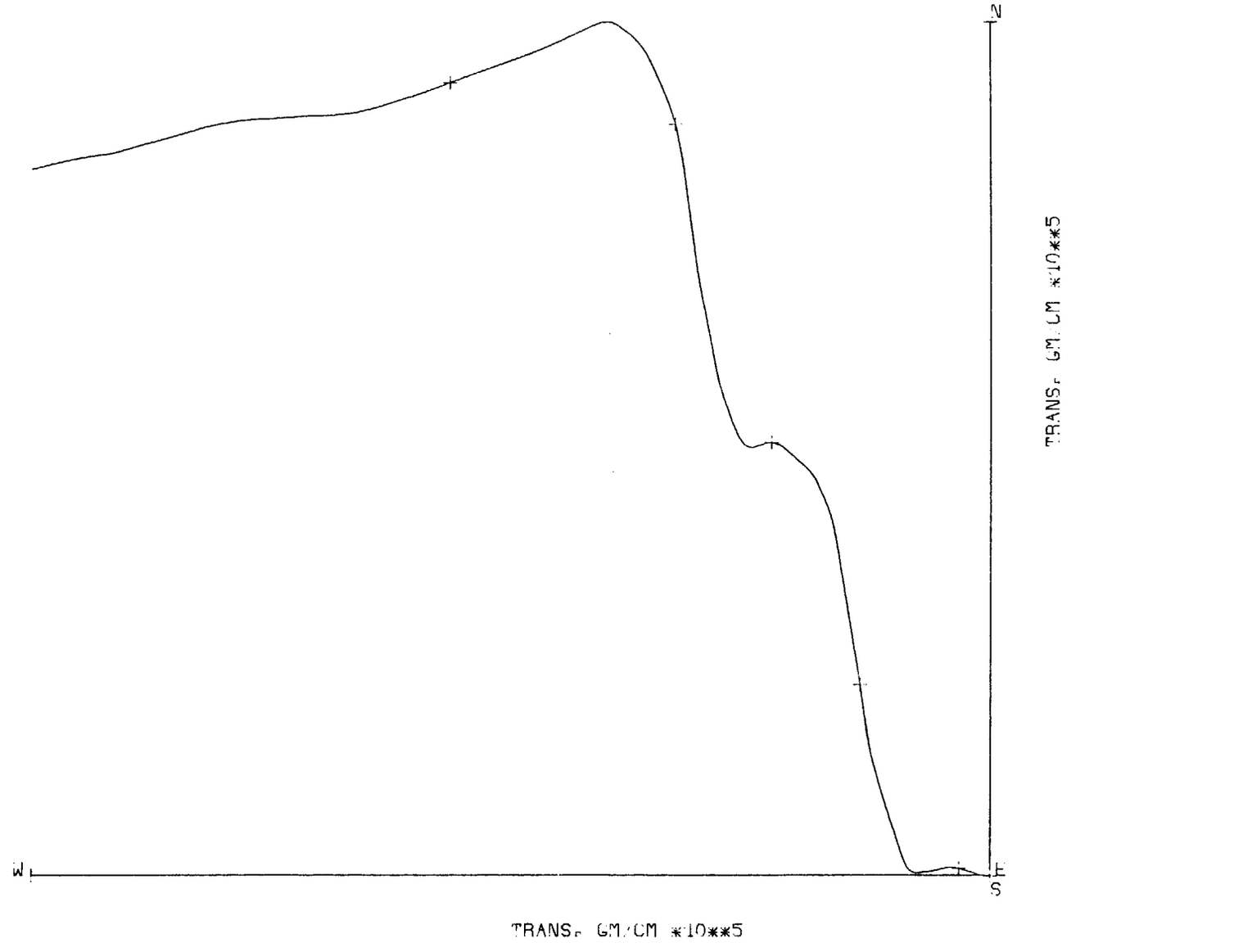
METER 238 DATE 12 1 77 SWD STN. A HT. 6M Y SED. WAVES 8SEC.
N
S
W
TRANS. GM/CM *10**5
TRANS. GM/CM *10**5

Fig. B3

METER 260 DATE 13 5 77 SWD STN. A HT. GM Y SED. WAVES 8SEC.

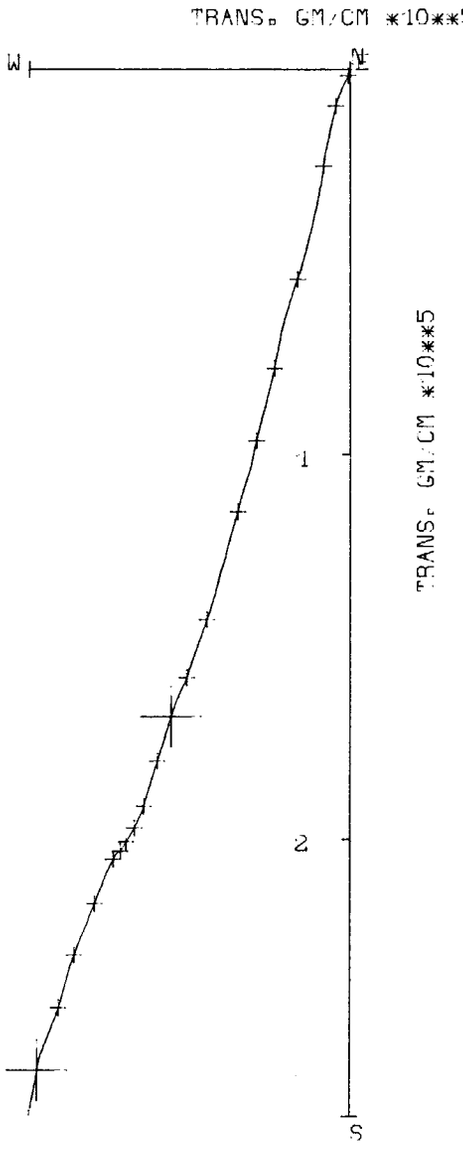

Fig. B4

METER 238 DATE 18 7 77 SWD STN.A HT.6M Y SED. WAVES 8SEC.

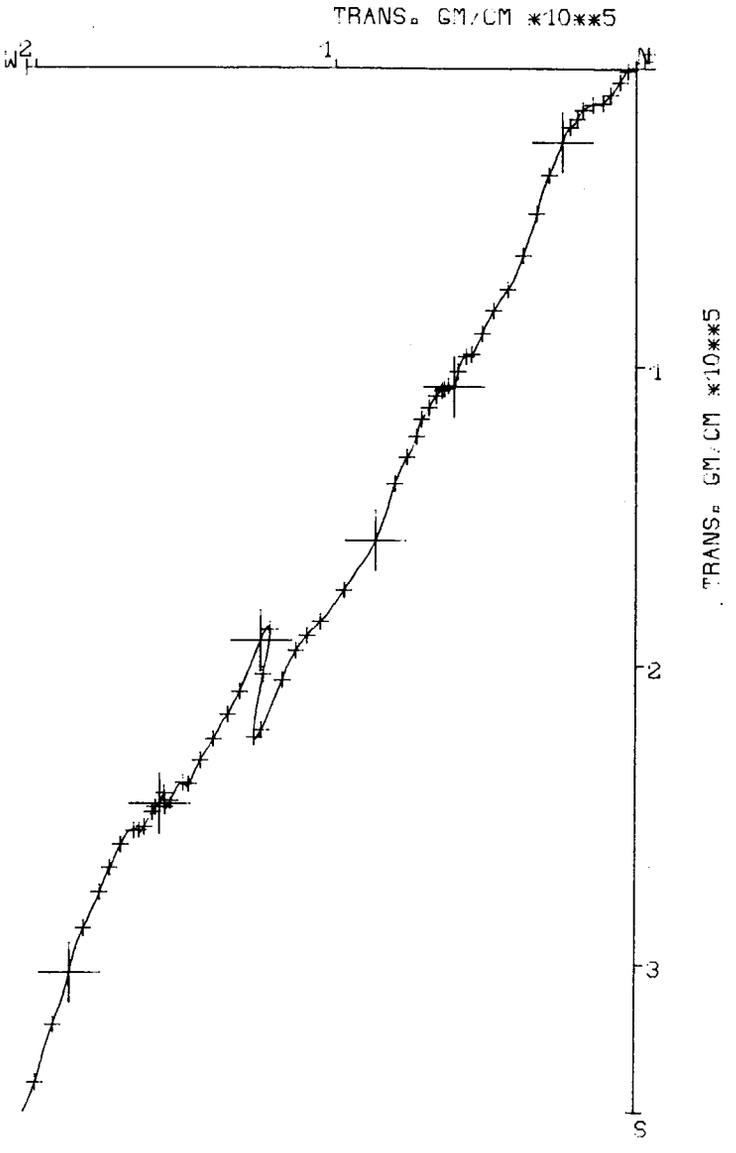

Fig. B5

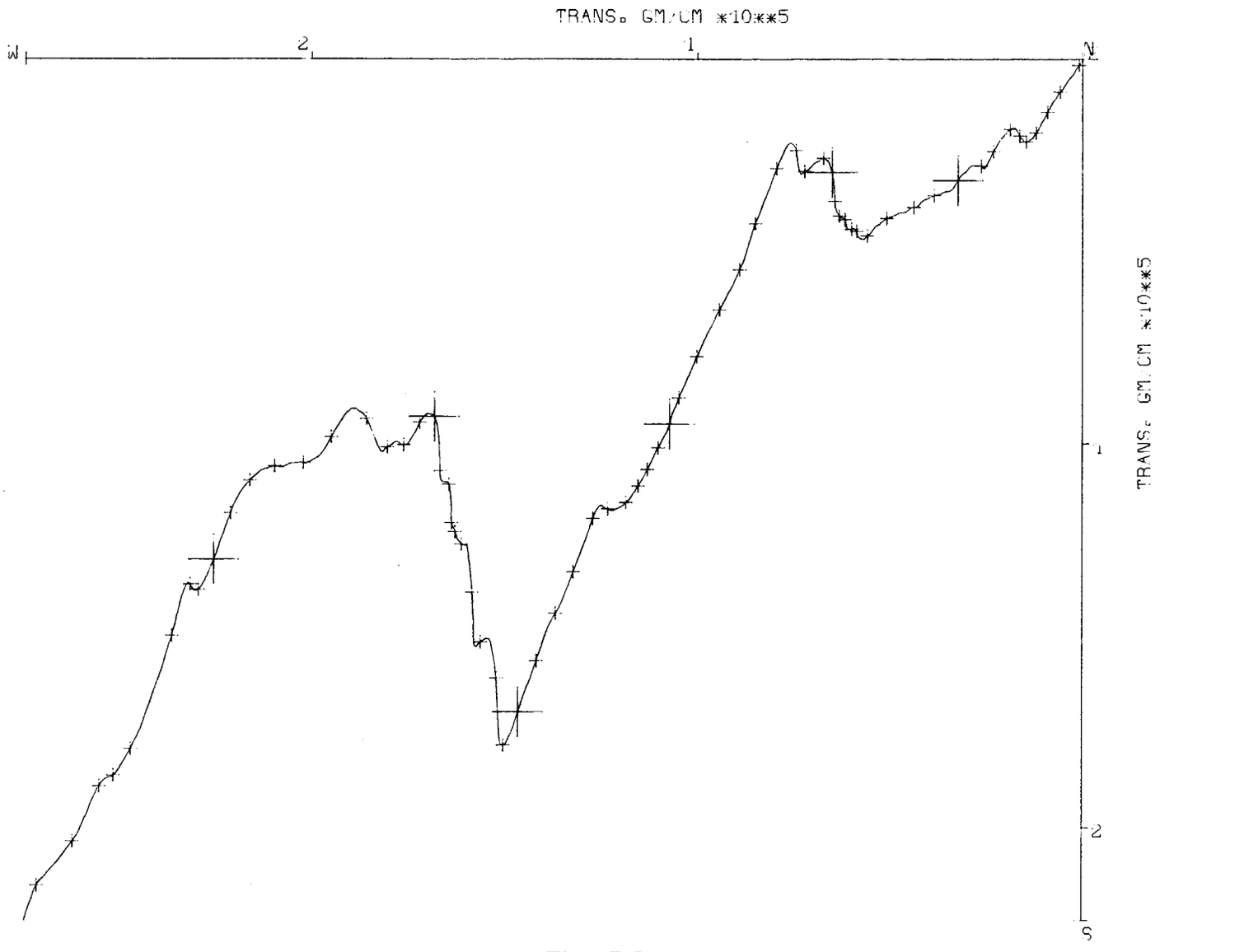
METER 629 DATE 19 9 77 SWD STN. A HT. GM Y SED. WAVES 8SEC.
TRANS. GM/CM *10**5
W
2
1
N
TRANS. GM/CM *10**5
1
2
S

Fig. B6

METER 534 DATE 10 4 78 SWD STN. A HT. 6M Y SED. WAVES 8SEC.

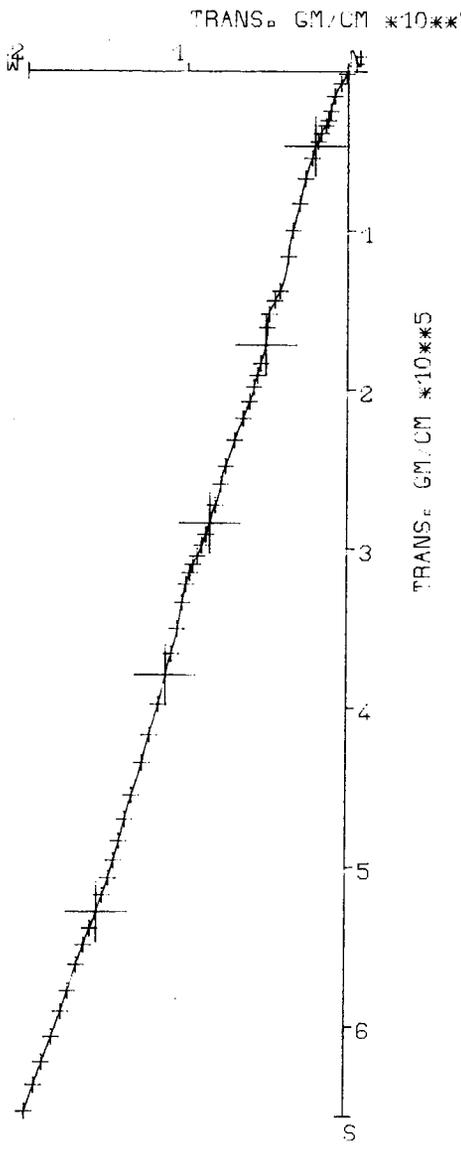

Fig. B7

METER 560 DATE 16 6 78 SWD STN.A HT.GM Y SED. WAVES 8SEC.

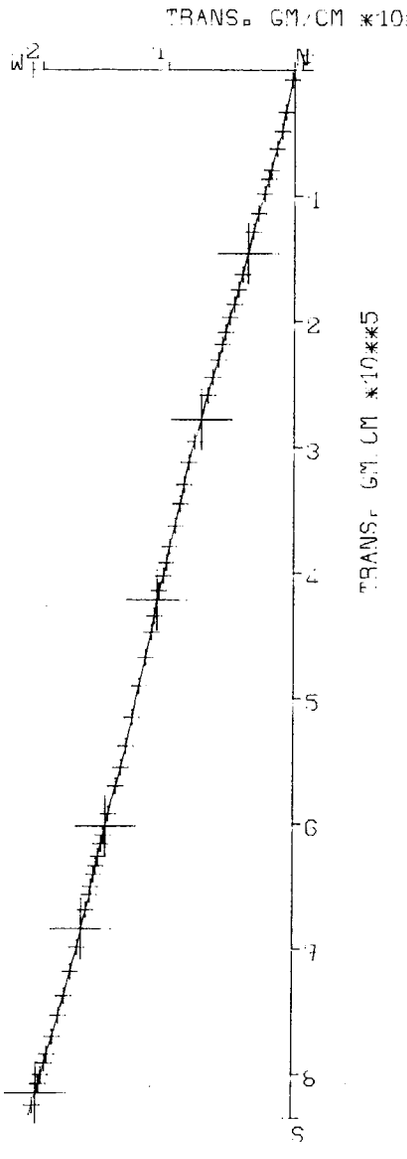

Fig. B8

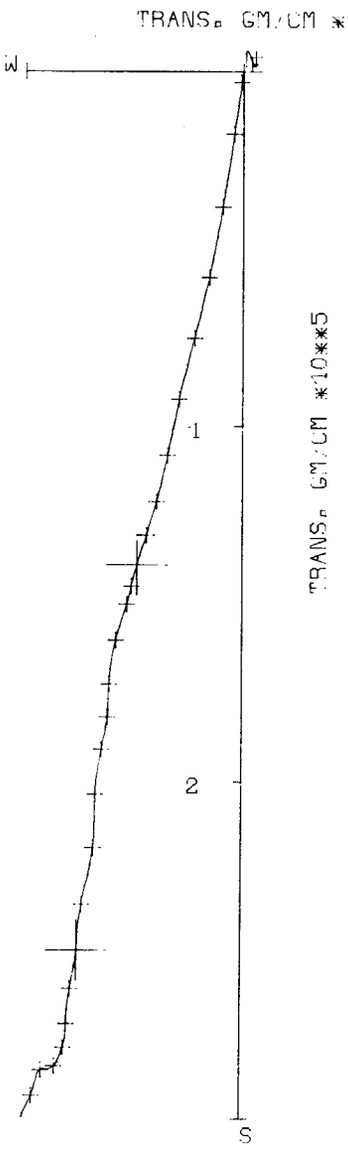
METER 260 DATE 17 8 78 SWD STN. A- HT. 6M Y SED. WAVES 8SEC.
TRANS. GM/CM *10**5
W
N
1
2
S
TRANS. GM/CM *10**5

Fig. B9

METER 560 DATE 27 10 78 SWD STN.A HT.6M Y SED. WAVES 8SEC.

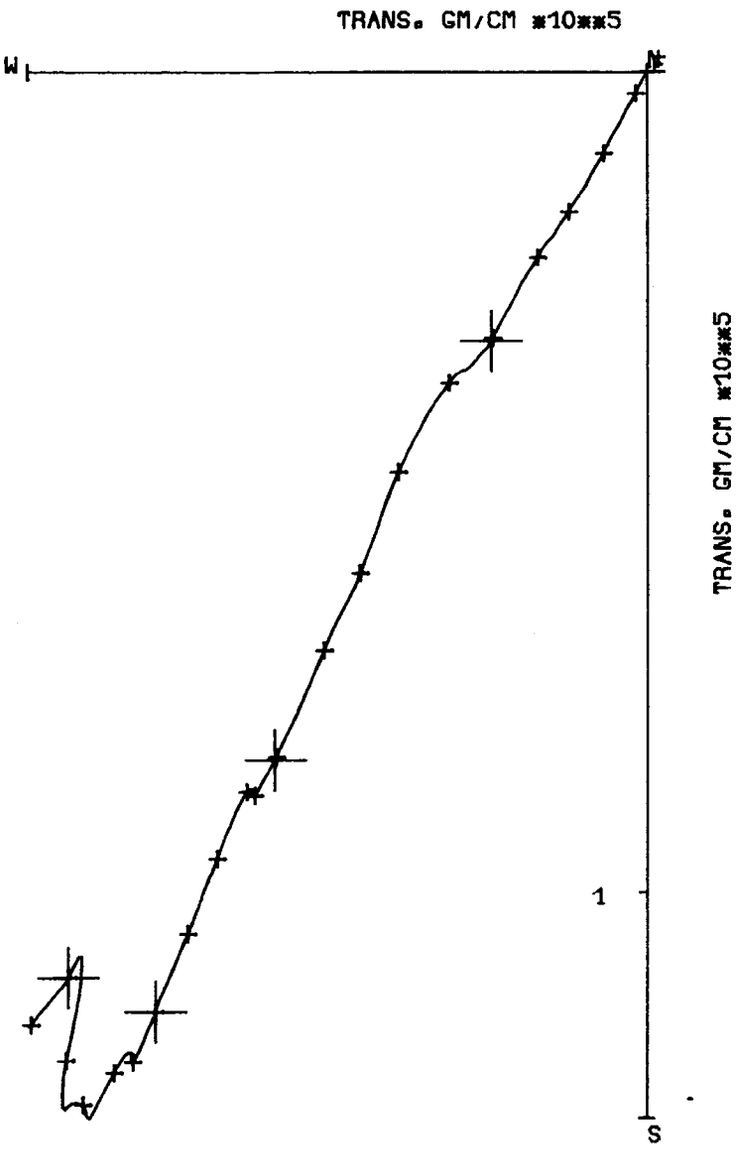

Fig. B10

METER 534 DATE 11 4 79 SWD STN.A HT.6M Y SED. WAVES 8SEC.

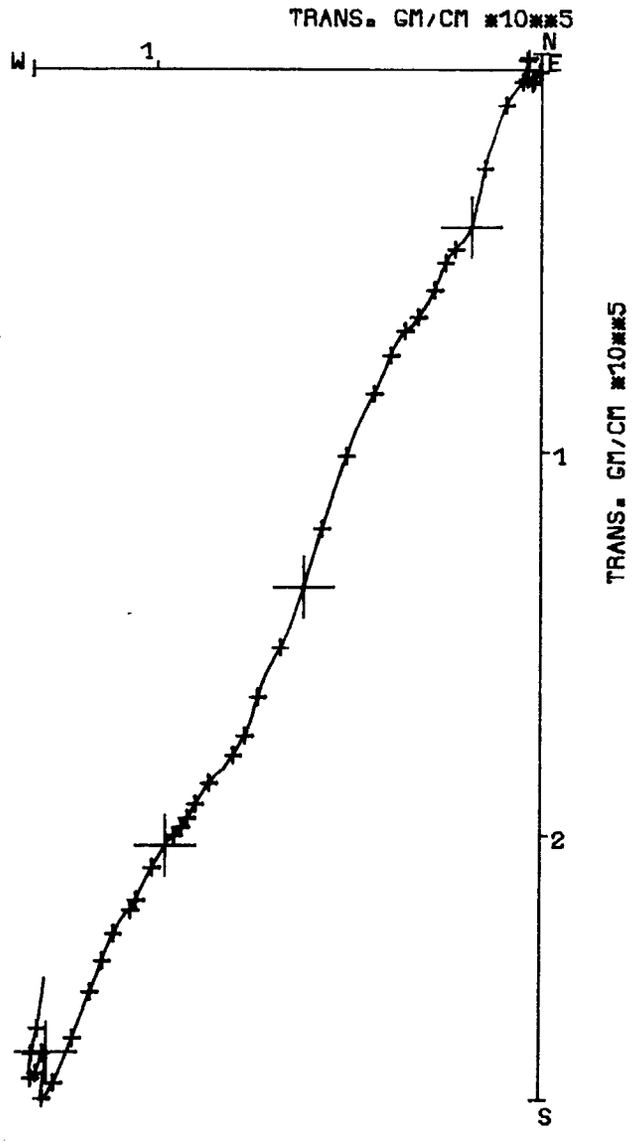

Fig. B11

METER 392 DATE 9 2 75 SWD STN.B HT.10M Y SED. WAVES 8SEC.

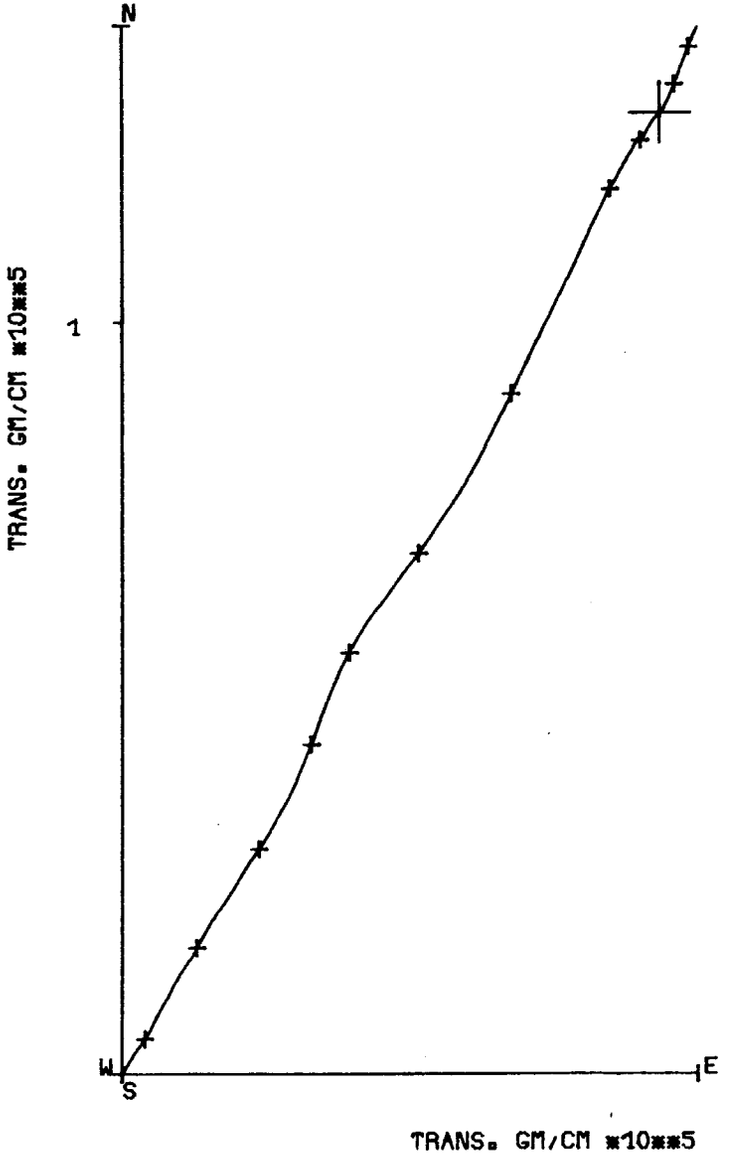

Fig. B12

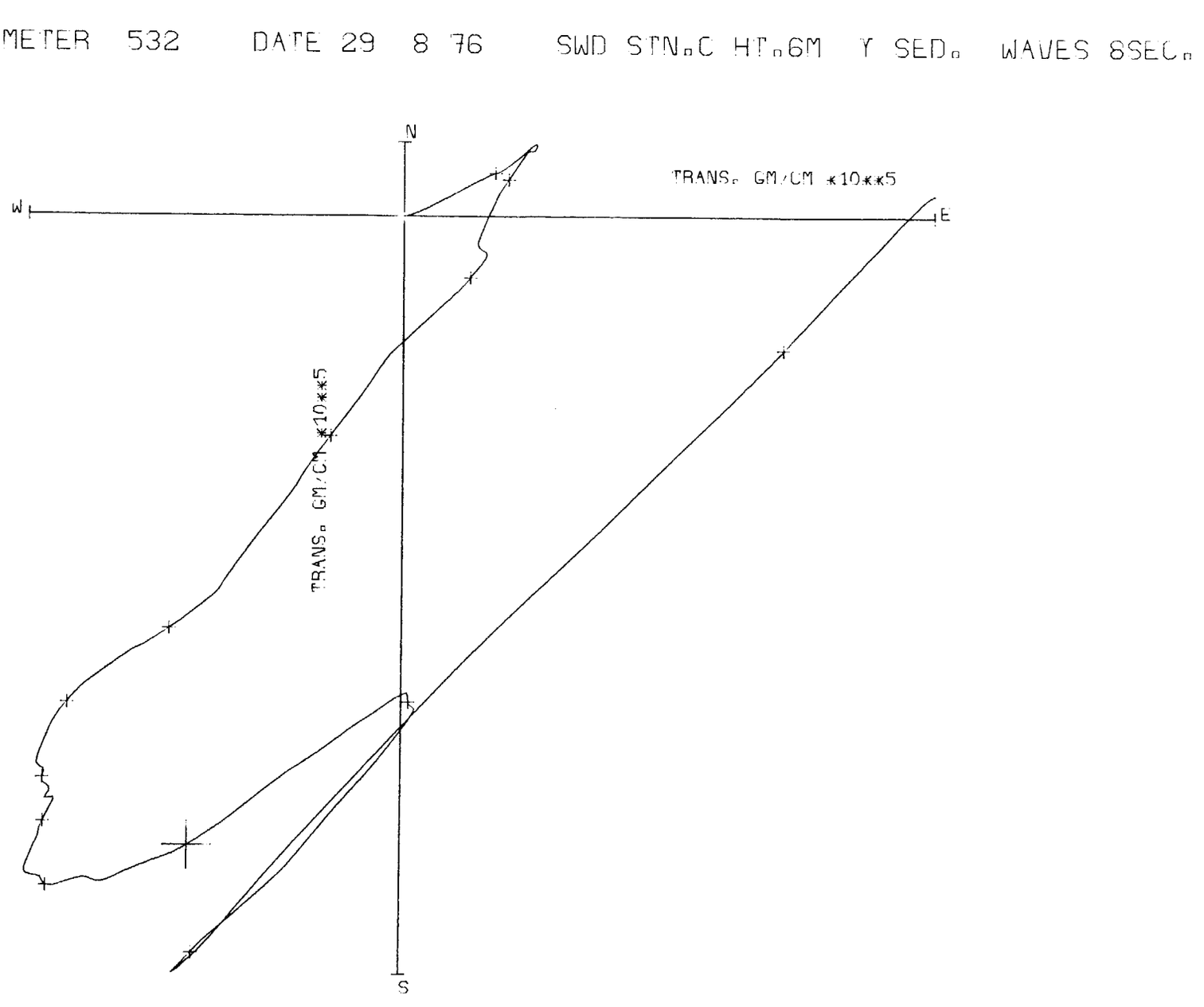
METER 532 DATE 29 8 76 SWD STN.C HT.6M Y SED. WAVES 8SEC.
N
W
E
S
TRANS. GM/CM *10**5
TRANS. GM/CM *10**5

Fig. B13

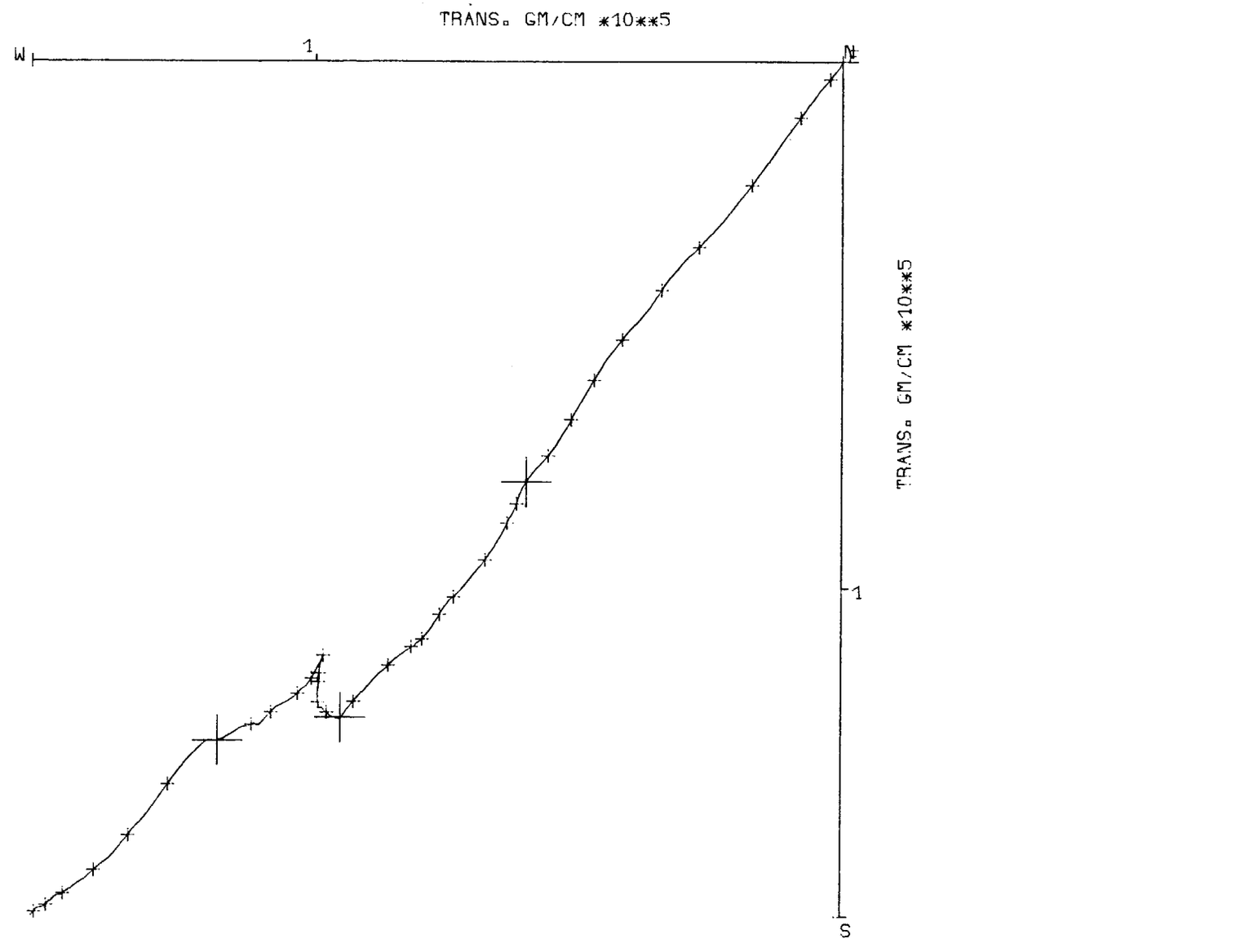
METER 669 DATE 17 8 78 SWD STN.D HT.6M Y SED. WAVES 8SEC.
TRANS. GM/CM *10**5
W
1
N
TRANS. GM/CM *10**5
1
S

Fig. B14

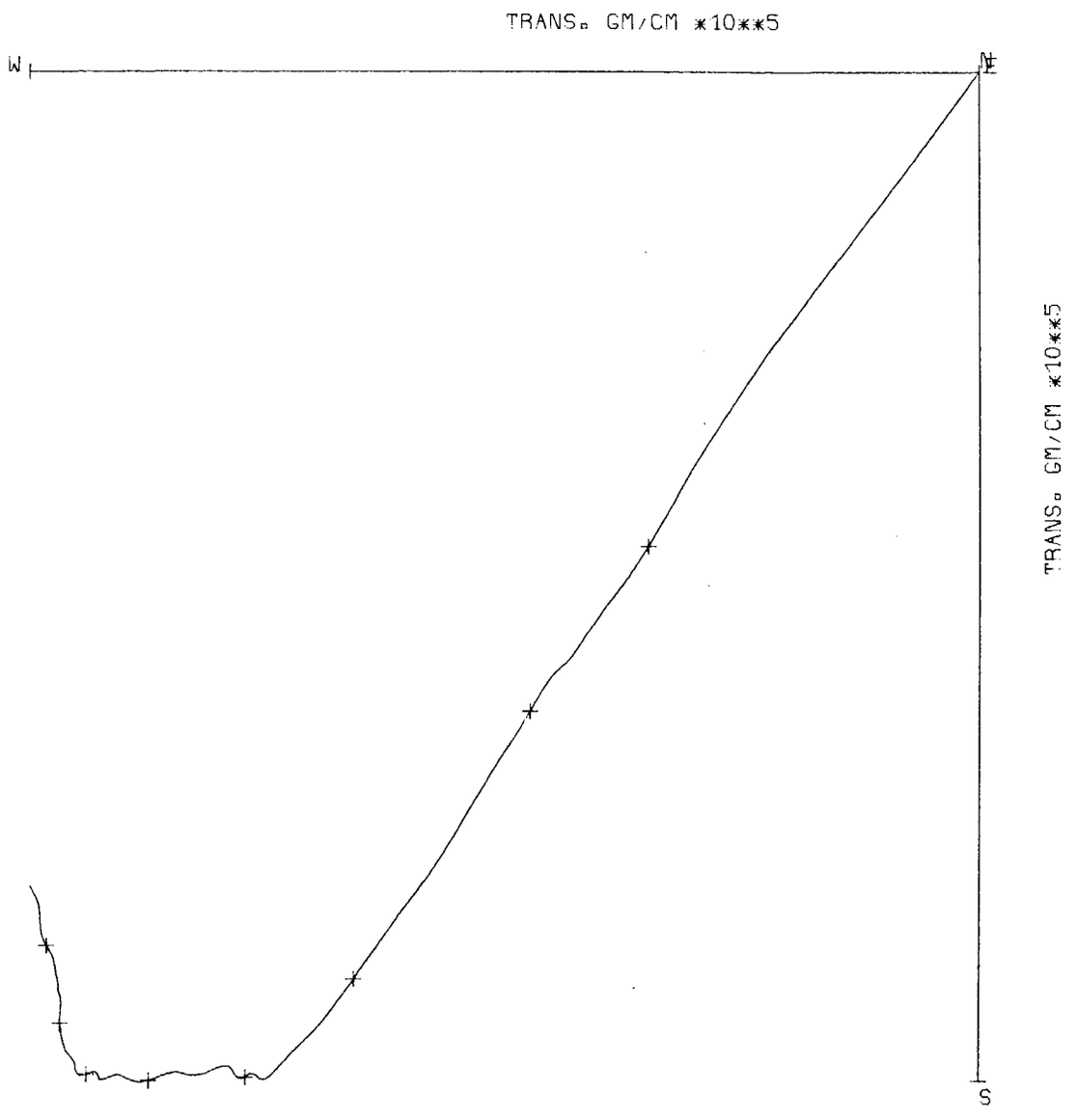
METER 669 DATE 1 10 78 SWD STN.D HT.6M Y SED. WAVES 8SEC.
TRANS. GM/CM *10**5
W
E
TRANS. GM/CM *10**5
S

Fig. B15

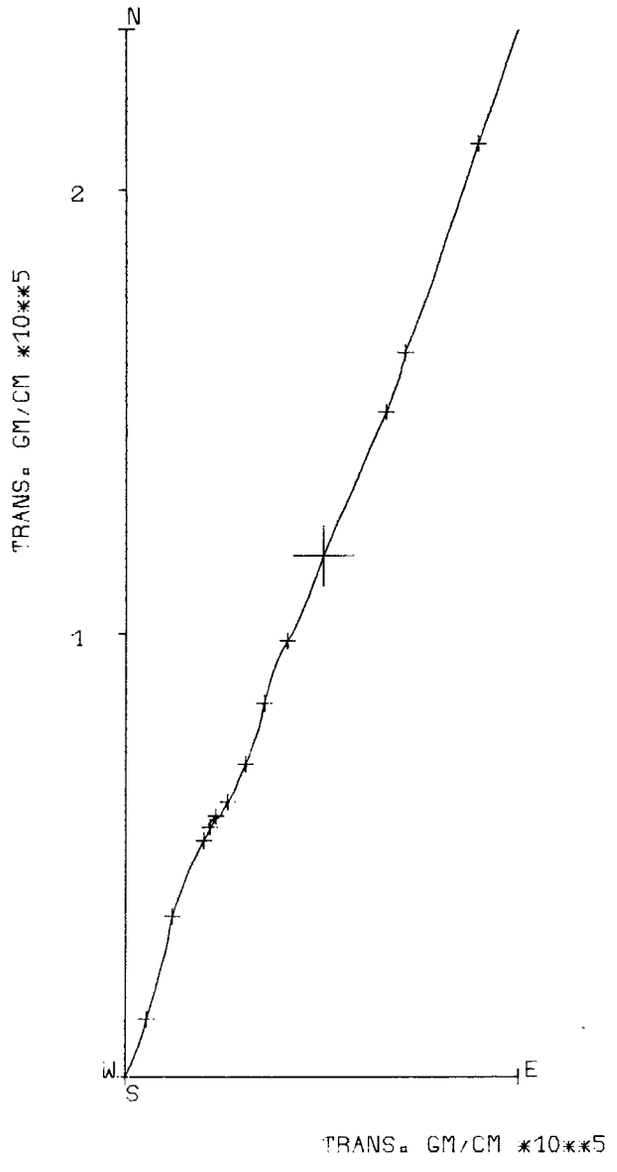
METER 667 DATE 29 8 76 SWD STN.E HT.7M Y SED. WAVES 8SEC.
N
2
1
W
S
E
TRANS. GM/CM *10**5
TRANS. GM/CM *10**5

Fig. B16

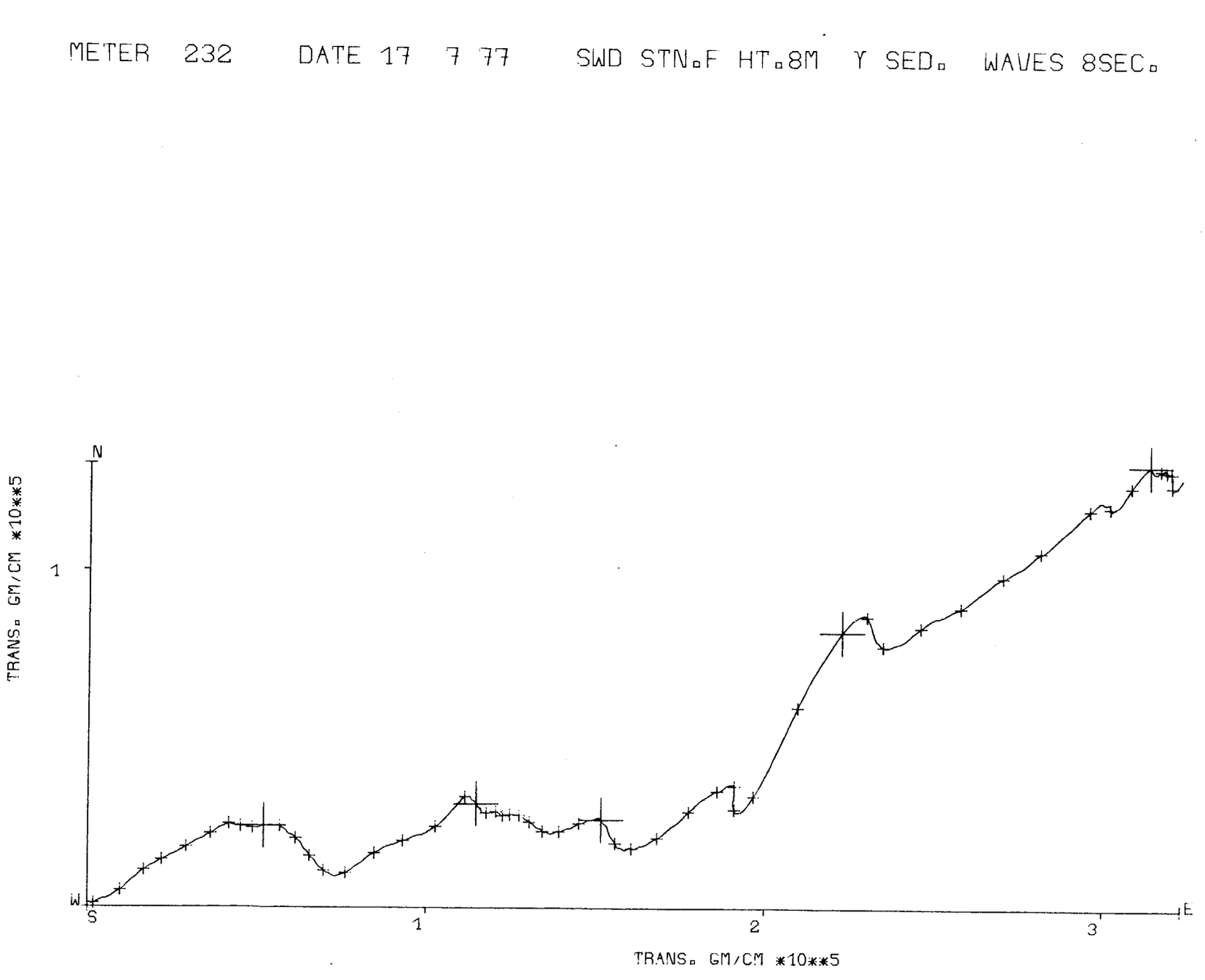
METER 232 DATE 17 7 77 SWD STN.F HT.8M Y SED. WAVES 8SEC.
N
W
S
E
1
1
2
3
TRANS. GM/CM *10**5
TRANS. GM/CM *10**5

Fig. B17

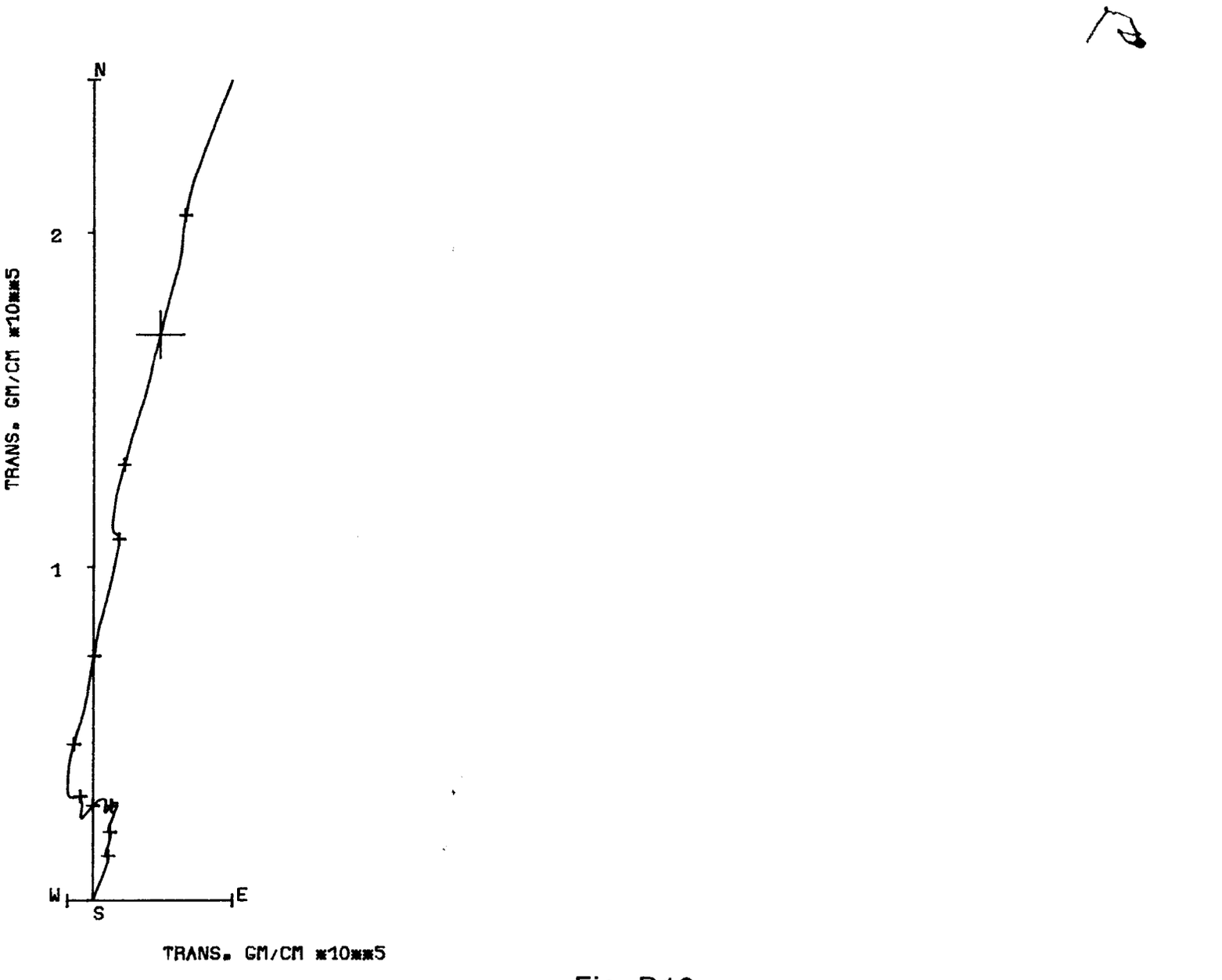
METER 534 DATE 19 4 75 SWD STN.G HT.6M T SED. WAVES 8SEC.
N
2
1
W
E
S
TRANS. GM/CM *10**5
TRANS. GM/CM *10**5

Fig. B18

METER 680 DATE 19 4 75 SWD STN.H HT.6M Y SED. WAVES 8SEC.

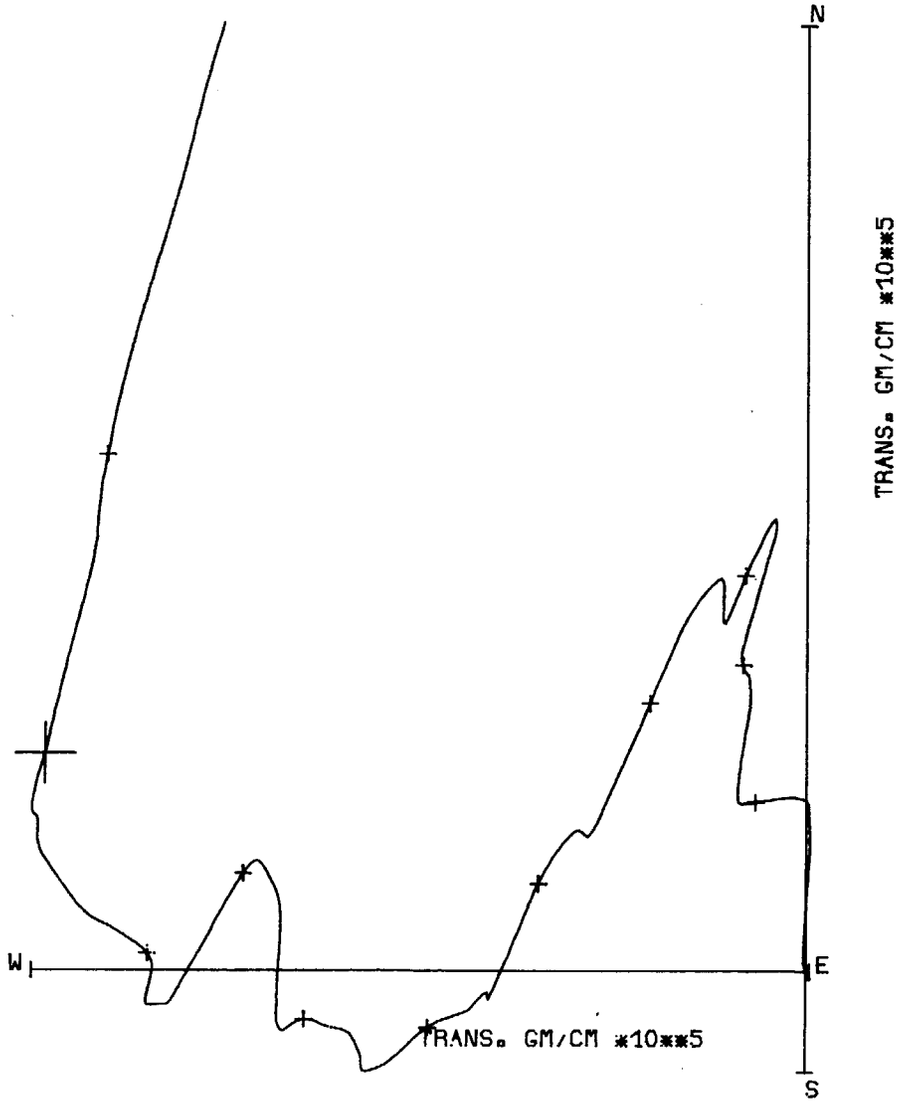

Fig. B19

METER 626 DATE 30 8 76 SWD STN.J HT.5M Y SED. WAVES 8SEC.

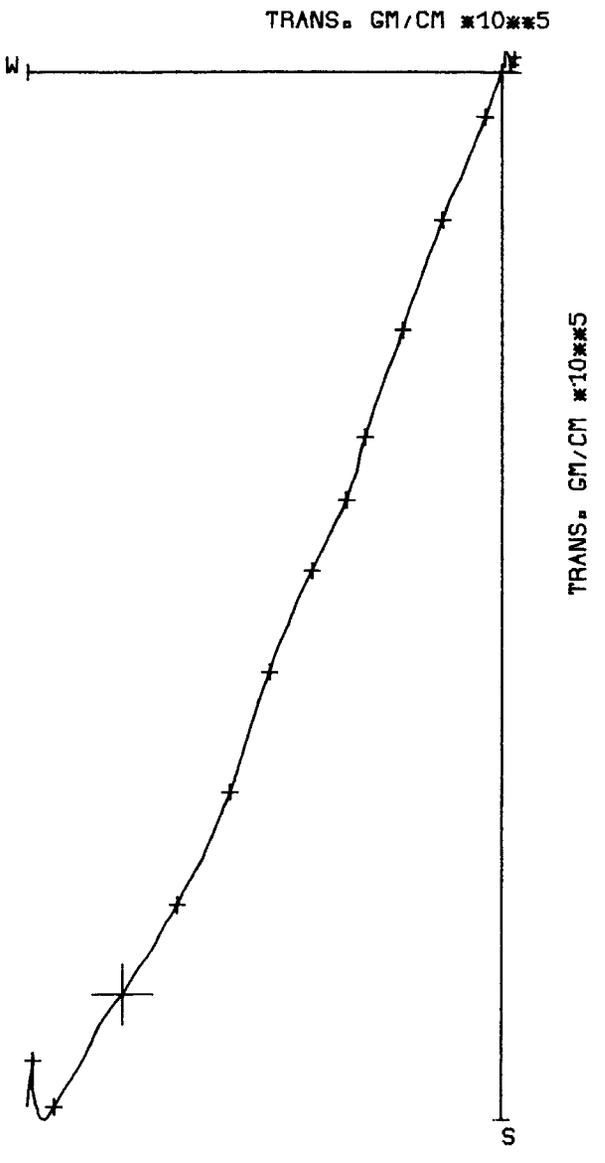

Fig. B20

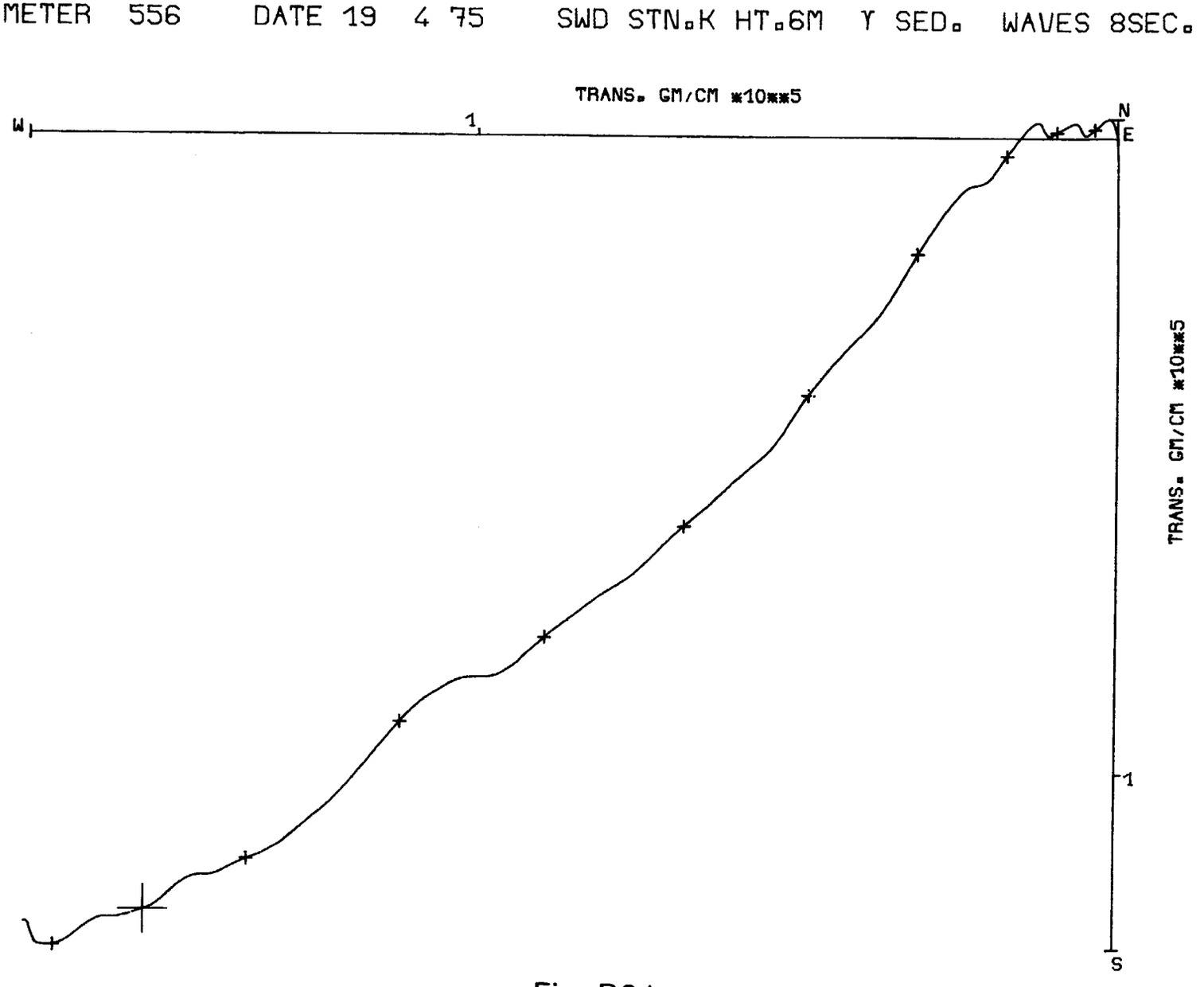
METER 556 DATE 19 4 75 SWD STN.K HT.6M T SED. WAVES 8SEC.
TRANS. GM/CM *10**5
W
1
N
E
1
S
TRANS. GM/CM *10**5

Fig. B21

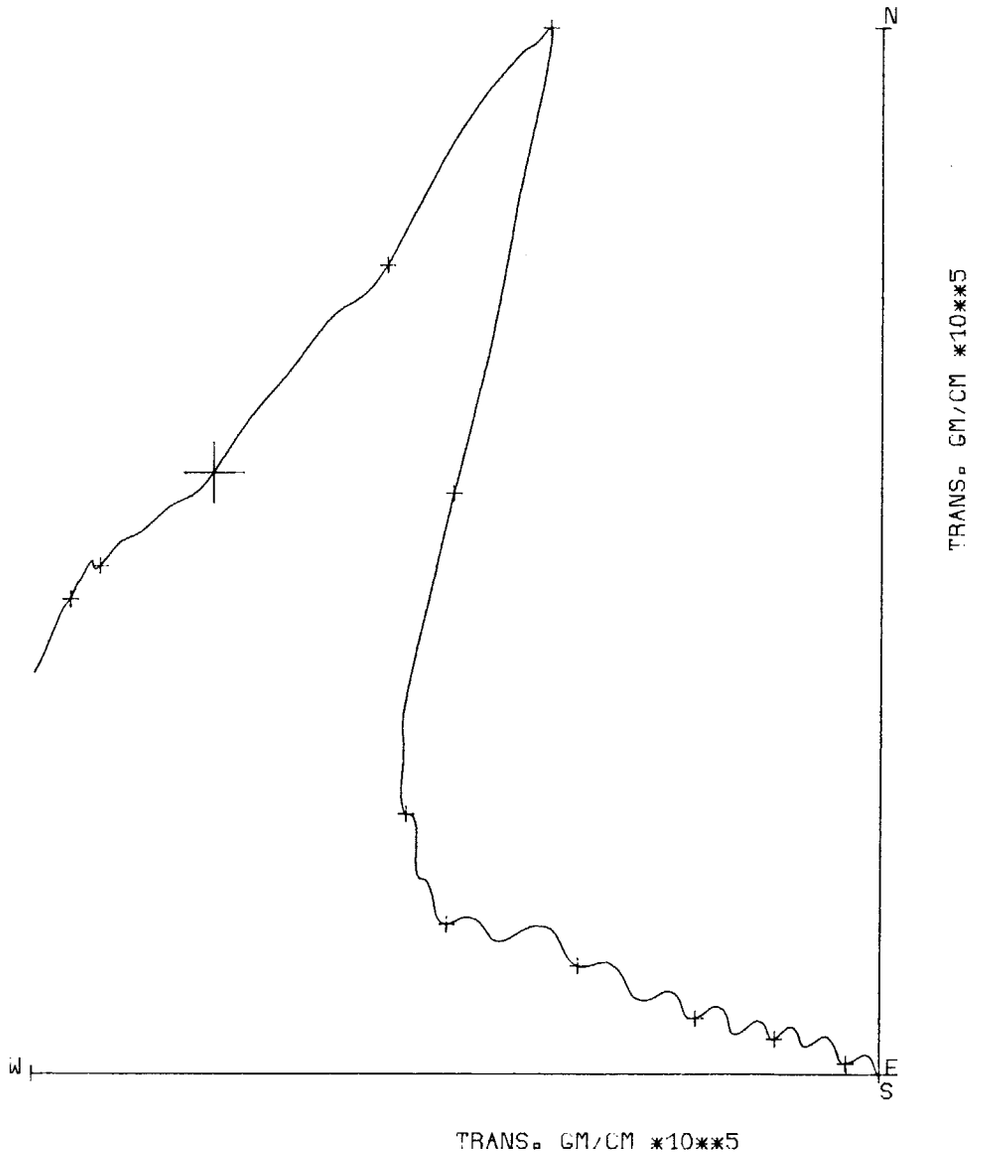
METER 295 DATE 9 2 75 SWD STN.L HT.10M Y SED. WAVES 8SEC.
N
W
E
S
TRANS. GM/CM *10**5
TRANS. GM/CM *10**5

Fig. B22

METER 267 DATE 30 8 76 SWD STN.M HT.6M Y SED. WAVES 8SEC.

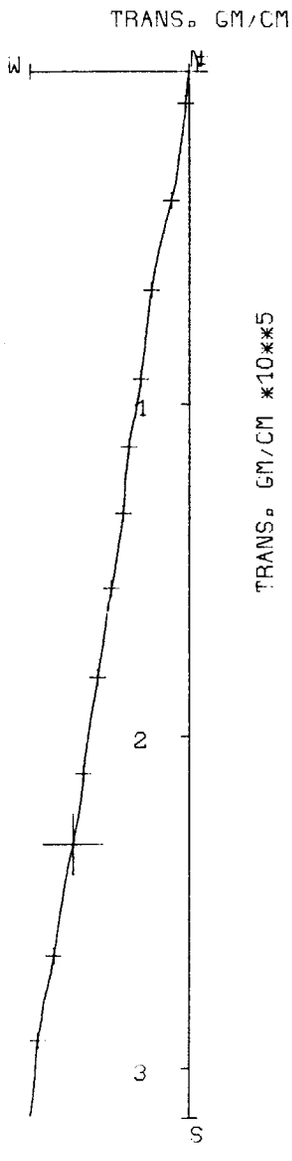

Fig. B23

METER 594 DATE 1 9 76 SWD STN. N HT. 3M Y SED. WAVES 8SEC.

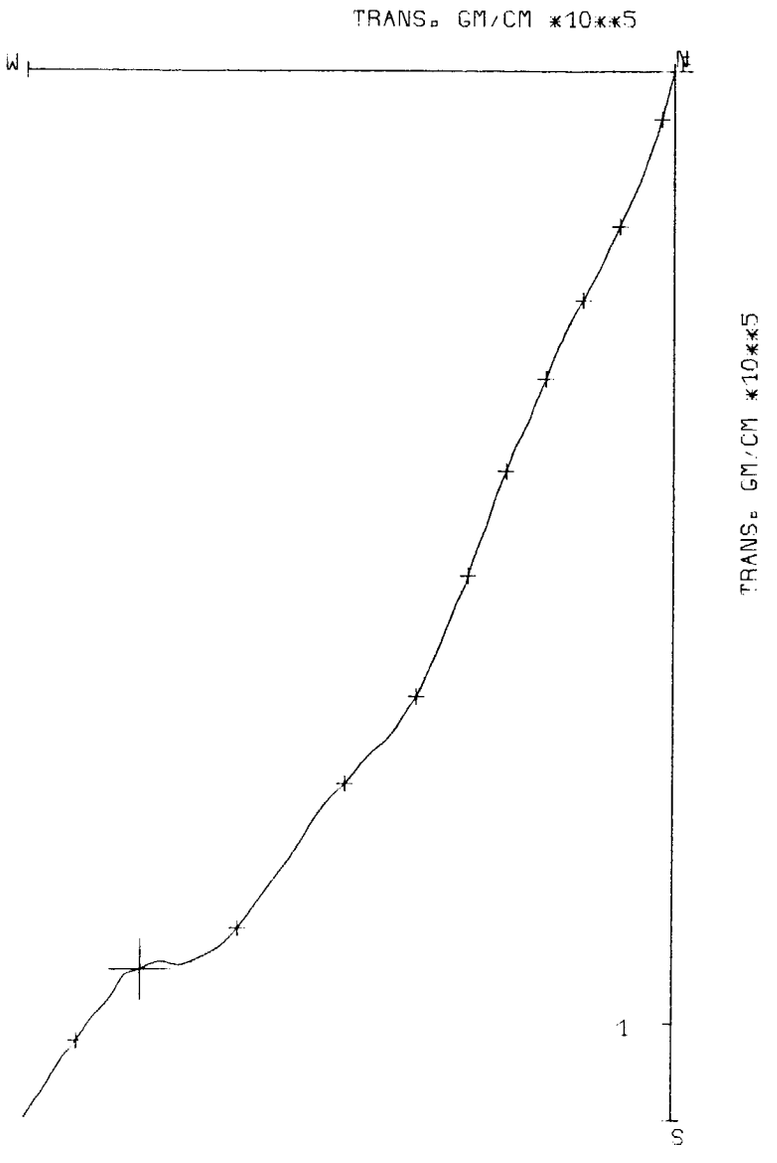

Fig. B24

METER 534 DATE 1 9 76 SWD STN.P HT.2M Y SED. WAVES 8SEC.

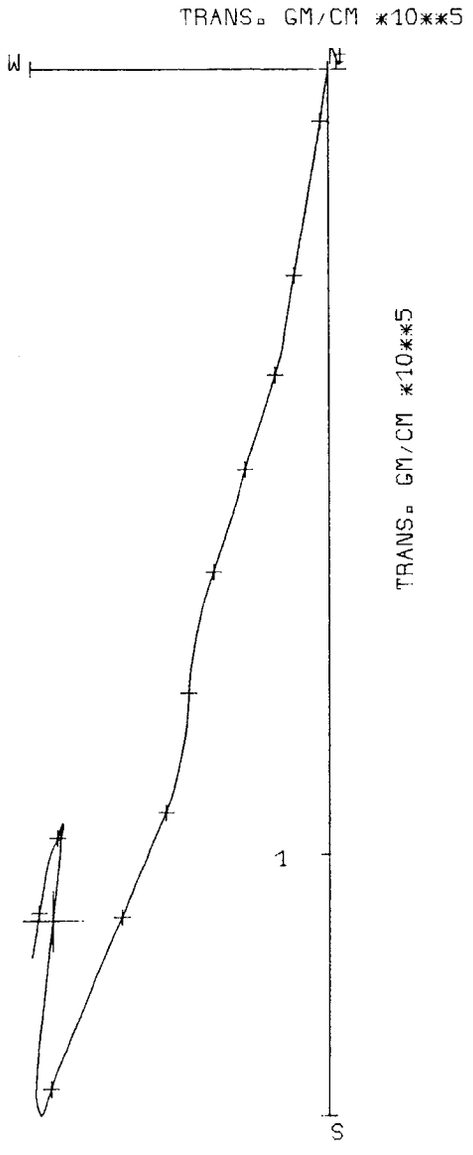

Fig. B25

METER 629 DATE 19 4 75 SWD STN.Q HT.6M Y SED. WAVES 8SEC.

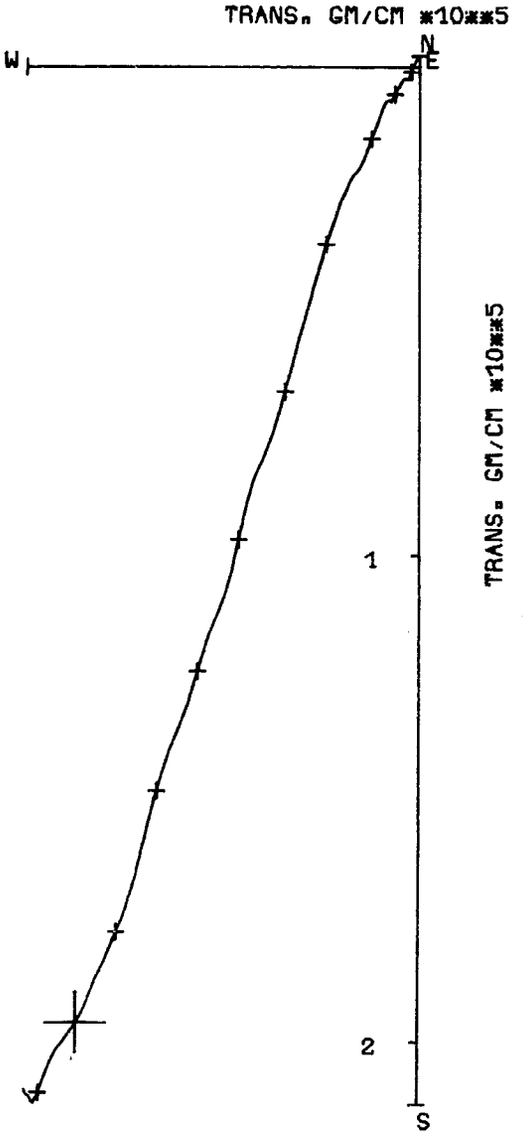

Fig. B26

METER 567 DATE 8 2 75 SWD STN.R HT.10M Y SED. WAVES 8SEC.

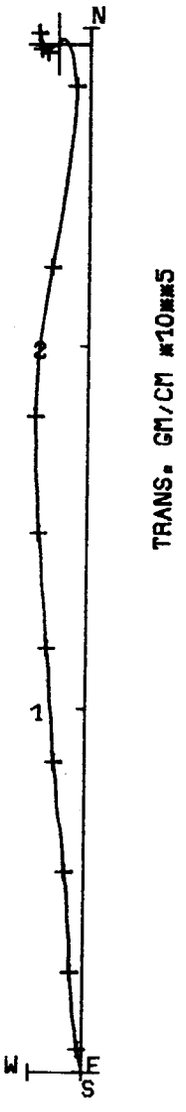

TRANS. GM/CM *10**5

Fig. B27

METER 232 DATE 30 8 76 SWD STN.S HT.5M Y SED. WAVES 8SEC.

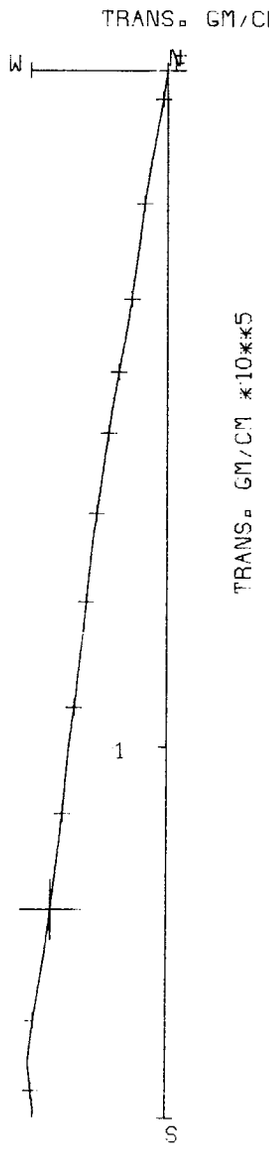

Fig. B28

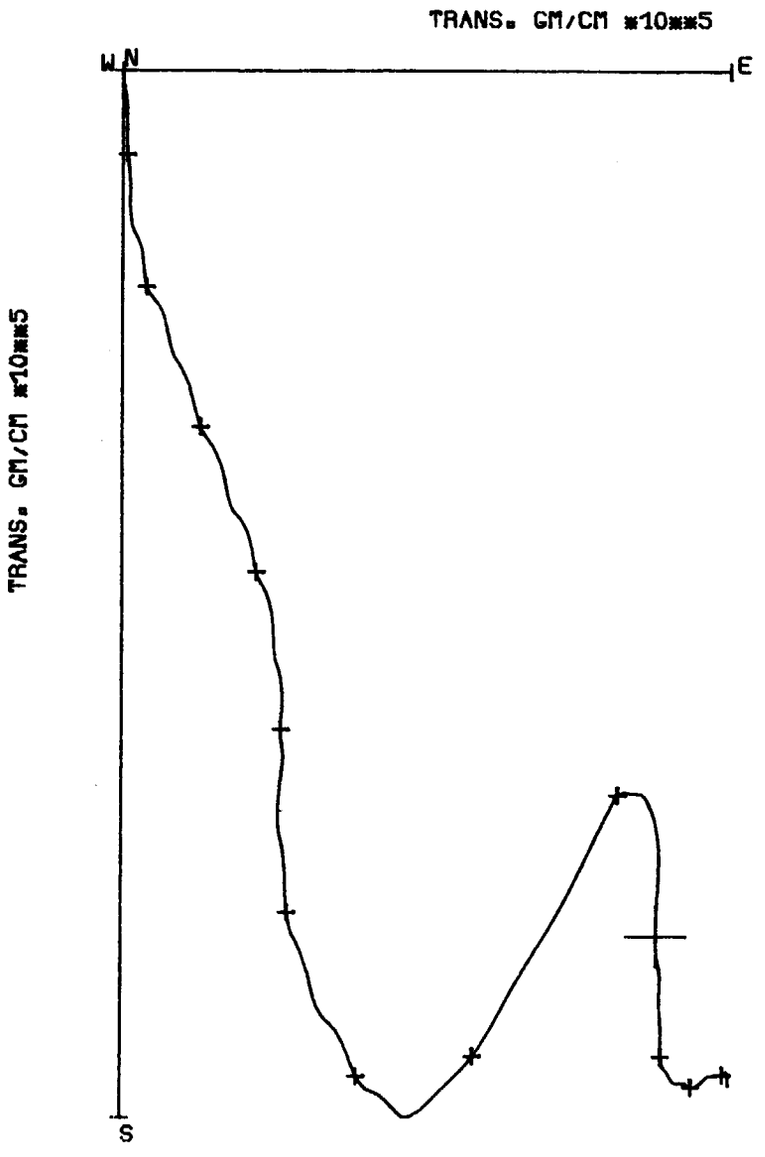
METER 570 DATE 8 2 75 SWD STN.T HT.10M Y SED. WAVES 8SEC.
TRANS. GM/CM *10**5
W
N
E
S
TRANS. GM/CM *10**5

Fig. B29

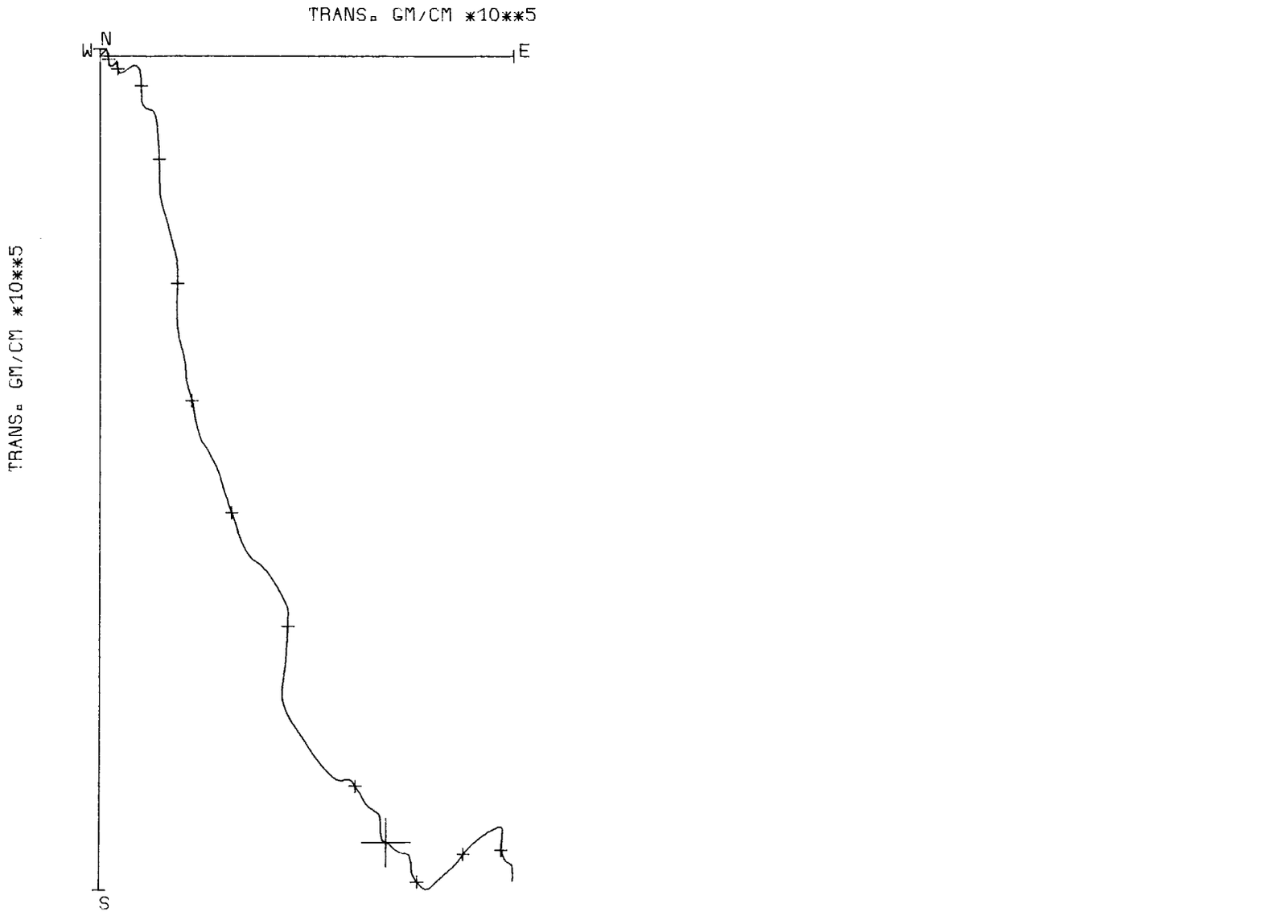
METER 663 DATE 19 4 75 SWD STN.V HT.6M Y SED. WAVES 8SEC.
TRANS. GM/CM *10**5
N
W
E
S
TRANS. GM/CM *10**5

Fig. B30

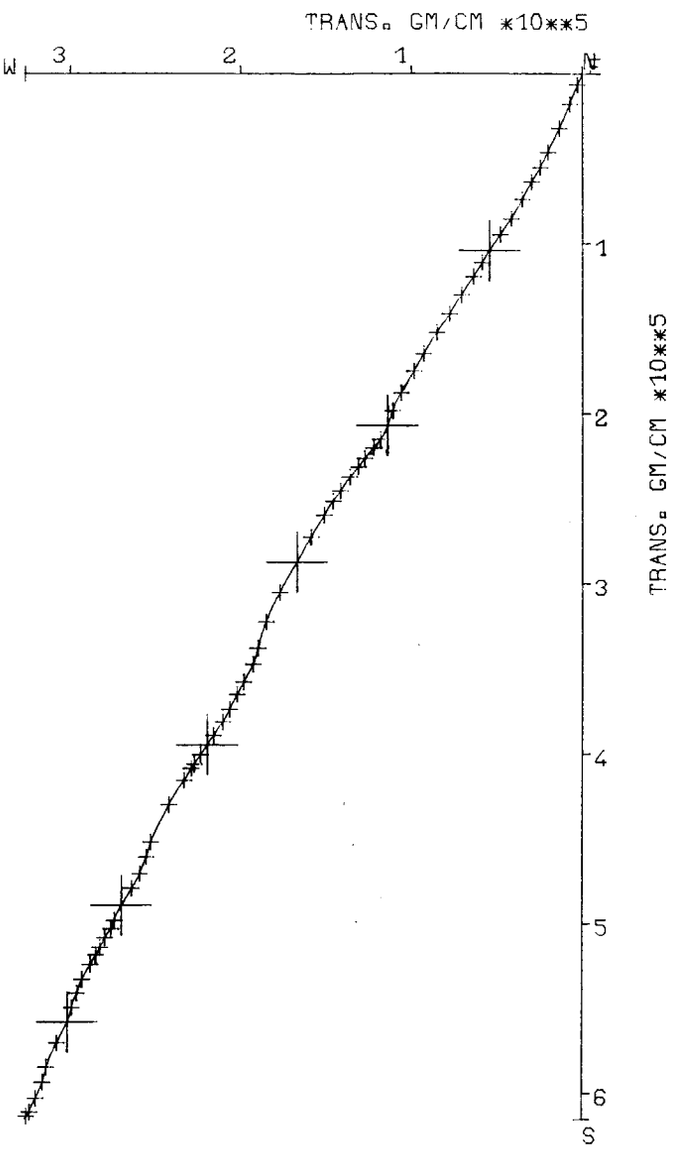
METER 534 DATE 17 8 78 SWD STN.W HT.8M T SED. WAVES 8SEC.
TRANS. GM/CM *10**5
W
3
2
1
N
1
2
3
4
5
6
S
TRANS. GM/CM *10**5

Fig. B31

METER 560 DATE 16 7 77 SWD STN.X HT.6M Y SED. WAVES 8SEC.

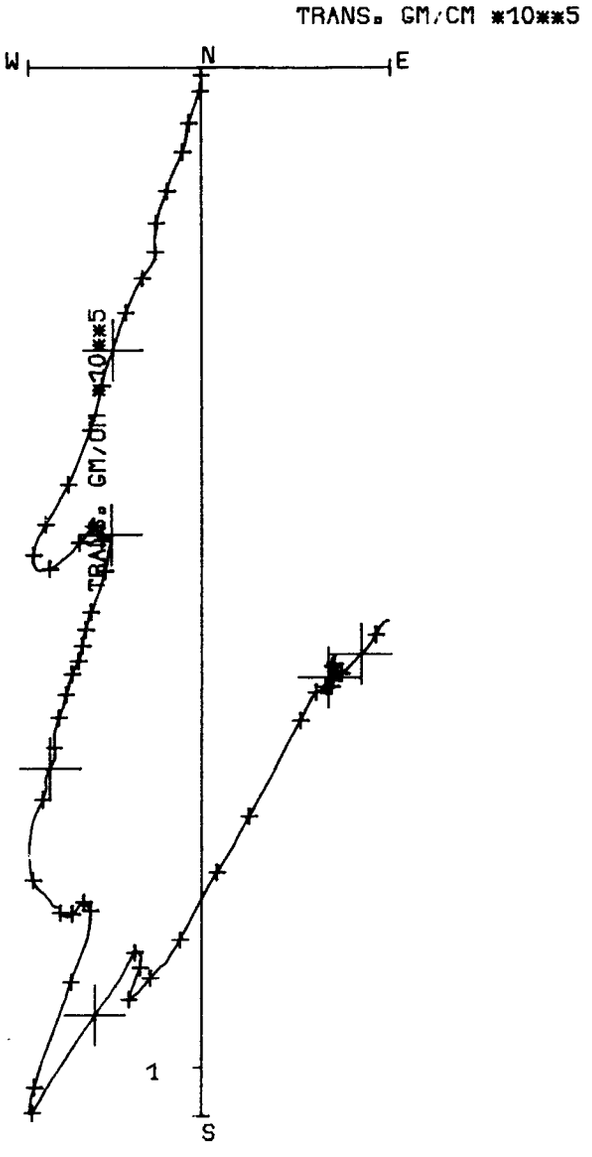

Fig. B32

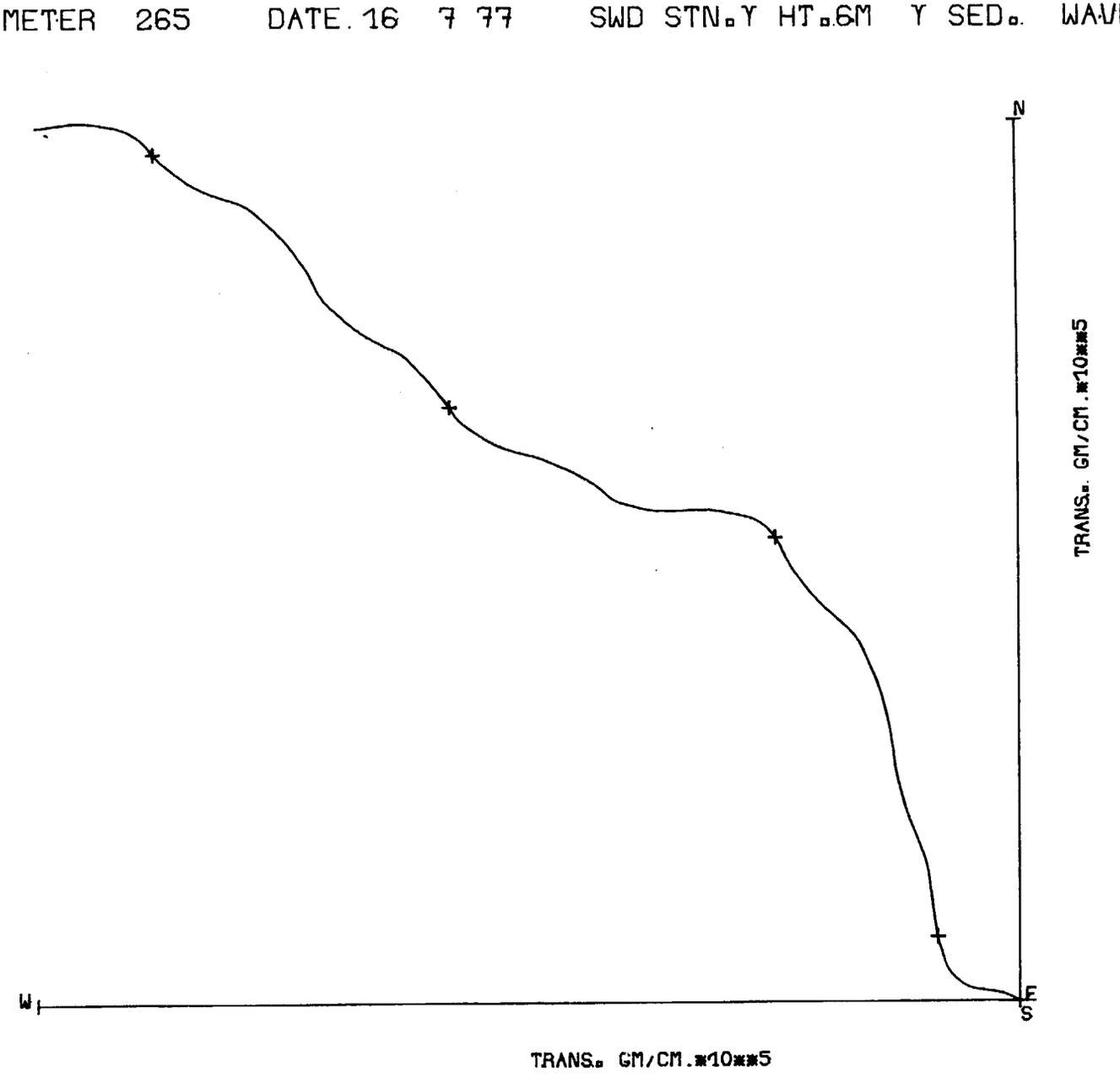
METER 265 DATE. 16 7 77 SWD STN. Y HT. 6M Y SED. WAVES 8SEC.
N
W
E
S
TRANS. GM/CM.**10**5
TRANS. GM/CM.**10**5

Fig. B33

METER 237 DATE 16 7 77 SWD STN.Z HT.8M Y SED. WAVES 8SEC.

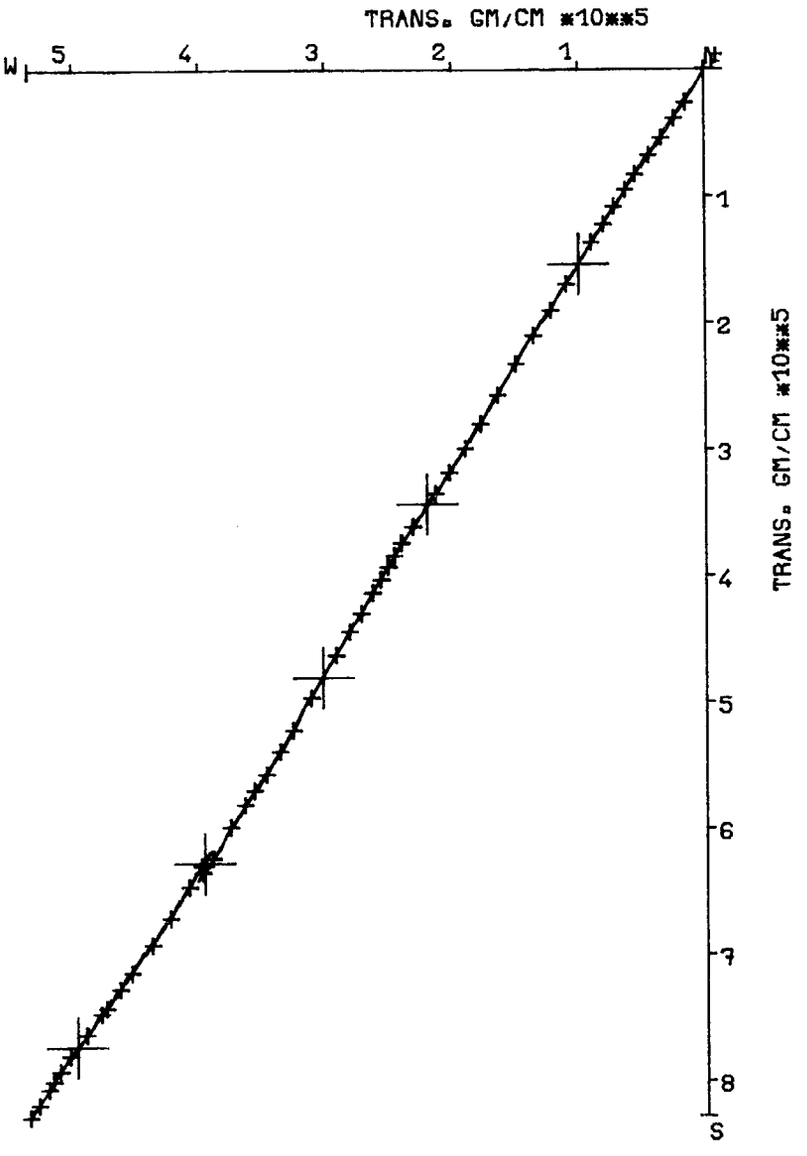

Fig. B34